Answers to the Reviewers' comments

We would like to thank the reviewers for carefully reading the manuscript and for their constructive comments, which helped us to improve our work. The comments are written with blue colour in Italic font. Our answers are given with normal font.

Reply to Reviewer #1

Comments

The manuscript presents results from the global chemistry climate model ECAM on changes regarding DNA weighted UV radiation with regard to changes in total ozone, cloud cover and surface albedo. UV data derived from the model are validated with respect to past UV data from 13 ground-based stations providing solar UV measurements while the simulated ozone is compared to SBUV ozone.

The results are discussed as three groups, defined by North and South high latitudes and middle latitudes, and model results are retrieved at the locations of the 13 ground-based stations.

The key findings presented in the manuscript are that model and measurements agree fairly well, giving support to the simulations of the future scenarios. Cloud cover is generally decreasing, leading to increased solar radiation, apart from the high latitudes, where no significant changes are observed. UV trends are a combination of ozone changes (mostly ozone recovery), and cloud cover changes, while at high latitudes, decreased surface albedo in the second half of the next century have a significant influence on the surface UV radiation.

The manuscript is well written, the references are extensive and cover the current status of the field as far as I can judge. The results are interesting and therefore the manuscript is in principle worth to be published.

Answer:

We thank the reviewer for the comments. We find very useful the reviewer's view of the key findings of our work, and we have incorporated them in the conclusions together with an appropriate acknowledgement in the Acknowledgements. We have answered all comments and made the appropriate changes to the manuscript. Important updates are that we added UV irradiance data from Sodankylä station in the plots for the

northern high latitudes (3 stations now instead of 2), and we prepared new figures using zonally averaged data for the three latitudinal bands.

In brief, the figures in the revised manuscript are as follows:

- Figure 1. DNA active irradiance (station based). Same as before, but now for 3 stations in the northern high latitudes instead of 2. Notation of simulations changed.
- Figure 2. Scatter plots of DNA active irradiance data (station-based) from Figure 1. New figure.
- Figure 3. Ozone and clouds (station based). Same as before, but now for 3 stations in the northern high latitudes instead of 2. Notation of simulations changed.
- Figure 4. Time series for the near global mean (station based). Same as before. Notation of simulations changed.
- Figure 5. Time series for the northern high latitudes (station based). Same as before, but now for 3 stations in the northern high latitudes instead of 2. Notation of simulations changed.
- Figure 6. Time series for the southern high latitudes (station based). Same as before. Notation of simulations changed.
- Figure 7. Time series of surface albedo for Barrow and Palmer. Same as before. Notation of simulations changed.

The new figures showing all latitude averaged results are presented in the updated Supplement as follows:

- Figure S1. Ozone and clouds from the global products (zonal based). New figure.
- Figure S2. Time series for the near global mean (zonal based). New figure.
- Figure S3. Time series for the northern high latitudes (zonal based). New figure.
- Figure S4. Time series for the southern high latitudes (zonal based). New figure.

However I have serious concerns with the novelty of the research and its added value with respect to already published papers, foremost the one published in 2020 by the same main author, Eleftheratos, K., Kapsomenakis, J., Zerefos, C. S., Bais, A. F., Fountoulakis, I., Dameris, M., Jöckel, P., 821 Haslerud, A. S., Godin-Beekmann, S., Steinbrecht, W., Petropavlovskikh, I., Brogniez, C., Leblanc, T., Liley, 822 J. B., Querel R., and Swart, D. P. J.: Possible Effects of Greenhouse Gases to Ozone Profiles and DNA

Active 823 UV-B Irradiance at Ground Level, Atmosphere, 11, 228, doi:10.3390/atmos11030228, 2020.

The authors discuss this manuscript at length, so they are aware that there is a need for distinction. However it seems that the main difference in this manuscript with respect to the previous work are the addition of a few ground-based stations at which the model results are analysed (13 instead of 5, of which 4 are identical). The conclusions of the manuscript are very similar to the previous manuscript, with some differences by distinguishing three latitudinal bands.

Answer:

The reviewer raised serious concerns about the novelty of the research and its added value with respect to the previous study by Eleftheratos et al., pointing out that there is need for distinction. We have added the following text in the Introduction, in order to distinct the new study from the previous one:

"It is important to clarify the novelty of this research and its added value with respect to the previous study, and to point out the main differences and similarities. The objective of this research is to study how total ozone, DNA active irradiance and cloud cover might change in the future at high latitudes due to the increasing GHGs in comparison to the near global mean (50^o N–50^o S). Also, to estimate the part of the DNA active irradiance change that can be explained by ozone and cloud changes in the future using multiple linear regression (MLR) statistical analysis. The previous study by Eleftheratos et al. (2020) did not look at high latitudes and did not apply MLR analysis to quantify the related contributions to the DNA weighted UV irradiance. The previous work analysed 5 stations between 50^o N and 50^o S. The new study is enriched with more stations at the near global scale (13 instead of 5 stations, of which 4 are identical) and, in addition, it includes analysis of averages in latitudinal bands, which was not done in the previous study, thus providing more complete results".

We hope that these clarifications will satisfy the reviewer's concerns about the novelty of the study.

The reviewer also commented that "*the conclusions of the manuscript are very similar to the previous manuscript, with some differences by distinguishing three latitudinal bands*". Our conclusions for the near global mean are indeed similar to the previous manuscript, which is why we give more attention to the high latitudes that were not studied in the previous manuscript. We point out that DNA active irradiance is expected to change differently at high latitudes than at near-global scale after around 2050. It will continue to decline at high latitudes mainly due to ozone recovery (cloud cover changes

are not significant), while it is expected to increase on a near-global scale affected by the reduction of cloud cover from climate change. This opposite behaviour is not a finding of the previous study, and we believe it is worth sharing with the scientific community. Of course, it is an outcome that emerges from the simulations of a single climate-chemistry model, and as such, it may well turn out to be true or false. Verification of the results from other model simulations would be useful. It is important to note that our free running simulations were designed according to the definitions for the reference and sensitivity simulations provided by the IGAC and SPARC communities to address emerging science questions, improve process understanding and support upcoming ozone and climate assessments (Eyring et al., 2013).

Reference

Eyring, V., Lamarque, J.-F., Hess, P., Arfeuille, F., Bowman, K., Chipperfield, M., Duncan, B., Fiore, A., Gettelman, A., Giorgetta, M., Granier, C., Hegglin, M., Kinnison, D., Kunze, M., Langematz, U., Luo, B., Martin, R., Matthes, K., Newman, P., Peter, T., Robock, A., Ryerson, A., Saiz-Lopez, A., Salawitch, R., Schultz, M., Shepherd, T., Shindell, D., Stähelin, J., Tegtmeier, S., Thomason, L., Tilmes, S., Vernier, J.-P., Waugh, D., and Young, P.: Overview of IGAC/SPARC Chemistry-Climate Model Initiative (CCMI) Community Simulations in Support of Upcoming Ozone and Climate Assessments, SPARC Newsletter, 40, 48-46, 2013.

Since the model used in the analysis is a global model, the restriction to 13 specific sites must be for good reason. The only reason I can see is that this allows comparison between the ground based UV stations with the model at these locations, in order to validate the model. I am not convinced by this argument for the following reasons:

• The model has a resolution of 3°x3°, which is a huge area for which the point measurement has to be representative for. I doubt that this is the case for several stations where the surrounding area is inhomogeneous, such as mountain tops (Mauna Loa, Sonnblick, Zugspitze), or in valleys (Aosta), or by being in a town with very heterogeneous surroundings (sea, mountains, tropospheric ozone and aerosols such as Athens).

• The correlation for DNA weighted UV irradiance is actually not very good, and the figures in the supplementary material show quite different behaviour. A general comment is that the correlation is not the only measure for the agreement between two datasets, but also the slope between two datasets (from a scatter plot), are significantly different from one, showing that the model results disagree quite significantly from the

measurements, see Table S1 with a summary of the statistics. For me these comparisons do not support any validation of the model.

Answer:

Yes, the reason for the restriction to specific sites was because it allowed comparison between the ground-based UV stations and the model at these locations. We did not have any better way to test the model simulations with real measurements. We agree with the reviewer's comment that these comparisons do not support any validation of the model, which is why we do not use the word "validation" in the text but the word "evaluation", which is more appropriate.

More specifically, the resolution of the model of 3^o x 3^o is indeed a large area for which the point measurement has to be representative for. We thank the reviewer for bringing this up, and we have made a note on these comments in the revised Section 3.1, as follows:

"We note here that the model has a resolution of about 3° x 3°, which is a large area for which the point measurement has to be representative for. As such, for stations where the surrounding area is inhomogeneous, such as mountain tops (Mauna Loa, Sonnblick, Zugspitze), or in valleys (Aosta), or by being in a town with very heterogeneous surroundings (sea, mountains, tropospheric ozone and aerosols such as Athens), the model simulations of DNA active irradiance are not expected to be fully representative of the specific UV sites. Thus, the correlation between modelled and measured DNA weighted UV irradiance is not very good at some stations, as shown in the figures provided in the supplementary material. For the same reason, the slope between two datasets can deviate significantly from unity (see Supplement Table S1). Therefore, the comparisons at the individual stations provide a qualitative evaluation of the model's variability, but cannot be considered as a strict validation of the model."

• *The comparisons were performed for past to present data, using a model with prescribed dynamics. However the results of the manuscript are obtained using a free-running model, which as the authors write themselves, has serious shortcomings. The Appendix A discusses this fact, which is appreciated.*

Answer:

Indeed, the results of the manuscript were obtained using a free-running model, which has shortcomings during the period of the observed ozone depletion as discussed in

Appendix A. Nevertheless, after the 1980's the model seems to reproduce quite well the observed ozone variability.

• ozone and Cloud cover are obtained from satellite measurements, which also give a global product.

Answer:

We now analyse the global products of ozone and Cloud cover from satellite measurements and compare them with the respective model simulations. We have added a new figure in the Supplement, as Figure S1, showing the comparisons for ozone and Cloud cover using the zonally averaged data. The results of the statistical comparisons are in line with those from the station averaged data.

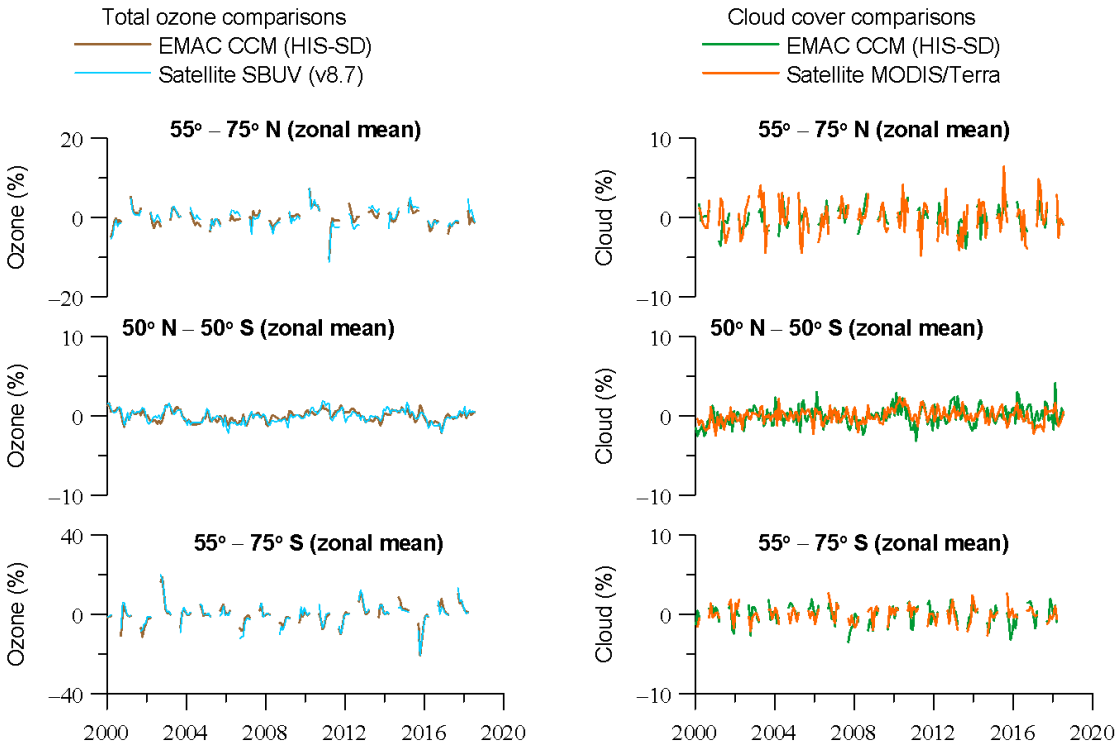

Figure S1. (a) Comparison of zonally averaged ozone column from model simulations and satellite measurements for the northern high latitudes (55°–75° N) (upper panel), the near-global mean (50° N–50° S) (middle panel) and the southern high latitudes (55°–75° S) (lower panel). **(b)** Same as **(a)** but for zonally averaged cloud cover. The y-axes show monthly de-seasonalized anomalies (in %) relative to the long-term monthly mean (2000–2018). Shown are monthly anomalies from March to September for the northern high latitudes, and from September to March for the southern high latitudes. For 50° N–50° S, we present all months.

• The authors themselves mention that some stations might not be very representative, being close to the shore (Barrow and Palmer, line 493).

Answer:

We have added one more station in the northern high latitudes, namely Sodankylä in Finland. The UV irradiance data for Sodankylä were provided by Dr. Kaisa Lakkala and cover the period 1990-2021. The analysis of the model data for Sodankylä was performed by Dr. Kostas Douvis from the Academy of Athens. These two scientists have been added in the list of co-authors. The figures and tables referring to the average of northern high latitude stations have been updated.

Therefore the benefit of restricting the analysis of the model results to only 13 point locations does not compensate for the results obtained if the model results were analysed as a whole, for example in latitudinal bands, or by selecting specific regions where future changes are expected to be very different (Europe versus Asia, Sahara, …).

Answer:

We now complement the analysis presented in Section 3.2 with zonally averaged data, in order not to restrict the analysis of the model results to only 13 locations according to the reviewer's comment, but to analyse model results for example in latitudinal bands. We have added three new figures in the Supplement that show the changes from the free running simulations for the near global mean, the northern and southern high latitudes based on latitudinal averages. The three new figures are presented below. The results from the analysis of averaging the model data in latitudinal bands are in the same direction with that from the station averages. The results are discussed in Section 3.2. The new figures based on zonally averaged data for the near global mean, the northern and southern high latitudes are the Supplement Figures S2, S3 and S4, respectively.

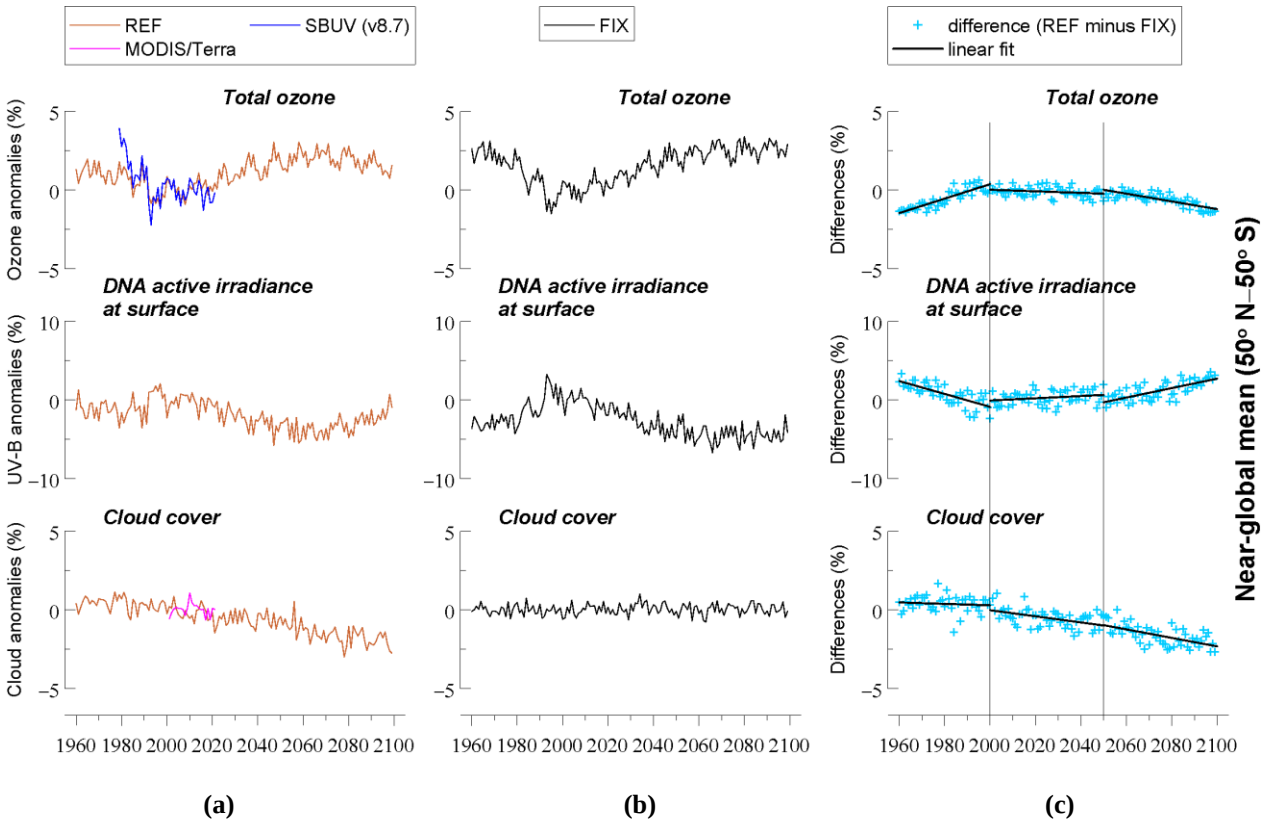

Figure S2. Changes in zonal mean total ozone, zonal mean DNA active irradiance and zonal mean cloud cover for the near global mean (50° N – 50° S), based on simulations with increasing and fixed GHGs mixing ratios. **(a)** REF is the simulation with increasing GHGs according to RCP-6.0. **(b)** FIX is the simulation with fixed GHGs emissions at 1960 levels. **(c)** Difference between the two model simulations, indicating the impact of increasing GHGs. The y-axes in (a) and (b) show yearly averaged data (in %) calculated from de-seasonalized monthly data. The monthly data were de-seasonalized relative to the long-term monthly mean (1990–2019) and were expressed in %. For 50° N–50° S we used all months to calculate the annual average.

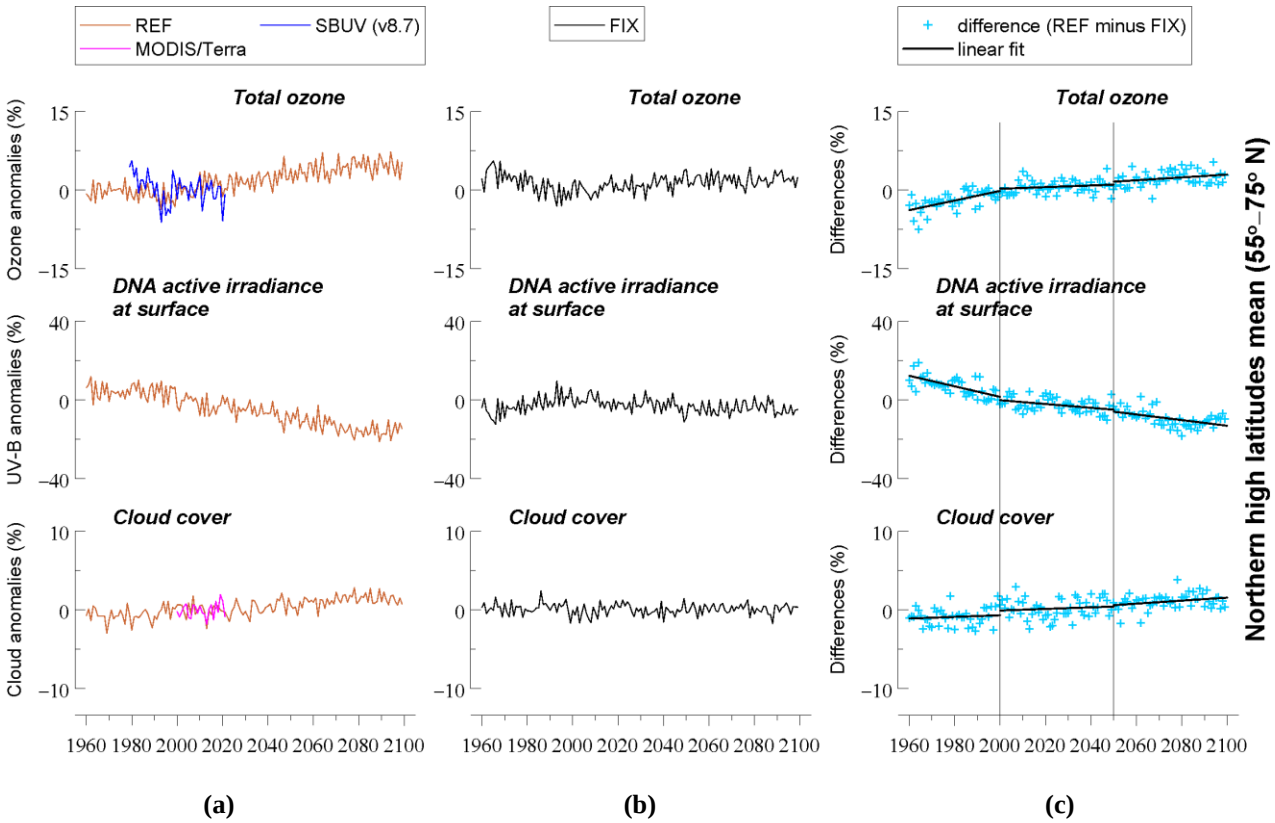

Figure S3. Same as Figure S2 but for northern high latitudes (55° – 75° N). The y-axes in (a) and (b) show yearly averaged data (in %) calculated from de-seasonalized monthly data. For the northern high latitudes, the annual average refers to the average of monthly anomalies from March to September.

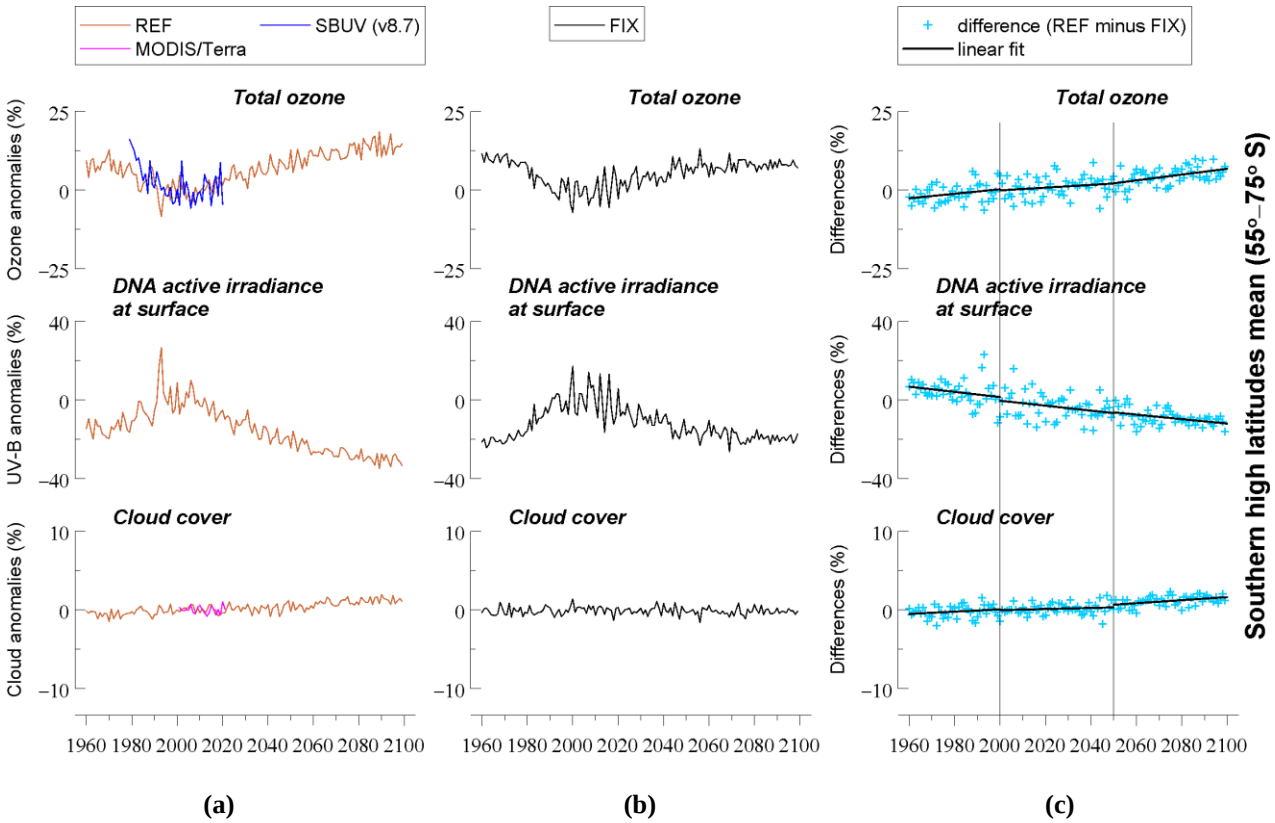

Figure S4. Same as Figure S2 but for southern high latitudes (55° – 75° S). The y-axes in (a) and (b) show yearly averaged data (in %) calculated from de-seasonalized monthly data. For the southern high latitudes, the annual average refers to the average of monthly anomalies from September to March.

Some Specific comments

– The simulations of the future climate did not take into account possible solar variabilities (grand minimum, as discussed in Anet, J., Rozanov, S. Muthers, et al., Impact of a potential 21st century "grand solar minimum" on surface temperatures and stratospheric ozone, Geophys. Res. Lett., 40, 4420–4425, doi:10.1002/grl.50806, 2013, and Arsenovic, P., Rozanov, J. Anet, et al., Implications of potential future grand solar minimum for ozone layer and climate, Atmos. Chem. Phys., 18, 3469–3483, doi: 10.5194/acp-18-3469-2018, 2018.

Answer:

The simulations of the future climate were setup to account for the solar variability according to Jöckel et al. (2016), as follows:

"The future solar forcing, used for the projections, has been prepared according to the solar forcing used for CMIP5 simulation of HadGEM2-ES, where the SSTs and SICs are taken from Jones et al. (2011; see also Sect. 3.3 of Jöckel et al., 2016). It consists of repetitions of an idealized solar cycle connected to the observed time series in July 2008. This has been applied consistently for all projections with prescribed SSTs (RC2-base) and the same holds also for the SC-simulations. Here, we deviate from the CCMI recommendations consisting of a sequence of the last four solar cycles (20–23) (see Sect. 3.4 of Jöckel et al., 2016)."

We now explain this in the revised Section 2.3.

New reference added in the References:

Jones, C. D., Hughes, J. K., Bellouin, N., Hardiman, S. C., Jones, G. S., Knight, J., Liddicoat, S., O'Connor, F. M., Andres, R. J., Bell, C., Boo, K.-O., Bozzo, A., Butchart, N., Cadule, P., Corbin, K. D., Doutriaux-Boucher, M., Friedlingstein, P., Gornall, J., Gray, L., Halloran, P. R., Hurtt, G., Ingram, W. J., Lamarque, J.-F., Law, R. M., Meinshausen, M., Osprey, S., Palin, E. J., Parsons Chini, L., Raddatz, T., Sanderson, M. G., Sellar, A. A., Schurer, A., Valdes, P., Wood, N., Woodward, S., Yoshioka, M., and Zerroukat, M.: The HadGEM2-ES implementation of CMIP5 centennial simulations, Geosci. Model Dev., 4, 543–570, https://doi.org/10.5194/gmd-4-543-2011, 2011.

– Future changes in aerosol loading are expected to be significant in some areas of the globe, having a strong impact on the UV radiation reaching the surface.

Answer:

We agree that future changes in aerosol loading will have a strong impact on the UV radiation reaching the surface. In all simulations analyzed here, we used prescribed aerosol distributions. Since the aerosol distributions have been prescribed, there is no aerosol output for these simulations that we could use to examine the impact of aerosols on the UV radiation.

In the revised Section 2.3, we clarify that:

"In all simulations analyzed here, we used prescribed aerosol distributions. The prescribed aerosol effects are separated into the aerosol surface area, representing chemical effects via heterogeneous chemistry, and the radiative properties influencing the radiation budget (Sect. 3.7 of Jöckel et al., 2016). Due to a glitch, the stratospheric volcanic aerosol was not considered correctly in the free running simulations (Sect. 3.12.1 of Jöckel et al., 2016). Therefore, the dynamical effects of large volcanic eruptions (e.g. Mt. Pinatubo 1991; El Chichón 1982) are essentially not represented in the simulations, except for the contribution to the tropospheric temperature signal induced by the prescribed SSTs. For the specified dynamics simulations, however, this has been corrected. Since the aerosol distributions have been prescribed, there is no aerosol output for these simulations that we could look at. As such, we cannot investigate the impact of future changes in aerosol loading on the UV radiation reaching the surface."

– The significance of the results are mainly described by correlation coefficient and p values. The supporting figures, for example Figure 1, however show that the variability between the model and ground based stations is very large. Even though scatter plots are also not the method of choice, they would give a better indication how two datasets would scatter, and the slope and associated fitting uncertainties would give an indication on how well the two datasets agree. I would have preferred the authors to have used other metrics as well, such as uncertainties (at the 95% confidence level) derived from the statistical models.

Answer:

The reviewer wanted to see scatter plots and describe the significance of the results with more statistical parameters. We have added the scatter plots, as suggested by the

reviewer, in a new figure. The new figure is Figure 2. The regression lines have been added. The related statistics (slope, error of slope and root mean square error) are now discussed in the text. Section 3.1 has been revised.

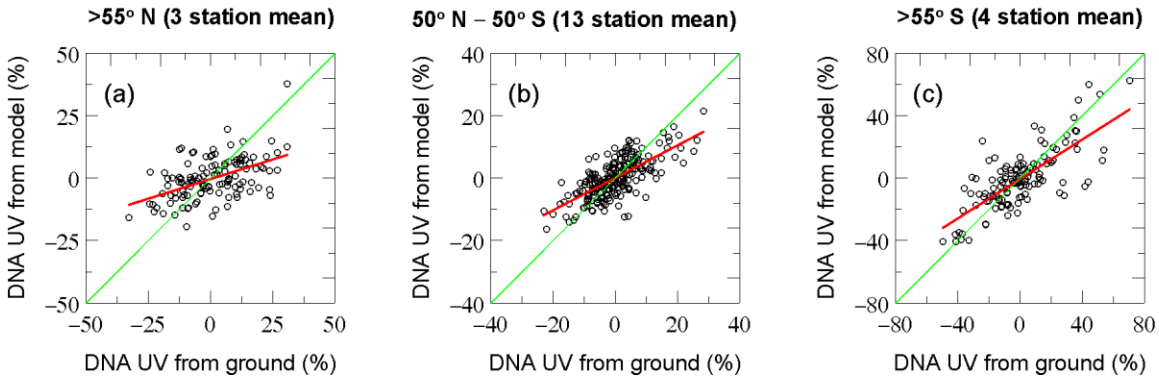

Figure 2. Scatter plots of DNA active irradiance from simulated and ground-based data shown in Figure 1 for **(a)** 3 UV stations in the northern high latitudes (>55° N), **(b)** 13 UV stations from 50° N to 50° S and **(c)** 4 UV stations in the southern high latitudes (>55° S).

– The statistical approach of using a MLR technique is interesting, but why did not the authors include in equation 7 also the surface albedo, instead of treating it separately in the following section?

Answer:

The reason for treating it separately in the following section is because we did not analyse surface albedo for all stations but only for Barrow and Palmer.

In the revised manuscript, we have applied equation 7 to the zonal means of 55° – 75° N and 55° – 75° S, also including the surface albedo parameter. The results are included in Section 3.4, as follows:

"In order to better represent the northern and southern high latitudes, we also applied the MLR model to the large-scale zonal means of 55° – 75° N and 55° – 75° S. For the northern high latitude zone, the findings are in the same direction as those found for Barrow. We estimate that ~31% of the DNA active irradiance trend is determined by the trend in ozone, and that ~14% and ~32% of the DNA active radiation trend are explained by trends in clouds and surface albedo, respectively. For the southern high latitude zone, we estimate that the largest part of the DNA active irradiance trend is determined by the trend in ozone, and that the contributions of cloud and albedo trends are small."

– The datasets would have been ideally suited to be analysed using the very powerful Dynamical Linear Modelling (DLR), for example, Alsing, (2019) dlmmc: Dynamical linear model regression for atmospheric time-series analysis. Journal of Open Source Software, 4(37), 1157, https://doi.org/10.21105/joss.01157, and Laine, M., Latva-Pukkila, N., and Kyrölä, E.: Analysing time-varying trends in stratospheric ozone time series using the state space approach, Atmos. Chem. Phys., 14, 9707–9725, https://doi.org/10.5194/acp-14-9707-2014, 2014.

Answer:

Yes, they would, but we do not have experience with the Dynamical Linear Modelling. We leave this kind of analysis for a future study.

– Figure 1: 50N-50S, there is a striking difference between model and measurements around the year 2012, of about 15%, which seem not be seen in either ozone or cloud cover. Did the authors investigate this feature?

Answer:

We thank the reviewer for noticing this. By mistake we had plotted the wrong line from the model. We now plot the new correct line, and the striking difference is not there anymore. Figure 1 and related statistics in Table 2a have been corrected. The corrected Figure 1 is as follows:

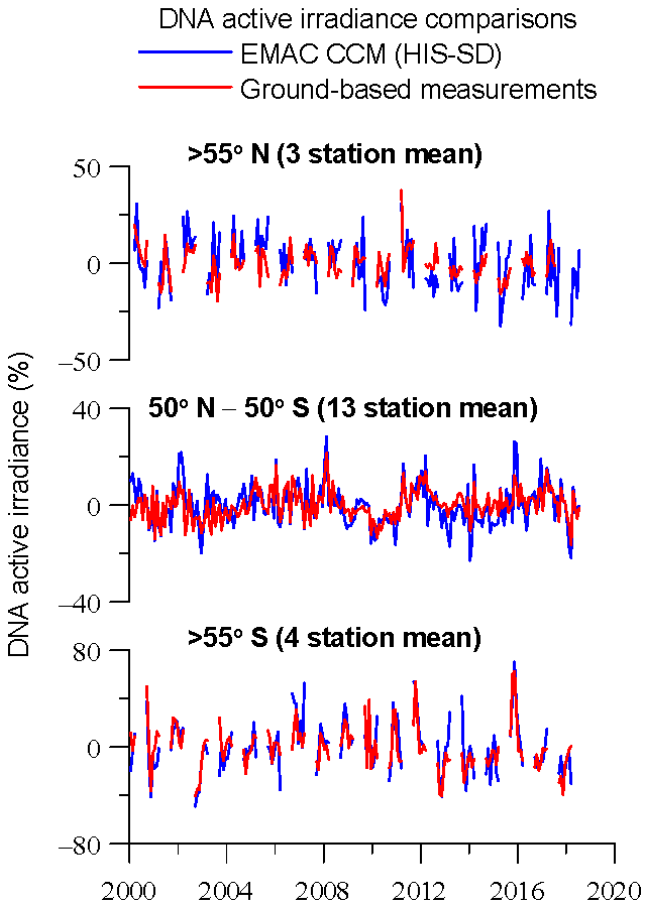

Figure 1. Comparison of model simulations of DNA active irradiance with averages of ground-based measurements at 3 UV stations in the northern high latitudes (>55° N) (upper panel), 13 UV stations from 50° N to 50° S (middle panel) and 4 UV stations in the southern high latitudes (>55° S) (lower panel). The y-axis shows monthly de-seasonalized DNA active irradiance data (in %). The monthly data at each station were de-seasonalized by subtracting the long-term monthly mean (2000–2018) pertaining to the same calendar month and were expressed in %. Then, the average over each geographical zone was estimated by averaging the de-seasonalized data of the stations belonging to each geographical zone. Shown are data from March to September for the northern high latitudes and from September to March for the southern high latitudes.

– In the figures from the supplement, the model variabilities of the DNA weighted irradiance are much larger than the corresponding measurements for : Barrow, Villeneuve d'Ascq, Aosta, Lauder, Ushuaia, while they are in better agreement for Summit, Thessaloniki, Boulder, Mauna Loa, or Alice Springs. For Athens, between approx. 2012 and 2015 the measurements are significantly higher than the model results, why is that so?

Answer:

As it is now clarified in the revised Section 3.1, the main reason for these differences in the variability of the DNA weighted irradiances is that we compare averages for 3° x 3° pixels (model simulations) with measurements performed at specific sites (representing narrow areas in the corresponding pixels). Thus, environmental features within the model pixel – that do not affect the station where measurements are performed – may lead to increased variability for the model with respect to the station. For example, the sites of Aosta, Lauder and Ushuaia are surrounded by very high mountains where surface albedo varies significantly in the year and affects strongly the levels of UV irradiance. The measurement sites however are at lower altitudes and changes in surface albedo do not affect strongly the levels of surface UV irradiance. In other sites (e.g., Villeneuve d'Ascq) environmental conditions are possibly less variable with respect to the average conditions in the pixel wherein they belong. Other sites (e.g., Summit, Thessaloniki, Boulder, Mauna Loa, or Alice Springs) are possibly more representative for the average conditions in the pixels wherein they belong. For Athens, the most possible explanation for the much higher measured UV relative to the UV simulated by the model in 2011 – 2014 is again that the model cannot accurately capture changes in air quality (e.g., aerosols, tropospheric ozone etc.) at the city since it represents a much wider area. We were not able to find aerosol optical properties in the UV for the same period for the site in order to verify our assumption but we intend to further investigate these differences in the future.

We make a note on these comments in the updated Supplement of this study.

– The cloud cover from Modis/Terra and the model show no correlation for most stations, apart for example for Aosta, which is slightly better. Can the authors provide some comments why some stations show better agreement than others?

Answer:

It would be nice if we obtained good model – satellite correlations from all datasets. We would have perfect model simulations and perfect satellite measurements at all locations. Frankly speaking, we cannot say which of the two datasets is responsible for the smaller agreement at some stations or if both are. But statistically speaking, we find that the majority of the stations (13 of 20 stations) show medium to good correlations (between 0.5 and 0.7), 5 stations show small to medium correlations (between 0.3 and 0.5), and only 2 stations show no correlation. The stations that show no correlation are Summit and South Pole. Both stations are high-altitude sites located at high latitudes with year-round snow cover and albedos of larger than 0.95. Multiple scattering

between the surface and clouds greatly reduces cloud effects (Nichol et al., 2003). Mauna Loa (MLO) is also a high-altitude site. MLO is interesting, not only because it is also at high altitude, but because there are often clouds below the station, which enhance downwelling radiation similar to the effect of high albedo. Both in Antarctica and MLO, UV radiation is scattered up either by snow or a cloud layer, and then Rayleigh-scattered down to increase downwelling irradiance. However, we find that the correlation is 0.592 for the cloud case in MLO, suggesting that other contributing processes might account for somewhat successful cloud simulations in the EMAC model which would require further investigation. The stations with small to medium correlations (between 0.3 and 0.5) are Haute Provence, Athens, Lauder, Ushuaia and Palmer. We remind that all correlations were derived from de-seasonalized data, i.e. data after removing the mean seasonal cycle of the period 2000-2018. This was performed because we wanted to evaluate the long-term variability of cloud cover and not its seasonal cycle.

We make a note on these comments in the updated Supplement of this study.

Reference

Nichol, S. E., Pfister, G., Bodeker, G. E., McKenzie, R. L., Wood, S. W., and Bernhard, G.: Moderation of cloud reduction of UV in the Antarctic due to high surface albedo, J. Applied Meteorology, 42, 1174–1183, DOI: https://doi.org/10.1175/1520-0450(2003)042<1174:MOCROU>2.0.CO;2, 2003.

Reply to Reviewer #2

The manuscript presents valid and useful analysis with adequate source data, solid statistical analysis and interpretation and reasonable (but not spectacular or unexpected) conclusions. I am favourable on the scientific merits of this work despite the fact that a very similar analysis (now enriched with more data here) has already been published before by the same first author (I do not see this as an obstacle for publication). I only have the following comments which I would like to see addressed (numbers indicate the respective manuscript lines):

Answer:

We would like to thank the reviewer for the useful comments and for finding our work worthy of publication despite of our previously published paper. All comments have been answered and the text has been revised accordingly.

GENERAL

1-3: The title oversells the role of GHGs. The analysis of UV changes is done for simulations with and without time-varying GHGs and without doubt, modelled changes (=increases) of GHGs are driving the UV changes. But the actual UV change is mainly brought about by cloud changes (driven by changes in GHGs) that correctly the manuscript places in primary focus.

Answer:

The reviewer correctly writes that the actual UV change is mainly brought about by cloud changes (driven by changes in GHGs). We have revised the title of the paper to also mention the cloud changes, as follows:

"Ozone, DNA active UV radiation and cloud changes for the near global mean and at high latitudes due to enhanced greenhouse gas concentrations".

100-109: In direct relation to my comment for lines 1-3 and perhaps to justify the prominent insertion of the GHGs in the title, 1-2 additional lines should elaborate on why/how the GHG changes drive the cloud changes (that actually effect the UV changes).

Answer:

We now discuss why/how the GHG changes can drive the cloud changes, as follows:

"Norris et al. (2016) provided evidence for climate change in the satellite cloud record. They estimated fewer clouds over the mid-latitudes from 1983 to 2009 and concluded that the observed and simulated cloud change patterns are consistent with poleward retreat of mid-latitude storm tracks, expansion of subtropical dry zones, and increasing height of the highest cloud tops at all latitudes. The primary drivers for these changes were found to be the increasing GHG concentrations and a recovery from volcanic radiative cooling (Norris et al., 2016). In the same direction, Schneider et al. (2019) showed that stratocumulus clouds, some of the planet's most effective cooling systems, become unstable and break up into scattered clouds under increasing GHG concentrations. Their results also showed that less clouds will trigger additional surface warming in addition to that from the rising CO_2 levels (Schneider et al., 2019). Both studies provided indications that increasing GHGs can affect clouds, which in turn can affect the UV radiation changes."

Two references have been added:

Norris, J. R., Allen, R. J., Evan, A. T., Zelinka, M. D., O'Dell, C. W., and Klein, S. A.: Evidence for climate change in the satellite cloud record, Nature, 536, 72–75, doi: 10.1038/nature18273, 2016.

Schneider, T., Kaul, C. M., and Pressel, K. G.: Possible climate transitions from breakup of stratocumulus decks under greenhouse warming, Nature Geoscience, 12, 163–167, https://doi.org/10.1038/s41561-019-0310-1, 2019.

177-178: From the way it is written, I deduce that the reference simulation includes additional 10 years of run for spin-up, while the sensitivity one, no. Is this correct? If yes, does this affect the ozone simulation? Ideally, shouldn't the runs be identical (with only difference the time-varying GHGs)?

Answer:

Indeed, the reference simulation (RC2-base-04) includes 10 year spin-up (1950-1960) to overcome the original initial conditions chosen for 1950, in particular the initialized distributions of the chemical compounds, in order to get the model on the RCP-6.0 track. From 1960 onwards, both simulations (the reference and the sensitivity SC2-

fGHG-01) both follow the RCP-6.0 scenario with the GHG kept at 1960 levels for the sensitivity simulation.

In other words, SC2-fGHG-01 was "branched off" from the reference and both share the same spin-up period.

As such, the only difference from 1960 to 2100 is indeed the time-varying vs. constant GHG.

267-268: The importance of this comment goes beyond technicalities so I insert it here. Currently the manuscript, throughout the figures, labels the three model runs according to their original names given by the modellers for specific reasons but are not necessary for the journal paper reader (in contrast they make harder following the figure content). The model run labels in the figure must be short and intuitive, for example:
SC1SD-Base02 -> HIS (for historical/hindcast)
RC2-Base04 -> SCE (for time-varying GHGs)
SC2-fGHG-01 -> FIX (for fixed GHGs)

Answer:

The notation of our simulations has been used in previous publications as well, and it largely follows the CCMI notation: R stands for Reference, C for CCMI phase 1, SD for specified dynamics (i.e. nudged), and base for "basic setup" vs. anything else, for instance fGHG for fixed Greenhouse Gases. The number determines either the correct realisation after n-1 attempts or the ensemble member.

In particular "SD" is an important indicator for the setup, because it distinguishes specified dynamics from free running simulations.

Since this notation has been used in other publications as well, we are hesitating to change them; however, since the reviewer thinks it is hard for the reader to follow the figure content, we will change the notation as follows:

In the description we once introduce "our" names and later use the suggested abbreviations, for instance:

- SC1SD-base-02 --> further abbreviated as HIS-SD for historical specified dynamics
- RC2-base-04 --> further denoted as REF for reference, and
- SC2-fGHG-01 --> further denoted as FIX for fixed GHGs.

590-592: how many Sigmas is this uncertainty range defined for? please clarify.

Answer:

We have revised the lines which now mention the Sigmas as follows:

“We conducted a separate analysis on total cloud cover variability and trends through the 21st century, using the available simulations from the CCMI-1 REF-C2 set, which showed that the EMAC CCM results fall well within the range of uncertainty (i.e., ± 2σ), and is close to the ensemble average (± 1σ)."

TECHNICAL

176: Move the description of the runs in a different paragraph for easier reading.

Answer: Done

179-185: " Furthermore, we have analyzed the ...". The description of the EMAC RC1SD-base-10 can preceed the description of the scenario runs.

Answer: Done

186-192: Further description of the scenario runs must be merged with the previous one in lines 176-179.

Answer: Done

211-225: The deseasonalisation definitions and the t-test formula for the correlation coefficient formula may be introduced as a "statistical methods (or formulas)" sub-section in a Data and Methods Section.

Answer: Done. We have moved the lines to a new Section 2.4 “Statistical methods”.

256: replace "and of the parameters" with "and the parameters"

Answer: Done

408-423: the mathematics (equations etc) used for the statistical tests for difference may be introduced as a "statistical methods (or formulas)" sub-section (same as in comment for lines 211-225) in a Data and Methods Section.

Answer: Done. We have moved the lines to a new Section 2.4 “Statistical methods”.

Ozone ~~and,~~ DNA active UV radiation and cloud changes for the near global mean and at high latitudes due to enhanced greenhouse gas concentrations

Kostas Eleftheratos[1,2], John Kapsomenakis[3], Ilias Fountoulakis[4,5], Christos S. Zerefos[2,3,6], Patrick Jöckel[7], Martin Dameris[7], Alkiviadis F. Bais[8], Germar Bernhard[9], Dimitra Kouklaki[1], Kleareti Tourpali[8], Scott Stierle[10], J. Ben Liley[11], Colette Brogniez[12], Frédérique Auriol[12], Henri Diémoz[5], Stana Simic[13], Irina Petropavlovskikh[14], Kaisa Lakkala[15,16], Kostas Douvis[3]

[1]Department of Geology and Geoenvironment, National and Kapodistrian University of Athens, Athens, Greece
[2]Center for Environmental Effects on Health, Biomedical Research Foundation of the Academy of Athens, Athens, Greece
[3]Research Centre for Atmospheric Physics and Climatology, Academy of Athens, Athens, Greece
[4]Institute for Astronomy, Astrophysics, Space Applications and Remote Sensing, National Observatory of Athens (IAASARS/NOA), Athens, Greece
[5]Aosta Valley Regional Environmental Protection Agency (ARPA), Saint-Christophe, Italy
[6]Navarino Environmental Observatory (N.E.O), Messenia, Greece
[7]Deutsches Zentrum für Luft- und Raumfahrt, Institut für Physik der Atmosphäre, Oberpfaffenhofen, Germany
[8]Department of Physics, Aristotle University of Thessaloniki, Thessaloniki, Greece
[9]Biospherical Instruments Inc., San Diego, CA 92110, USA
[10]NOAA Global Monitoring Laboratory, Boulder, CO 80305, USA
[11]National Institute of Water & Atmospheric Research (NIWA), Lauder, New Zealand
[12]Univ. Lille, CNRS, UMR 8518 - Laboratoire d'Optique Atmosphérique, F-59000 Lille, France
[13]Institute for Meteorology and Climatology, University of Natural Resources and Life Sciences, Vienna 1180, Austria
[14]Cooperative Institute for Research in Environmental Sciences, University of Colorado, Boulder, CO, USA
[15]Space and Earth Observation Centre, Finnish Meteorological Institute, Sodankylä, Finland
[16]Climate Research Programme, Finnish Meteorological Institute, Helsinki, Finland

Correspondence to: Kostas Eleftheratos (kelef@geol.uoa.gr)

Abstract. This study analyses the variability and trends of ultraviolet-B (UV-B, wavelength 280–320 nm) radiation that can cause DNA damage, which are caused by climate change due to enhanced greenhouse gas (GHG) concentrations. The analysis is based on DNA active irradiance, total ozone, total cloud cover, and surface albedo calculations with the EMAC Chemistry-Climate Model (CCM) free running simulations following the RCP-6.0 climate scenario for the period 1960–2100. The model output is evaluated with DNA active irradiance ground-based measurements, satellite SBUV (v8.7) total ozone measurements and satellite MODIS/Terra cloud cover data. The results show that the model reproduces the observed variability and change of total ozone, DNA active irradiance, and cloud cover for the period 2000-2018 quite well according to the statistical comparisons. Between 50° N–50° S, the DNA-damaging UV radiation is expected to decrease until 2050 and to increase thereafter, as it was shown previously by Eleftheratos et

al. (2020). This change is associated with decreases in the model total cloud cover and ~~insignificant~~ negative trends in total ozone after about 2050 due to increasing GHGs. The new study confirms the previous work by adding more stations over low and mid-latitudes (13 instead of 5 stations). In addition, we include estimates from high latitude stations with long-term measurements of UV irradiance (~~2~~–3 stations in the northern high latitudes and 4 stations in the southern high latitudes greater than 55°). In contrast to the predictions for 50° N–50° S, it is shown that DNA active irradiance will continue to decrease after the year 2050 over high latitudes because of upward ozone trends. At latitudes poleward of 55° N, we estimate that DNA active irradiance will decrease by ~~10.6~~8.2 ± ~~3.7~~3.8% from 2050 to 2100. Similarly, at latitudes poleward of 55° S, DNA active irradiance will decrease by 4.8 ± 2.9% after 2050. The results for the high latitudes refer to the summer period and not to the seasons when ozone depletion occurs, i.e., in late winter and spring. The contributions of ozone, cloud and albedo trends on the DNA active irradiance trends are estimated and discussed.

1 Introduction

The observed depletion of stratospheric ozone in the middle and high latitudes in the 1980s and the 1990s was followed by a general stabilization in the 2000s and by signs of recovery in the 2010s (Solomon et al., 2016; Weber et al., 2018; Krzyścin and Baranowski, 2019). The general behavior of ozone in the last 4 decades motivated research into the response of UV variability to ozone variability during periods with and without ozone decline. UV-B radiation is of special importance because of its effects on human health and the environment. In the short-term, the biological effects of UV-B radiation on humans include skin effects (erythema, photodermatitis) and eye effects (keratitis, conjunctivitis). Long-term effects include skin cancer, skin aging and cataracts. UV radiation can also damage the immune system and DNA (Lucas et al., 2019, Section 3.2 and references therein).

Changes in UV-B radiation and their relation to the depletion of the ozone layer in the stratosphere are being studied since the early 1990s (e.g., Blumthaler and Ambach, 1990; McKenzie, 1991; Bais and Zerefos, 1993; Bais et al., 1993). Early measurements of solar UV irradiance suggested that the long-term increase of the strongly ozone dependent wavelength of 305 nm was solely attributed to the observed stratospheric ozone decline and that it was not the result of improvements of air quality in the troposphere and changes in environmental conditions (Kerr and McElroy, 1993; Zerefos et al., 1998). Later studies based on longer atmospheric measurements looked at the effects of cloud cover, aerosols, air pollutants and surface reflectance on the long-term UV variability (e.g., Bernhard et al., 2007; den Outer et al., 2010; Kylling et al., 2010; Douglass et al., 2011). Over Canada, Europe, and Japan, it was found that the observed positive change in UV-B irradiance could not be explained solely by the observed ozone change and that a large part of the observed UV increase was attributed to tropospheric aerosol decline, the so-called brightening effect (Wild et al., 2005), since cloudiness had no significant trends (Zerefos et al., 2012). At

high latitudes on the other hand, it was found that the long-term variability of UV-B irradiance was not affected by aerosol trends but by ozone trends (Eleftheratos et al., 2015).

Further efforts to understand the interactions between solar UV radiation and related geophysical variables were done by Fountoulakis et al. (2018). They concluded that the long-term changes in UV-B radiation vary greatly over different locations over the Northern Hemisphere, and that the main drivers of these changes are changes in aerosols and total ozone. Updated analysis of total ozone and spectral UV data recorded at four European stations during 1996–2017 revealed that long-term changes in UV are mainly driven by changes in aerosols, cloudiness, and surface albedo, while changes in total ozone play a less significant role (Fountoulakis et al., 2020b). Over higher latitudes, part of the observed changes may be attributed to changes in surface reflectivity and clouds (Fountoulakis et al., 2018 and references therein). Dedicated studies assessing trends of UV radiation in Antarctica provided further evidence that the UV indices are now decreasing in Antarctica during summer months, but not yet during spring when the ozone hole leads to large UV index variability (Bernhard and Stierle, 2020). The downward trends in UV index during summer are associated with upward trends in total ozone.

Long-term predictions of UV radiation are governed by assumptions about the future state of the ozone layer, changes in clouds, changes in tropospheric pollution, mainly aerosols, and changes in surface albedo. Unpredictable volcanic eruptions, increasing emissions of GHGs, effects from growing air traffic, changes in air quality and changes in the oxidizing capacity of the atmosphere induce uncertainties to long-term predictions of ozone and therefore to UV radiation levels (Madronich et al., 1998). The Environmental Effects Assessment Panel of the United Nations Environment Programme publishes the most recent global environmental effects from the interactions between stratospheric ozone, UV radiation and climate change. The Panel noted that future changes in UV radiation will be influenced by changes in seasonality and extreme events due to climate change (Neale et al., 2021). Simulations of surface UV erythemal irradiance by Bais et al. (2011) showed that UV irradiance will likely return to its 1980 levels by the first quarter of the 21st century at northern mid and high latitudes, and 20-30 years later at southern mid- and high latitudes. After reaching this level, UV will continue to decrease towards 2100 in the Northern Hemisphere because of the continuing increases in total ozone due to circulation changes induced by the increasing GHG concentrations, whereas it is highly uncertain whether UV will reach its 1960s levels by 2100 in the Southern Hemisphere (Bais et al., 2011). However, in the Arctic, large, seasonal loss of column ozone could persist for much longer that commonly appreciated. Projections of stratospheric halogen loading and humidity with General Circulation Model (GCM)-based forecasts of temperature, suggested that conditions favorable for large Arctic ozone loss could persist or even worsen until the end of this century, if future GHG concentrations continue to steeply rise. Consequently, anthropogenic climate change has the potential to partially counteract the positive effects of the Montreal Protocol in protecting the Arctic ozone layer (von der Gathen et al., 2021). CCM simulations of DNA-damaging UV variability analyzed by Eleftheratos et al. (2020) showed that UV irradiance will likely increase at low and mid-latitudes during the second half

of the 21st century due to decreases in cloud cover driven by climate change caused by enhanced GHG concentrations.

GHG changes can be an important driver of cloudiness changes. Norris et al. (2016) provided evidence for climate change in the satellite cloud record. They estimated fewer clouds over the mid-latitudes from 1983 to 2009 and concluded that the observed and simulated cloud change patterns are consistent with poleward retreat of mid-latitude storm tracks, expansion of subtropical dry zones, and increasing height of the highest cloud tops at all latitudes. The primary drivers for these changes were found to be the increasing GHG concentrations and a recovery from volcanic radiative cooling (Norris et al., 2016). In the same direction, Schneider et al. (2019) showed that stratocumulus clouds, some of the planet's most effective cooling systems, become unstable and break up into scattered clouds under increasing GHG concentrations. Their results also showed that less clouds will trigger additional surface warming in addition to that from the rising CO2 levels (Schneider et al., 2019). Both studies provided indications that increasing GHGs can affect clouds, which in turn can affect the UV radiation changes.

In this work we investigate the UV variability and trends for the near global mean (50° N–50° S) and at high latitudes due to the expected increase of GHG concentrations in the future. We show that DNA active irradiance will continue to decrease after 2050 at high latitudes due to the prescribed evolution of greenhouse gases in contrast to regions located between 50º N and 50º S where it is shown to increase. The year 2050 was chosen as a mid-point to evaluate the trends as it divides the 21st century into two equal periods, 2000-2049 and 2050-2099, but most importantly because it was noted that for a Representative Concentration Pathway (RCP) of 6.0, the Chemistry-Climate Model Initiative (CCMI, phase 1) simulations project that global total column ozone will return to 1980 values around the middle of this century (Dhomse et al., 2018). Our study confirms the previous work by Eleftheratos et al. (2020), which focused on ozone profiles from five well-maintained lidar stations at low and mid-latitudes. Here, we add more ozone and UV stations in mid-latitudes and include estimates from high latitude stations with long-term measurements of UV radiation. The analysis aims to investigate whether the increase of DNA active radiation predicted for mid-latitudes in view of climate change, will also be observed at high latitudes. To address the issue, we use the same methodology as Eleftheratos et al. (2020), in which we compare two CCM simulations; one with increasing GHGs according to RCP-6.0 and one with fixed GHGs emissions at 1960 levels. The variability of ozone from the model simulations is evaluated against solar backscatter ultraviolet radiometer 2 (SBUV/2) satellite ozone data. The variability of DNA active irradiance from the model simulations is evaluated against ground-based DNA active radiation measurements, and the variability of simulated cloud cover is evaluated against cloud fraction data from the MODerate-resolution Imaging Spectroradiometer (MODIS)/Terra v6.1 satellite dataset.

It is important to clarify the novelty of this research and its added value with respect to the previous study, and to point out the main differences and similarities. The objective of this research is to study how total ozone, DNA active irradiance and cloud cover might change in the future at high latitudes due to the

increasing GHGs in comparison to the near global mean (50º N–50º S). Also, to estimate the part of the DNA active irradiance change that can be explained by ozone and cloud changes in the future using multiple linear regression (MLR) statistical analysis. The previous study by Eleftheratos et al. (2020) did not look at high latitudes and did not apply MLR analysis to quantify the related contributions to the DNA weighted UV irradiance. The previous work analysed 5 stations between 50º N and 50º S. The new study is enriched with more stations at the near global scale (13 instead of 5 stations, of which 4 are identical) and, in addition, it includes analysis of averages in latitudinal bands, which was not done in the previous study, thus providing more complete results.

The study is organized as follows. Section 2 describes the data sources and methodology. Section 3 shows the variability and projections of DNA-damaging UV radiation at high latitude stations in comparison to mid-latitude stations, and, finally, Section 4 summarizes the main results.

2 Data sources

2.1. Ground-based data

We have analyzed DNA-weighted UV irradiance data at ~~19~~ 20 ground-based (GB) stations listed in Table 1. Although the DNA action spectrum tends to exaggerate UV effects on humans, mammals, etc., (as it was determined with bacteria and viruses and does not take the wavelength dependence of the skin's transmission into account), it is the appropriate action spectrum for studying the detrimental biological effects of solar radiation and the effective dose of UV radiation in producing skin cancer (Setlow, 1974).

Most of the stations listed in Table 1 contribute spectral UV data to the data repository of the Network for the Detection of Atmospheric Composition Change (NDACC, www.ndacc.org) at https://www-air.larc.nasa.gov/pub/NDACC/PUBLIC/stations/~~https://ftp.cpc.ncep.noaa.gov/ndacc/station/~~ (last access ~~10 February~~4 September 2022) (De Mazière et al., 2018) and have been reported among those possessing high-quality long term UV irradiance measurements (McKenzie et al., 2019). Sites not part of NDACC are Aosta, Athens, Sodankylä, and Thessaloniki. Data from these stations are of high-quality as well (e.g., Fountoulakis et al., 2018; Fountoulakis et al., 2020a; Kosmopoulos et al., 2021; Lakkala et al., 2008). The high quality of the spectral UV measurements is ensured by applying strict calibration and maintenance protocols.

We have calculated monthly mean irradiances from noon averages for all stations listed in Table 1 (average of measurements ± 45 minutes around local noon) and compared them with the DNA active irradiance data from an EMAC sensitivity simulation (internally named SC1SD-base-02), with specified dynamics representing the recent past (2000-2018) as a means for model evaluation. The comparisons are presented in Section 3.1 and in the Supplementary materials of this study for each station separately.

2.2. Satellite data

We have analyzed the daily solar backscatter ultraviolet radiometer 2 (SBUV/2) ozone profile and total ozone data, selected to match the UV stations' locations. The data are available from April 1970 to the present, with nearly continuous data coverage from November 1978. The satellite ozone data coverage is from backscatter ultraviolet radiometer (BUV) to solar backscatter ultraviolet radiometer 2 (SBUV-2; Bhartia et al., 2013), as follows: Nimbus-4 BUV (05/1970–04/1976), Nimbus-7 SBUV (11/1978–05/1990), NOAA-9 SBUV/2 (02/1985–01/1998), NOAA-11 SBUV/2 (01/1989–03/2001), NOAA-14 SBUV/2 (03/1995–09/2006), NOAA-16 SBUV/2 (10/2000–05/2014), NOAA-17 SBUV/2 (08/2002–03/2013), NOAA-18 SBUV/2 (07/2005–11/2012), NOAA-19 SBUV/2 (03/2009–present) and Suomi NPP OMPS (12/2011–present). We calculated daily averages by averaging the measurements from all available SBUV instruments, and then we calculated monthly means from daily averages according to Zerefos et al. (2018).

Cloud fraction monthly mean data were taken from the MODIS/Terra v6.1 dataset for the period 2000–2020. We include estimates of the variability in cloudiness around each of the ground-based monitoring stations listed in Table 1. The cloud data were taken at a spatial resolution of 3° × 3° around each monitoring station. We have calculated the correlation coefficients between the de-seasonalized monthly time series of cloud fraction from MODIS/Terra and EMAC CCM for their common period (03/2000–07/2018), in order to evaluate the model simulations. The seasonal component was removed from the series by subtracting from each monthly value the 2000–2018 seasonal mean. Analytical estimates are provided in Section 3.1 and in the Supplementary materials.

2.3. EMAC Chemistry climate model (CCM) simulations

We use the same CCM simulations and methodology as described by Eleftheratos et al. (2020). The simulations come from the European Centre for Medium-Range Weather Forecasts – Hamburg (ECHAM) / Modular Earth Submodel System (MESSy) Atmospheric Chemistry (EMAC) model. The EMAC model is designed to study the chemistry and dynamics of the atmosphere (Jöckel et al., 2016). The resolution applied here is 2.8º x 2.8º in latitude and longitude, with 90 model levels reaching up to 0.01 hPa (about 80 km).

~~Two free-running hind-case and projection simulations have been analyzed, both based on boundary conditions following the RCP 6.0 scenario: the reference simulation RC2-base-04 (1960–2100, with additional 10 years spin-up; Jöckel et al., 2016) and the sensitivity simulation SC2-fGHG-01 (1960–2100), in which the GHG mixing ratios have been kept on 1960 levels (Dhomse et al., 2018). Furthermore, we~~We have analyzed the EMAC RC1SD-base-10 (Jöckel et al., 2016) and SC1SD-base-02 simulation results of ozone, DNA active irradiance, and total cloud cover (in %). These simulations have been performed in a "specified dynamics" (SD) setup, i.e., nudged with ECMWF ERA-Interim reanalysis data (Dee et al., 2011) for the periods January 1979 – December 2013 (RC1SD-base-10) and January 2000 – July 2018 (SC1SD-base-02), respectively, and are therefore particularly suited for a direct comparison with observations such

as ground-based and satellite measurements as presented in Section 3.1 and Appendix A. We note that the SD simulation RC1SD-base-10 (which starts in 1979) is used for the comparisons during the period of ozone depletion as the SC1SD-base-02 doesn't cover that period (the 80's and 90's).

Two free running hind-case and projection simulations have been analyzed, both based on boundary conditions following the RCP-6.0 scenario: the reference simulation RC2-base-04 (1960–2100, with additional 10 years spin-up; Jöckel et al., 2016) and the sensitivity simulation SC2-fGHG-01 (1960–2100), in which the GHG mixing ratios have been kept on 1960 levels (Dhomse et al., 2018). The RC2-base-04 and SC2-fGHG-01 simulations were forced with sea surface temperatures (SSTs) and sea ice concentrations (SICs) from the Hadley Centre Global Environment Model version 2 – Earth System (HadGEM2-ES) Model (Collins et al., 2011; Martin et al., 2011). These simulations were performed for the Coupled Model Intercomparison Project – Phase 5 (CMIP5) multi-model data sets in the frame of the Program for Climate Model Diagnosis and Intercomparison (PCMDI). For years up to 2005, the data of the "historical" simulation with HadGEM2-ES is used. Afterwards, the RCP-6.0 simulation, which is initialized with the historical simulation, has been employed (Jöckel et al., 2016, and reference therein). The future solar forcing, used for the projections, has been prepared according to the solar forcing used for CMIP5 simulation of HadGEM2-ES, where the SSTs and SICs are taken from Jones et al. (2011; see also Sect. 3.3 of Jöckel et al., 2016). It consists of repetitions of an idealized solar cycle connected to the observed time series in July 2008. This has been applied consistently for all projections with prescribed SSTs (RC2-base) and the same holds also for the SC-simulations. Here, we deviate from the CCMI recommendations consisting of a sequence of the last four solar cycles (20–23) (see Sect. 3.4 of Jöckel et al., 2016).

The UV-B radiation calculated by the photolysis scheme (JVAL) (Sander et al., 2014) is weighted with the DNA damage potential of Setlow (1974) with the parameterization by Brühl and Crutzen (1989). The DNA damaging irradiance of the NDACC database is again based on the action spectrum by Setlow (1974) and parameterized using Eq. (2) of Bernhard et al. (1997). The different parameterization of the DNA action spectrum in the EMAC CCM simulations and the GB measurements will likely lead to small difference between the two datasets. For example, the radiative amplification factors (RAFs) for the two parameterizations may not be identical, which may lead to seasonal variations because RAFs are solar zenith angle and ozone dependent. To reduce such differences, we only compared de-seasonalized data. The seasonal component at each station was removed by subtracting the long-term monthly mean (2000–2018) from each individual monthly value. The monthly departures were then expressed in percent of the long-term monthly mean.

Ozone and total cloud cover data from the two RC2-base-04 and SC2-fGHG-01 free running simulations for the stations listed in Table 1 have been analyzed as well and respective de-seasonalized monthly means were derived. Here, the monthly data were de-seasonalized with respect to the 30-year long-term monthly mean (1990–2019).

We note here that by a separate analysis (not shown) on total cloud cover variability and trends through the 21st century, using the available simulations from the CCMI-1 REF-C2 set (e.g., Eyring et al., 2013), the EMAC models results fall well within the range of uncertainty, close to the ensemble average.

In all simulations analyzed here, we used prescribed aerosol distributions. The prescribed aerosol effects are separated into the aerosol surface area, representing chemical effects via heterogeneous chemistry, and the radiative properties influencing the radiation budget (Sect. 3.7 of Jöckel et al., 2016). Due to a glitch, the stratospheric volcanic aerosol was not considered correctly in the free running simulations (Sect. 3.12.1 of Jöckel et al., 2016). Therefore, the dynamical effects of large volcanic eruptions (e.g. Mt. Pinatubo 1991; El Chichón 1982) are essentially not represented in the simulations, except for the contribution to the tropospheric temperature signal induced by the prescribed SSTs. For the specified dynamics simulations, however, this has been corrected. Since the aerosol distributions have been prescribed, there is no aerosol output for these simulations that we could look at. As such, we cannot investigate the impact of future changes in aerosol loading on the UV radiation reaching the surface.

In the following sections, to assist the reader to easily follow the figure content, we change the notation of our simulations as follows:

- SC1SD-base-02: further abbreviated as HIS-SD for historical specified dynamics
- RC2-base-04: further denoted as REF for reference, and
- SC2-fGHG-01: further denoted as FIX for fixed GHGs.

2.4. Statistical methods

In Section 3.1, we evaluate the variability of DNA active irradiance from the model simulations with station measurements for a nearly 20-year period (2000–2018). The comparisons were based on regression analyses between the simulated and observed DNA active irradiance monthly data after removing variations related to the seasonal cycle. The monthly data at each station were de-seasonalized by subtracting the long-term monthly mean (2000–2018) pertaining to the same calendar month.

We have calculated the Pearson's correlation coefficients, R, between the simulated and measured DNA active irradiance (Eq. 1) and tested them for statistical significance using the t–test formula for the correlation coefficient with n–2 degrees of freedom (Eq. 2) (von Storch and Zwiers, 1999):

$$R = \frac{\sum_{i=1}^{n}(x_i - \bar{x})(y_i - \bar{y})}{\sqrt{\sum_{i=1}^{n}(x_i - \bar{x})^2}\sqrt{\sum_{i=1}^{n}(y_i - \bar{y})^2}} \quad (1)$$

Where x refers to the measured and y to the simulated data.

$$t = R\sqrt{\frac{n-2}{1-R^2}} \quad (2)$$

The same procedure was followed for the comparisons between the simulated and satellite derived total ozone and cloud cover datasets for the period 2000–2018, which are presented in Section 3.1.

In Section 3.3, we apply a statistical test to compare the regression slopes in DNA active irradiances before and after the year 2050. The null hypothesis, that the two slopes are statistically equal ($H_0: b_1 = b_2$), is tested against the alternative hypothesis that the two slopes are not statistically equal ($H_1: b_1 \neq b_2$). The difference in slopes is tested with the statistic:

$$t = \frac{b_1 - b_2}{s_{(b_1-b_2)}} = \frac{b_1 - b_2}{\sqrt{s_{b_1}^2 + s_{b_2}^2}} \quad (3)$$

With $n_1 + n_2 - 4$ degrees of freedom, according to Eq. (11.20) of Armitage et al. (2002). The parameter $s_{(b_1-b_2)}$ is the standard error of $(b_1 - b_2)$. The parameters b_1 and b_2 are the slopes before and after 2050 in each geographical zone, and n_1 and n_2 are the numbers of data before and after 2050, respectively. The test was performed using de-seasonalized monthly values but also with the averages shown in Figures 4c, 5c, 6c, calculated from de-seasonalized data. Both ways gave similar statistical results. In Section 3.3 we provide the results using the de-seasonalized monthly values.

The equation for the slope of the regression line, using *x* as the time variable and *y* as the DNA active irradiance variable, is:

$$b = \frac{\sum(x-\bar{x})(y-\bar{y})}{\sum(x-\bar{x})^2} \quad (4)$$

The residual mean square for the first group (1960-2049), $s_{b_1}^2$, is estimated as follows:

$$s_{b_1}^2 = \frac{\sum_{(1)}(y-Y_1)^2}{n_1-2} = \frac{S_{yy1} - S_{xy1}^2/S_{xx1}}{n_1-2} \quad (5)$$

And the corresponding mean square for the second group (2050-2099), $s_{b_2}^2$, as follows:

$$s_{b_2}^2 = \frac{\sum_{(2)}(y-Y_2)^2}{n_2-2} = \frac{S_{yy2} - S_{xy2}^2/S_{xx2}}{n_2-2} \quad (6)$$

Here, S_{yy} is the standard deviation of DNA active irradiance, S_{xx} is the standard deviation of time and S_{xy} is their covariance, for the first (1960-2049) and second (2050-2099) groups, respectively.

If $|t| > t_{critical\ (n_1+n_2-4)}$, then the null hypothesis, H_0: the slopes are equal, is rejected at the significance level a, and the alternative hypothesis (the two slopes are statistically different) is accepted.

3 Results and discussion

3.1 Evaluation of EMAC CCM simulations for the present

~~DNA active irradiance data from station observations and model simulations have been compared, for a nearly 20 year period (2000–2018). The comparisons were based on regression analyses between the simulated and observed DNA active irradiance monthly data after removing variations related to the seasonal cycle. The monthly data at each station were de-seasonalized by subtracting the long-term monthly mean (2000–2018) pertaining to the same calendar month.~~

The time series of de-seasonalized DNA active irradiance data are presented in Figure 1. The figure compares model calculations of DNA active irradiance from the ~~SC1SD-base-02~~HIS-SD simulation with ground-based measurements at stations described in Section 2. The upper panel refers to the average of de-seasonalized data at ~~two~~ three stations in the northern high latitudes, the middle panel refers to the respective average of thirteen stations between 50° N and 50° S, and the lower panel to the respective average of four stations in the southern high latitudes. The comparisons refer to the period 2000–2018. We note that this is a composite dataset, obtained with the same set of stations (both in the model and in the observations). All timeseries start from the same year in the model, but not all timeseries start from the same year in the observations.

~~We have calculated the Pearson's correlation coefficients, R, between the two datasets and tested them for statistical significance using the t-test formula for the correlation coefficient with n-2 degrees of freedom (von Storch and Zwiers, 1999):~~

$$t = R\sqrt{\frac{n-2}{1-R^2}} \quad (1)$$

~~The correlations between the simulated and ground-based DNA active irradiance data are statistically significant. The results are presented in Table 2a. The de-seasonalized data from the model agree quite well with those measured from the ground, except for Barrow, Zugspitze, and Reunion Island, where they show smaller correlation coefficients (0.342, 0.266, and 0.295, respectively) which may be related with the coarse resolution of the model simulations (2.8°x2.8°). The correlation results between the two data sets at~~

~~each station separately are presented in Supplement Table S1. The R values are highly statistically significant (>99%).~~

The results show that the correlations between the simulated and ground-based DNA active irradiance data are statistically significant. Figure 1, however, shows that the variability between the simulated and ground-based data can be different. To have a better indication how the two datasets are scattered, Figure 2 presents the respective scatter plots. We have added the linear regression line and the y=x line which shows how much the slope of the fit deviates from the 1:1 line. The statistical results (correlation coefficient, slope, error, t-value, p-value, and root mean square error (RMSE)) are summarized in Table 2a.

The comparison for the near-global mean shows that the correlation coefficient between the simulated and observed DNA active irradiances is +0.709, the slope of the fit is 0.521, its error is 0.035, and the RMSE is 4.423. For the northern high latitudes, the statistical results are estimated to be R = 0.518, slope = 0.657, error of slope = 0.129, RMSE = 9.543. The respective results for the southern high latitudes are R = 0.746, slope = 0.879, error of slope = 0.070, RMSE = 14.766. It appears that the slope of the regression fit for the near-global mean is small; however, the RMSE, which is the measure of the differences between the simulated and observed values, is also small. A RMSE of 0 would indicate a perfect fit to the data, something that is never achieved in practice. It also appears that the respective RMSE of the residuals (i.e., simulated minus observed values) are larger at high latitudes; this is because it was derived from larger differences of de-seasonalized data at the northern high latitudes and even larger at the southern high latitudes.

The regression analysis results between the two data sets at each station separately are presented in Supplement Table S1. We note here that the model has a resolution of 2.8° x 2.8°, which is a large area for which the point measurement has to be representative for. As such, for stations where the surrounding area is inhomogeneous, such as mountain tops (Mauna Loa, Sonnblick, Zugspitze), or in valleys (Aosta), or by being in a town with very heterogeneous surroundings (sea, mountains, tropospheric ozone and aerosols such as Athens), the model simulations of DNA active irradiance are not expected to be fully representative of the specific UV sites. Thus, the correlation between simulated and measured DNA weighted UV irradiance is not very good at some stations, as shown in the figures provided in the supplementary material. For the same reason, the slope between two datasets can deviate significantly from unity (see Supplement Table S1). Therefore, the comparisons at the individual stations provide a qualitative evaluation of the model's variability, but cannot be considered as a strict validation of the model. We provide here indicative estimates for individual stations, which give very good to excellent correlations: a) Summit, Greenland: R = +0.709, slope = 0.757, error of slope = 0.081, p-value <0.0001, N = 88, b) Hoher Sonnblick, Austria: R = +0.673, slope = 0.946, error of slope = 0.075, p-value <0.0001, N = 192, c) Boulder, CO, USA: R = +0.748, slope = 0.677, error of slope = 0.047, p-value <0.0001, N = 163, d) Arrival Heights, Antarctica: R = +0.939, slope = 1.000, error of slope = 0.033, p-value <0.0001, N = 126.

The same procedure was followed to evaluate simulated ozone and cloud cover. Figure ~~2~~ 3 shows (a) ozone calculations from the ~~SC1SD-base-02~~HIS-SD simulation compared to satellite SBUV retrievals and (b) shows simulated cloud cover compared to cloud cover from MODIS/Terra. It appears that the variability of ozone from the model simulation follows exceptionally well the variability of ozone from the satellite retrievals. It also appears that the variability of cloud cover from the model simulation is quite well correlated with the variability from the satellite observations (see Tables 2b and 2c). The respective comparisons using zonally averaged data for the northern high latitudes (55º – 75º N), the near global mean (50º N – 50º S) and the southern high latitudes (55º – 75º S) are presented in Supplement Figure S1. The regression results (R, slope, error of slope, t-value, p-value, and RMSE) for the large-scale latitudinal averages are presented in Supplement Table S2 and they are in line with the results from the station averages.

The Supplement Table ~~S2~~ S3 presents analytically the comparisons of total ozone between the EMAC CCM calculations and SBUV satellite retrievals. The correlations between the two different data sets are statistically significant at confidence level greater than 99.9% at all stations under study. The correlation results for four indicative stations are: a) Summit, Greenland: R = +0.927, slope = 0.791, error of slope = 0.028, p-value <0.0001, N = 131, b) Hoher Sonnblick, Austria: R = +0.902, slope = 0.803, error of slope = 0.026, p-value <0.0001, N = 223, c) Boulder, CO, USA: R = +0.854, slope = 0.757, error of slope = 0.031, p-value <0.0001, N = 223, d) Arrival Heights, Antarctica: R = +0.896, slope = 0.655, error of slope = 0.029, p-value <0.0001, N = 128.

The Supplement Table ~~S3~~ S4 presents the respective comparisons for cloud cover. The cloud observations come from MODIS/Terra. The correlation results for these four stations are: a) Summit, Greenland: R= +0.196, slope = 0.069, error of slope = 0.031, p-value = 0.025, N = 131, b) Hoher Sonnblick, Austria: R = +0.556, slope = 0.619, error of slope = 0.062, p-value <0.0001, N = 222, c) Boulder, CO, USA: R = +0.539, slope = 0.482, error of slope = 0.051, p-value <0.0001, N = 222, d) Arrival Heights, Antarctica: R = +0.537, slope = 0.949, error of slope = 0.133, p-value <0.0001, N = 129.

3.2 Future changes in ozone and DNA active irradiance

In the previous section we evaluated the SD simulation SC1SD-base-02 with satellite and ground-based measurements. In this section we use the EMAC CCM simulations to investigate the evolution of DNA active irradiance and ~~of~~ the parameters that affect its long-term variability into the future. More specifically, we have analyzed the free-running simulation of the EMAC CCM, namely RC2-base-04, with increasing GHGs according to RCP-6.0 at the stations under study. An evaluation of the free running simulation RC2-base-04 with the SD simulation SC1SD-base-02 is provided in Appendix A. It helps to evaluate the quality of the results of the free running model system with respect to the SD simulation and the observations of the stations, and it serves as a "bridge" from the observations via the SD simulation results to the results of the (longer-term) free-running model simulation.

We followed the same methodology as Eleftheratos et al. (2020), to examine the effect of increasing GHGs on the evolution of DNA active radiation. We have compared the free-running simulation RC2-base-04 with the sensitivity simulation SC2-fGHG-01 where GHGs are kept constant at 1960 levels (see also Appendix A). The difference between the two free-running simulations gives us an estimate of the desired result.

We have prepared a series of figures to demonstrate the two different simulations and the differences between them. Figure ~~3~~ 4 is based on 13 UV stations between 50º north and south. Figure ~~4~~ 5 shows the results for the northern high latitude stations and Figure ~~5~~ 6 for the southern high latitude stations. The top panel refers to the evolution of total ozone anomalies from 1960 to 2100; the middle panel refers to the evolution of DNA active irradiance and the lower panel to the evolution of clouds for the same period. The left panel shows the two simulations, i.e., the free-running simulation with increasing GHGs (~~RC2-base-04~~REF) versus the same simulation with fixed GHGs at 1960 levels (~~SC2-fGHG-01~~FIX) and the right panel shows their respective differences. Shown are annual averages calculated from monthly de-seasonalized data. The calculation of annual averages was done as follows: First, we de-seasonalized the monthly data at each station by subtracting the long-term monthly mean (1990–2019) pertaining to the same calendar month. Next, we calculated a monthly de-seasonalized time series for each geographical zone by averaging the monthly de-seasonalized data of the stations belonging to each geographical zone. The latter time series was used to estimate the annual data anomalies. For the northern high latitude stations, the annual average refers to the average of monthly anomalies from March to September, and for the southern high latitude stations, it refers to the average of monthly anomalies from September to March. For the stations between 50º N–50º S we used all months to calculate the annual average.

In addition, we have added with green squares the DNA-weighted UV irradiance anomalies averaged at the ground-based stations under study around local noon. We also include the total ozone anomalies from SBUV with blue dots and the respective cloud cover anomalies from MODIS/Terra (magenta triangles) averaged at the stations studied. The observational data have been added to show simply that the dispersion of the simulated data matches the dispersion of the measured data.

In the study by Eleftheratos et al. (2020) data from 5 stations between 50 degrees north and south were analyzed. Here, we examine for this latitude band 13 stations instead of 5 (Figure ~~3~~4). The new findings paint the same picture: an increasing trend in DNA active irradiance after the year 2050, associated with a decreasing trend in cloud cover due to the evolution of GHGs and ~~an insignificant~~a negative trend in total ozone (Figure ~~3c~~4c). Thus, our new results, based on 13 instead of 5 stations, confirm qualitatively the results of the previous study for 50º N–50º S. An offset between total ozone from SBUV and the free running simulation is evident in the 1980s, which is larger at 50º N–50º S. This is discussed later.

The focus now is at higher latitudes, which show a different picture than that of 50º N–50º S after the year 2050. At the northern high latitude stations (Figure ~~4~~5), DNA active irradiance (during the summer half year) shows a decreasing trend after 2050, total ozone shows an increasing trend after 2050 and cloud cover

does not show any obvious statistically significant trend. The estimated trends (in % per decade) and their standard errors are presented in Table 3. More specifically, we estimate that total ozone will increase by ~~2.4~~1.8 ± ~~0.9~~0.8% from 2050 to 2100 (t-value = ~~2.675~~2.169, p-value = ~~0.01019~~0.035), DNA active irradiance will decrease by ~~10.6~~8.2 ± ~~3.7~~3.8% (t-value = ~~–~~2.161~~–2.859~~, p-value = ~~0.00627~~0.036), and cloud cover will slightly increase by ~~1.3~~1.4 ± ~~2.0~~1.3% (t-value = ~~0.640~~1.061, p-value = ~~0.52496~~0.294). Accordingly, at the southern high latitude stations (Figure ~~5~~6), total ozone is estimated to increase by 4.2 ± 2.1% from 2050 to 2100 (t-value = 2.020, p-value = ~~0.04896~~0.049), DNA active irradiance is estimated to decrease by 4.8 ± 2.9% (t-value = –1.660, p-value = ~~0.10347~~0.103), and cloud cover will decrease insignificantly by 1.1 ± 1.7% (t-value = –0.604, p-value = ~~0.54842~~0.548).

The above estimates point to an increase in total ozone in the northern high latitudes by the end of the century on an almost year-round basis. In a recent study by von der Gathen et al. (2021), it was concluded that conditions favorable for large Arctic ozone loss during cold winters could persist or even worsen until the end of this century, if future abundances of GHGs continue to rise. As such, anthropogenic climate change has the potential to partially counteract the positive effects of the Montreal Protocol in protecting the Arctic ozone layer (von der Gathen et al., 2021). We examined the EMAC CCM projections regarding this finding. We have analyzed the ~~RC2-base-04~~REF and ~~SC2-fGHG-01~~FIX simulation results of ozone, DNA active irradiance, and cloud cover for January, February, and March for the ~~two~~ three northern high latitude stations, ~~Summit and Barrow~~Summit, Barrow and Sodankylä. The trend results are presented in Table 4, which shows the trends from the two simulations, and their differences, for the periods 1960–1999, 2000–2049 and 2050–2099.

It appears that in January and February, considered as the two coldest months of the year, the trends decrease from the first (2000–2049) to the second period (2050–2099), while in March (less cold month) the picture is different. More specifically, in January, the significant positive trend of ~~1.72~~1.53 ± ~~0.59~~0.64% per decade in 2000–2049 changes to ~~–0.02~~0.21 ± ~~0.63~~0.73% per decade in 2050–2099. In February, the significant positive trend of ~~2.09~~1.79 ± ~~0.63~~0.78% per decade in 2000–2049 decreases to ~~1.39~~0.58 ± ~~0.62~~0.71% per decade in 2050–2099. On the other hand, the trends in March are ~~0.65~~0.17 ± ~~0.49~~0.58% per decade in 2000–2049 and ~~0.83~~1.20 ± ~~0.39~~0.51% per decade in 2050–2099, and they agree with the general course of trends seen in Figure ~~4~~5. We end up to findings that are qualitatively in agreement with those concluded by von der Gathen et al. (2021) about the large seasonal losses of Arctic ozone during cold winters until the end of the century. We also attempted to estimate the trends in DNA active irradiance in the northern high latitude stations for January, February, and March. The results are presented in Table 4 for the two periods, 2000–2049 and 2050–2099, but due to the polar night at the northern high latitudes, UV values are very low in January and February, and the predicted trends have large standard errors. As such, they are not analyzed any further.

Another issue is that Figure ~~4a~~ 5a suggests that clouds will stay more or less constant over the Arctic. Other models predict that cloud cover in the Arctic will increase until the end of the century. With sea ice

diminishing in the Arctic, evaporation would increase, leading to more moisture in the air, resulting in more clouds, which in turn is expected to reduce UV radiation. For example, Fountoulakis and Bais (2015) analyzed changes in UV radiation projected for the Arctic. Comparison of Figure 1 (clear-sky trends) and Figure 2 (all-sky trends) of Fountoulakis and Bais (2015) suggests that UV changes between the future and the present will become more negative when clouds are also considered due to the projected increase in cloud attenuation. Our estimates indicate a significant cloud increase of ~~3~~2.2% from 1960 to 2100 (~1.4% from 2050 to 2100, not significant). These increases are small and are based on the average of ~~two~~ three stations only, ~~Summit and Barrow.~~ Summit, Barrow and Sodankylä, but they are in accordance with the results obtained for the whole latitudinal band of 55º–75º N (~2.7% from 1960 to 2100, p-value < 0.0001, and ~0.9% from 2050 to 2100, p-value = 0.05). Summit and Sodankylä are~~is~~ far away from the seashore and ~~is~~ are not affected by the ocean, while Barrow is located only 250 m away from the coast and is greatly affected by the ocean. Changes in cloudiness might be different at coastal and mainland sites. For Barrow (coastal site) we estimate a significant cloud increase of 5.5% in the period 1960–2100 (3% in the period 2050–2099), while for Summit (pure land site) we estimate an insignificant change of –0.1% in the period 1960–2100 (–0.4% in the period 2050–2100). For Sodankylä (also pure land site), we estimate an insignificant increase of 1.2% in the period 1960–2100 (p-value = 0.365), and of 1.6% in the period 2050–2100 (p-value = 0.446). Averaging large and small changes in cloudiness should finally result to moderate changes. These results generally agree with the results presented in other studies (Bais et al., 2015; Fountoulakis and Bais, 2015) for land areas of the Arctic (keeping also in mind that the results of the present study are averages for ~~two~~ three stations only). We note that the results presented in these two referenced studies were for RCPs 4.5 and 8.5, and thus not directly comparable with the results of our study. In a more recent study presenting RCP 6.0-based projections (Bais et al., 2019), it was shown that cloudiness changes at high latitudes would strongly affect the UV irradiance mainly over the ocean where the absence of sea ice would result to increased evaporation. For land, smaller and non-significant changes were reported (see Figure 8 of Bais et al., 2019), which is again in agreement with the results presented in our study. In another study (Figure 5 of Fountoulakis et al., 2014), changes in zonally averaged UV irradiance due to changes in cloudiness in 1950–2100 were estimated to be the order of 5–15% (depending on the RCP) for latitudes ~70 degrees. However, only changes over the ocean were considered in that study and not over land. Additional indications that our results should be considered representative of the ~~two~~ three stations under study and not the entire Arctic region is provided in Figure B1 (Appendix B), which shows the changes in zonal mean cloud cover for the Arctic region from the ~~RC2 base 04~~REF simulation. It appears that the zonal mean cloudiness is expected to increase more and more as move northward of 50º towards the North pole, indicating that the largest changes in cloud cover are likely to occur over the ocean and not over land.

For the period 1960–1999, the DNA active irradiance (summer half year) showed upward trends in all geographical zones following the downward trends of total ozone. Nevertheless, we should note that the examined simulation ~~RC2 base 04~~REF (simulation with full chemistry and increasing GHGs according to

RCP-6.0) seems to clearly underestimate the observed ozone depletion of the 1980s and 1990s in the geographical region 50º N–50º S (Figure ~~3~~4), but in the higher latitude regions (Figs. ~~4~~ 5 and ~~5~~6) the picture looks much better. This suggests that there may be a bias in the model, that might at least partly be caused by not considering all ozone depleting substances (ODSs), but only a subset (only CFC-11 and CFC-12 are considered; Jöckel et al., 2016). The ~~RC2-base-04~~REF simulation also underestimates the ozone depletion of the 1980s and 1990s in the northern high latitude stations (Figure ~~4~~5), but the picture is better than that of 50º N–50º S. The ~~SC2-fGHG-01~~FIX simulation seems to reproduce better the Arctic ozone depletion of the past. The latter, however, is coincidence; it only indicates that due to the higher dynamic variability of the northern (winter) stratosphere, the evolution of the ozone layer in the Arctic region is significantly affected by natural variability of the stratosphere due to planetary waves. The best agreement between the ~~RC2-base-04~~REF simulation and satellite measurements during the period of ozone depletion is found for the southern high latitudes, as can be seen from Figure ~~5~~6. As such, we can infer that the model simulations reproduce very well the observed ozone depletion of the past in particular in the southern higher latitudes, and less well in the northern higher latitudes. Nevertheless, the simulated decline of ozone during 1979–1999 and the minimum ozone values calculated by the model in the 1990s for the near global mean (50° N-50° S) and for the higher latitudes, are qualitatively in line with the satellite ozone observations, which is a good outcome. This is supported by Figure A1 (Appendix A), which shows the free running simulation ~~RC2-base-04~~REF against the SD simulation ~~SC1SD-base-02~~HIS-SD which starts in 2000. Because we wanted to evaluate the free running simulation for the period of ozone depletion, we also analyzed the SD simulation RC1SD-base-10 which starts in 1979. It appears that the ~~RC2-base-04~~REF simulation seems to reproduce well the negative ozone trends during the period of ozone depletion, but not the exact anomalies of a particular year. This is because the free running simulation has its own meteorological/synoptical sequence, and thus we cannot expect that the observed time series of the past is reproduced on a year-by-year basis in the free running simulation the same way is reproduced in the simulation with “specified dynamics”.

Finally, we should also refer to the recent assessment of the United Nations Environment Programme (UNEP) Environmental Assessment Panel (EEAP) (Bernhard et al., 2020), which compared projections of future UV radiation from two studies, Bais et al. (2019) and Lamy et al. (2019). We have compared our trend estimates, which are based on one model only, with the estimates provided in Table 1 of Bernhard et al. (2020), which are based on many models of the first phase of the Chemistry-Climate Model Initiative (CCMI-1) and should therefore be considered more robust than the estimates provided here. We clarify that it is only a qualitative comparison as our trends are based on DNA weighted irradiance while the table in Bernhard et al. (2020) refers to erythema. The DNA radiation amplification factor is about 2.1 while that for erythema is 1.2, which suggests that we would expect differences in trends by roughly a factor of 1.75. We also note that the table of Bernhard et al. (2020) shows zonal mean changes of the clear-sky UV index, whereas we estimate changes in DNA active irradiance based on station averages. Despite the inconsistencies in the radiation fields being compared, our trend estimates from the ~~RC2-base-04~~REF

simulation based on RCP-6.0 are qualitatively in line with the results presented by Bernhard et al. (2020) for the case of RPC-6.0. We estimate a statistically significant decrease in DNA active irradiance at the northern high latitude stations for the period 2015 to 2090 of about ~~–16~~ –17% (–16% for the zonal mean 55°–75° N). The numbers from Table 1 of Bernhard et al. (2020) for the northern high latitudes are –6% for the annual mean clear-sky UV index for the period 2015 to 2090, and –3%, –7%, –5% and –4% for January, April, July, and October, respectively. Our respective estimate for the southern high latitude stations is about –24% (–26% for the zonal mean 55°–75° S) and is also qualitatively in line with the negative trend estimates provided by Bernhard et al. (2020) for the southern high latitudes for the period 2015 to 2090 (–18% for the annual mean clear-sky UV index, and –8%, –6%, –6% and –23% for January, April, July, and October, respectively).

The above estimates are based on station averages. We have complemented the analysis presented in Figures 4, 5, 6 with zonally averaged data in order not to restrict the analysis of the model results to only 20 locations but to analyse the model results as a whole, for example in latitudinal bands. The Supplement Figures S2, S3, S4 show the changes from the free running simulations REF, FIX, and their differences, for the near global mean, the northern and southern high latitudes based on latitudinal averages. It appears that the results from the analysis of averaging the model data in latitudinal bands are in the same direction with that from the station averages. More specifically, for the near global mean we find similar results to those presented in Figure 4 for the station mean, but a stronger negative trend in total ozone after 2050 which together with the negative cloud trend drive the positive DNA active radiation trend after 2050. On the other hand, negative trends in ozone and clouds after 2050 are not observed in the northern or the southern high latitude belt.

We believe that the negative trends seen in the near-global mean after 2050 will result from the ongoing climate change that will affect ozone and clouds. It is well known that increasing GHG concentrations have led to tropospheric warming and stratospheric cooling over the last decades (Stocker et al., 2013; Zerefos et al., 2014). As a thermodynamic consequence, the troposphere has expanded and the height of the tropopause has increased (Santer et al., 2003). A recent study showed that the stratospheric layer has contracted substantially over the last decades due to increasing GHGs and will continue to contract under the RCP-6.0 scenario (Pisoft et al., 2021). Also, chemistry-climate and climate model projection results show an acceleration in Brewer-Dobson circulation in response to climate change (Butchard, 2014). These changes will not leave the ozone layer unaffected. Our model simulations for the near-global mean show a downward trend in total ozone after 2050, which will likely be shaped by the negative trends in the lower stratosphere due increasing GHGs. For clouds, it has been shown that increasing GHGs are responsible for less clouds over the mid-latitudes (Norris et al., 2016) and for breaking up stratocumulus clouds into scattered clouds (Schneider et al., 2019). Our simulations show that clouds will decrease in response to increasing GHGs, which is consistent with the indications from these studies.

The results based on the zonally averaged data fully support the basic finding of the paper that DNA active irradiance is expected to change differently at high latitudes than at near-global scale after around 2050. It will continue to decline at high latitudes mainly due to ozone recovery from the reduction of ODSs (cloud cover changes are not significant), while it is expected to increase on a near-global scale, affected by reductions in cloud cover and total ozone due to climate change. This of course is an outcome that emerges from the simulations of a single climate-chemistry model, and as such, it may well turn out to be true or false. Verification of the results from other model simulations would be important, but also important is the further investigation of cloud behaviour from the model simulations and their verification from high quality measurements. It is important to note that our free running simulations were designed according to the definitions for the reference and sensitivity simulations provided by the IGAC and SPARC communities to address emerging science questions, improve process understanding and support upcoming ozone and climate assessments (Eyring et al., 2013).

3.3 Statistical evaluation of differences between trends and statistical modelling

We have compared the regression slopes in DNA active irradiances before and after the year 2050. ~~The null hypothesis, that the two slopes are statistically equal ($H_0: b_1 = b_2$), is tested against the alternative hypothesis that the two slopes are not statistically equal ($H_1: b_1 \neq b_2$). The difference in slopes is tested with the statistic:~~

$$t = \frac{b_1 - b_2}{s_{(b_1 - b_2)}} = \frac{b_1 - b_2}{\sqrt{s_{b_1}^2 + s_{b_2}^2}} \quad (3)$$

~~With $n_1 + n_2 - 4$ degrees of freedom, according to Eq. (11.20) of Armitage et al. (2002). The parameters b_1 and b_2 are the slopes before and after 2050 in each geographical zone, and n_1 and n_2 are the numbers of data before and after 2050, respectively. The test was performed using de-seasonalized monthly values but also with the averages shown in Figures 3c, 4c, 5c, calculated from de-seasonalized data. Both ways gave similar statistical results. We provide here the results using the de-seasonalized monthly values.~~

~~The equation for the slope of the regression line, using x as the time variable and y as the DNA active irradiance variable, is:~~

$$b = \frac{\sum(x - \bar{x})(y - \bar{y})}{\sum(x - \bar{x})^2} \quad (4)$$

~~The residual mean square for the first group (1960-2049), $s_{b_1}^2$, is estimated as follows:~~

$$s_{b_1}^2 = \frac{\sum_{(1)}(y - Y_1)^2}{n_1 - 2} = \frac{S_{yy1} - S_{xy1}^2/S_{xx1}}{n_1 - 2} \quad (5)$$

And the corresponding mean square for the second group (2050-2099), $s_{b_2}^2$, as follows:

$$s_{b_2}^2 = \frac{\sum_{(2)}(y - Y_2)^2}{n_2 - 2} = \frac{S_{yy2} - S_{xy2}^2/S_{xx2}}{n_2 - 2} \quad (6)$$

Here, S_{yy} is the standard deviation of DNA active irradiance, S_{xx} is the standard deviation of time and S_{xy} is their covariance, for the first (1960-2049) and second (2050-2099) groups, respectively.

If $|t| > t_{critical\,(n_1+n_2-4)}$, then the null hypothesis, H_0: the slopes are equal, is rejected at the significance level α, and the alternative hypothesis (the two slopes are statistically different) is accepted.

Our calculations according to Eq. 3 show that at the significance level α = 0.05, the null hypothesis that the slopes are statistically equal, cannot be rejected for neither the northern, nor the southern high latitudes (>55º), and therefore we cannot conclude that there is any statistically significant difference between the trends in DNA active irradiance before and after 2050 in these two latitude zones. On the other hand, the null hypothesis is rejected for the latitude zone of 50º N–50º S, which means that the alternative hypothesis is accepted, and so the two trends before and after 2050 are statistically different. The statistical results are presented in Table 5.

We note here that the statistical test was also applied for the periods before 2050, i.e., the two periods 1960-1999 and 2000-2049, to test if their trends are statistically significant or not. In all latitudes it was found that the regression slope of the period 1960-1999 is not statistically significantly different from the regression slope of the period 2000-2049. As such, it appears that only after the year 2050 there appears to be a statistically significant change in the trends of DNA active irradiance because of the evolution of GHGs and only at latitudes between 50º N and 50º S. At latitudes poleward of 55º, the DNA active irradiance is more likely to continue to decrease due to the increasing ozone trends from the reduction of the concentrations of ODSs.

Moreover, we have applied multiple linear regression (MLR) analysis to examine the contribution of ozone and cloud trends to the estimated DNA active irradiance trends after the year 2050. The MLR model was applied to the differences between the two model simulations, RC2-base-04REF and SC2-fGHG-01FIX, which were estimated from monthly de-seasonalized data (*deseas*). The MLR model is of the following form:

$$deseas\ DNA\ active\ irradiance = a + \beta_{O_3} \cdot deseas\ O_3 + \beta_{cloud} \cdot deseas\ Cloud \quad (7)$$

Where, a is the intercept, β_{O_3} is the ozone coefficient and β_{cloud} is the cloud coefficient for the period 2050–2099. The regression coefficients and their standard errors are presented in Table 6a. These coefficients were derived from station mean data ~~and from zonal mean data~~, and hence might not be representative for the entire geographical zones. As can be seen, the coefficients β_{O_3} and β_{cloud} are highly statistically significant with small errors in all cases (p-values <0.001). We have used the regression coefficients to determine the part of the DNA active irradiance trends that are caused by trends in total ozone and cloud cover. We have derived the ozone-related DNA active irradiance trend by multiplying the regression coefficient between DNA active irradiance and ozone (β_{O_3}) with the trend in ozone for the period 2050–2099. Accordingly, we derived the respective cloud-related DNA active irradiance trend by multiplying the regression coefficient β_{cloud} with the cloud trend.

For the northern high latitude stations (>55° N), we estimate an ozone-related DNA active irradiance trend of about ~~–0.96~~ –0.72% per decade, indicating that ~~47~~39% of the DNA active irradiance trend (~~–2.04~~ –1.86% per decade) is caused by the trends in ozone. The respective cloud-related DNA active irradiance trend is smaller (~~–0.14~~ –0.21% per decade), which means that the cloud trend explains ~~7~~11% of the DNA active irradiance trend. Both parameters account for ~~54~~50% of the predicted DNA active irradiance trend. The remaining part of the DNA active irradiance trend is related to changes in other parameters, as for instance in surface albedo, as is discussed later in Section 3.4.

Similar results regarding the contribution of ozone and cloud trends to the predicted DNA active irradiance trend are also found for the southern high latitude stations (>55° S), but not for the stations averaged between 50° N and 50° S. The results are summarized in Table 6b. For the southern high latitude stations (>55° S), the ozone-related DNA active irradiance trend is –0.57% per decade and the cloud-related DNA active irradiance trend is +0.07% per decade. As such, ~59% of the DNA active irradiance trend (–0.96% per decade) is explained by ozone, and ~7% is explained by clouds.

For stations averaged between 50° N–50° S, we estimate that the ozone-related DNA active irradiance trend is +0.27% per decade, and the cloud-related DNA active irradiance trend is +0.33% per decade. The contribution of changes in cloudiness is larger than the contribution of changes in ozone (~41% compared to ~33%, respectively), and therefore, our findings support the previous results by Eleftheratos et al. (2020), who analyzed a smaller number of GB stations between 50° N–50° S than those used here.

3.4 Changes in surface albedo and relation to DNA active irradiance

In the previous section we showed that DNA active irradiance will continue to decrease after the year 2050 at high latitudes as a result of ozone change rather than cloud cover change. Another parameter affecting the solar UV variability at high latitudes is surface albedo (Weihs et al., 1999; Nichol et al., 2003; Weatherhead et al., 2005; Gröbner, 2012; Bais et al., 2019). In this respect, changes in surface albedo are expected to affect the long-term variability of surface UV-B irradiance. Figure 6 shows the changes in surface albedo simulated with the EMAC CCM at the two stations, Barrow in Alaska and Palmer in

Antarctica. More specifically the figure shows the differences between the two model simulations, the one with increasing GHGs (~~RC2-base-04~~REF) and the one with fixed GHGs (~~SC2-fGHG-01~~FIX), in order to account also for the effect of increasing GHGs on surface albedo changes according to the methodology applied in Section 3.2. The results refer to the summer seasons of the two hemispheres, where there is sufficient sunlight in the Arctic and the Antarctic. Table 7 summarizes the trends in the differences between the two model simulations, ~~RC2-base-04~~REF and ~~SC2-fGHG-01~~FIX, for the DNA active irradiance, total ozone, cloud cover and surface albedo at Barrow (Alaska) and Palmer (Antarctica) for the periods 1960–1999, 2000–2049 and 2050–2099. While variations in surface albedo are certainly of primary importance for high-latitude sites, they can play a non-negligible role even at mid-latitudes. However, they were not analyzed here.

From Figure ~~6~~ 7 it is clear that surface albedo decreases significantly by the end of the 21st century in view of the increasing GHG emissions. The decreases in surface albedo (Table 7) are larger in Barrow (Alaska) than Palmer (Antarctica). The trend for Barrow is qualitatively consistent with the conclusion by Bernhard (2011), showing that the ground at Barrow is covered by snow later and later at the start of winter. We also note that both, Barrow and Palmer, are coastal sites and are heavily affected by local conditions (e.g., how far sea ice gets to the station), which may not be simulated correctly. Therefore, we point out that the evolution of albedo at the two stations shown in Figure ~~6~~ 7 is representative for regional changes but may not accurately reflect changes at the exact location of these stations.

To assess the impact of the albedo changes on UV variability, we used surface albedo as additional explanatory variable in the MLR model of Eq. (7). We determined an additional regression coefficient, namely β_{albedo}, which explains the effect of albedo change on DNA active irradiance change at the two stations under study, Barrow and Palmer. We estimated an albedo-related DNA active irradiance trend, in the same way as described above, by multiplying the coefficient β_{albedo} with the trend in albedo differences between the two model simulations.

For Barrow, we estimate an ozone-related DNA active irradiance trend of about −0.87% per decade for the period 2050–2099, indicating that ~41% of the DNA active irradiance trend (−2.14% per decade) is caused by trends in ozone. The respective cloud-related DNA active irradiance trend is about −0.49% per decade, which means that the cloud trend explains ~23% of the DNA active irradiance trend. The surface albedo-related DNA radiation trend is about −0.45% per decade, explaining ~21% of the DNA active irradiance trend in the period 2050-2099. The model suggests that all parameters together explain ~85% of the DNA active irradiance trend, which however may not be such an unbiased result. This is because the effects of clouds and albedo are not independent, as assumed in the regression equation. For 100% albedo and non-absorbing clouds, clouds would barely attenuate UV radiation. For actual albedo and cloud conditions, clouds do attenuate, but the effect is greatly reduced by surface albedo because of multiple reflections between surface and cloud (Nichol et al., 2003).

At Palmer, the trends are smaller. The ozone-related DNA active irradiance trend is –0.46% per decade, the cloud-related DNA active irradiance trend is 0.43% per decade, and the albedo-related DNA active irradiance trend is –0.31% per decade. These trends together determine the small negative trend, which is predicted for the DNA active UV irradiance in the period 2050–2099 of about –0.33% per decade.

The above calculations indicate that the impact of albedo trends on DNA active irradiance trends due to the continuous increase of GHGs until the end of the 21st century is important and should not be ignored when studying the long-term changes of DNA active radiation reaching the ground. The model simulations at Barrow and Palmer suggest that the surface albedo changes might be larger at Barrow than Palmer according to Table 7. The model simulations also suggest that the northern high latitudes might experience larger changes in surface albedo than the southern high latitudes in the period 2050–2100 (Appendix C, Figures C1 and C2).

In order to better represent the northern and southern high latitudes, we also applied the MLR model to the large-scale zonal means of 55° – 75° N and 55° – 75° S. For the northern high latitude zone, the findings are in the same direction as those found for Barrow. We estimate that ~31% of the DNA active irradiance trend is determined by the trend in ozone, and that ~14% and ~32% of the DNA active radiation trend are explained by trends in clouds and surface albedo, respectively. For the southern high latitude zone, we estimate that the largest part of the DNA active irradiance trend is determined by the trend in ozone, and that the contributions of cloud and albedo trends are small.

4 Summary and Conclusions

We have studied changes in ozone ~~and,~~ DNA active irradiance and cloud cover due to the evolution of greenhouse gas concentrations in the near global mean (50° N–50° S) and in the northern and southern high latitudes, using the EMAC CCM simulations from 1960 to 2100.

The model simulations have been evaluated against ground-based UV irradiance measurements, satellite ozone observations from SBUV (v8.7) and satellite cloud fraction data from MODIS/Terra for the period 2000–2018. The evaluation results can be summarized as follows:

- Simulations of total ozone with specified dynamics (RC1SD-base-10 and ~~SC1SD-base-02~~HIS-SD) reproduce extremely well the variability of total ozone in the northern and southern high latitudes for the periods 1979–2013 and 2000–2018, respectively. The correlation analysis results between EMAC ~~SC1SD-base-02~~HIS-SD simulation and SBUV (v8.7) satellite ozone de-seasonalized data are: Northern high latitudes (~~2~~ 3 station mean), R = ~~+0.908~~+0.899, p-value <0.0001; Southern high latitudes (4 station mean), R = +0.892, p-value <0.0001; 50° N–50° S (13 station mean), R = +0.894, p-value <0.0001.
- The respective simulations of DNA active irradiance correlate quite well with ground-based UV measurements, as follows: Northern high latitudes (~~2~~ 3 station mean), R = ~~+0.518~~+0.504, p-value

<0.0001; Southern high latitudes (4 station mean), R = +0.746, p-value <0.0001; 50º N–50º S (13 station mean, R = +0.499, p-value <0.0001).

- Evaluation of cloud cover simulations against MODIS/Terra cloud fraction data gave good correlations as follows: Northern high latitudes (~~2~~ 3 stations mean), R = ~~+0.480~~+0.453, p-value <0.0001; Southern high latitudes (4 station mean), R = +0.485, p-value <0.0001; 50º N–50º S, R = +0.703, p-value <0.0001.

Between 50º N–50º S, the DNA-damaging UV radiation is expected to decrease until 2050 and to increase thereafter. This increase is associated with expected decreases in cloud cover and insignificant trends in total ozone, as it was shown previously by Eleftheratos et al. (2020). Our study however expands the previous work by adding more stations in low and mid-latitudes and by including estimates from high latitude stations with long-term measurements of UV irradiance.

In contrast to the predictions for 50º N–50º S, we estimate that DNA active irradiance will continue to decrease after the year 2050 in the northern and southern high latitudes (>55º) due to increasing ozone. More specifically, for the northern high latitude stations we estimate that total ozone will increase by ~~2.4~~1.8 ± ~~0.9~~0.8% from 2050 to 2100, DNA active irradiance will decrease by ~~10.6~~8.2 ± ~~3.7~~3.8% and that cloud cover will increase insignificantly by ~~1.3~~1.4 ± ~~2.0~~1.3%. Similarly, in the southern high latitude stations, total ozone is estimated to increase by 4.2 ± 2.1% from 2050 to 2100, DNA active irradiance is estimated to decrease by 4.8 ± 2.9% and cloud cover will decrease insignificantly by 1.1 ± 1.7%.

The statistical results have been confirmed by statistical tests. Statistical comparisons of the regression slopes before and after 2050 in the northern and southern high latitude stations under study showed that there are no statistically significant different trends in DNA active irradiance before and after that year. On the other hand, between 50º N–50º S the trends before and after 2050 were found to be statistically significantly different at the 0.05 significance level. The test confirmed the statistical result that DNA active irradiance will reverse sign and become positive after 2050 at stations between 50º N–50º S mainly due to cloud cover and ozone changes associated with climate change, something that is likely not to happen at high latitudes, where the DNA-damaging UV-B radiation is projected to continue its downward trend after 2050 mainly due to the continued increase of ozone from the reduction of ODSs. In addition, it should be mentioned, that the enhanced GHG concentrations will cool the stratosphere and therefore the stratospheric ozone content (especially in the middle and upper stratosphere) is expected to increase because the ozone depleting reactions (homogeneous gas phase reactions) will be getting slower. From Dhomse et al. (2018) we know that the (future) Arctic and the Antarctic stratosphere are developing differently in spring. In particular, the Arctic region is indicating a stronger reaction on enhanced GHG concentrations (most likely due to the dynamic feedbacks in the northern hemisphere, i.e., related to the planetary wave activity).

We clarify here that our findings for the high latitudes refer to the summer periods and not to the seasons when ozone depletion occurs, for which it has been shown that climate change will favor large spring loss

of Arctic column ozone in connection with extraordinary (persistent) cold stratospheric winters (with low planetary wave activity) in the future (von der Gathen et al., 2021). The best agreement between the ~~RC2-base-04~~REF simulation results and satellite measurements during the period of ozone depletion was found for the southern high latitudes. The ~~RC2-base-04~~REF simulation (full chemistry and increasing GHGs according to RCP-6.0) seems to underestimate the observed ozone depletion of the 1980s and 1990s for the near global mean (50° N–50° S) and at high latitudes of the Northern Hemisphere. This might at least partly be caused by not considering all ODSs, but only a subset (only CFC-11 and CFC-12 were considered). Despite this feature, the simulated ozone declines during 1979–1999 and the minimum ozone values calculated by the model in the 1990s for the northern mid- and high latitudes, are qualitatively in line with the satellite ozone observations.

Also, our analysis suggests that clouds might stay constant over the Arctic, while other models predict that cloud cover in the Arctic will increase during the next decades due to enhanced evaporation of water vapor by the sea-ice decrease. Our estimates, however, refer to two sites in the Arctic and not to the entire Arctic Ocean. As such, our results should be considered representative of the land sites under study and not of the entire Arctic or Antarctic regions. In addition, we cannot reliably evaluate the projection of cloud cover over time, using MODIS observations for a relatively short period. So, in the end we must trust that the physics coded in the model is correct. Hence, verification of our results using independent CCMs would be highly desired. We conducted a separate analysis on total cloud cover variability and trends through the 21st century, using the available simulations from the CCMI-1 REF-C2 set, which showed that the EMAC CCM results fall well within the range of uncertainty (i.e., ± 2σ), close to the ensemble average (± 1σ).

Moreover, we applied a multiple linear regression model to examine the contribution of ozone and cloud trends to the estimated DNA active irradiance trends after the year 2050. The model was applied to the differences between the two model simulations, ~~RC2-base-04~~REF and ~~SC2-fGHG-01~~FIX. It was found that ozone is the primary contributor accounting for about ~50% of the predicted trends in DNA active irradiance after 2050 both in the northern and in the southern high latitude stations.

The impact of surface albedo on DNA active irradiance trends due to the evolution of GHGs (RCP-6.0) has been examined at two stations, Barrow in the Arctic, and Palmer in the Antarctic. The model simulations suggest that declining trends in surface albedo are larger at Barrow than Palmer. The driving force for the decrease in Arctic surface albedo is by 70% the decrease in snow cover fraction over the Arctic land and sea-ice due to the increase in surface air temperature and decrease in snowfall (Zhang et al., 2019).

Unlike the Arctic sea-ice, which has consistently declined over the past four decades, the Antarctic sea-ice has shown little change (increase) from 1979 to 2015 but large regional and temporal variability (Maksym, 2019). A rapid decline in 2015–2018, far exceeding the decreasing rates seen in the Arctic (Parkinson, 2019), may have foreboded future changes in Antarctic sea-ice (Eayrs et al., 2021). The observed decline lowered the region's surface albedo, highlighting the importance of Antarctic sea-ice loss to the global snow and ice albedo feedback (Riihelä et al., 2021). This sea-ice reduction probably resulted from the

interaction of a decades-long ocean warming trend and an early spring southward advection of atmospheric heat, with an exceptional weakening of the Southern Hemisphere mid-latitude westerlies in late spring (Eayrs et al., 2021). Obviously, such abrupt declines cannot be predicted by the present-day model simulations. This is because the mechanisms for the Antarctic sea-ice variations are not yet well understood and future predictions are highly uncertain.

IPCC (2021) concluded that there has been no significant trend in Antarctic sea-ice area from 1979 to 2020, due to regionally opposing trends and large internal variability. In the Bellingshausen and Amundsen Seas, however, the observed sea-ice has shown decreasing trends (Maksym, 2019; Parkinson, 2019; Eayrs et al., 2021). Our estimates for Palmer, which is located at the coast of the Bellingshausen Sea, shows a negative trend in surface albedo from 1979 to 2020, which is in line with the negative trends in sea-ice observed in Bellingshausen and Amundsen Seas. The ~~RC2-base-04~~REF simulation shows that the surface albedo at Palmer will continue to decrease until 2100. This result should be considered representative of the Palmer station and its surroundings, and not of the entire Antarctic region.

The key findings presented in this study are that model and measurements agree fairly well, giving support to the simulations of the future scenarios. Cloud cover is generally decreasing, leading to increased solar radiation, apart from the high latitudes, where no significant changes are observed. Total ozone shows an increasing trend from the reduction of ODSs, while a decrease is observed after 2050 on a near-global scale due to the increase of GHGs. UV trends are a combination of changes in ozone and cloud cover, while at high latitudes, decreased surface albedo in the second half of the century has a significant influence on the surface UV radiation.

The above findings were based on the analysis of model simulations from 3 stations in the northern high latitudes, 4 stations in the southern high latitudes, and 13 stations in the near-global mean with contributions mainly from the mid-latitudes. A separate analysis using zonal means showed that the results from the analysis of the model data averaged over geographical zones are qualitatively in the same direction with those from the station averages. All simulations were based on a single CCM, and therefore, verification of the results from simulations of other models would be quite useful.

Appendix A Qualitative evaluation of free running CCM simulations against simulations with specified dynamics

In this appendix, we compare the free running ozone simulation ~~RC2-base-04~~REF, with the SD simulation RC1SD-base-10 and SBUV satellite ozone data (v8.7). The simulation with specific dynamics RC1SD-base-10 covers the period January 1979 – December 2013. The simulation has been used in recent assessments reports for stratospheric ozone studies (e.g., LOTUS, 2019). In addition to the nudging towards ECMWF ERA-Interim (Dee at al., 2011) reanalysis data (for details about the nudging setup see Jöckel et al., 2016) the simulation uses also sea surface temperatures and sea-ice concentrations from the ERA

Interim reanalysis data. Here, we use the SD simulation (RC1SD-base-10) to show that the free running simulation (~~RC2-base-04~~REF) is capable to qualitatively reflect the negative ozone trends of the 1980s and 1990s. The reason for quoting the RC1SD-base-10 simulation is because the ~~SC1SD-base-02~~HIS-SD simulation that is used in section 3.1 does not go back in time before 2000, and therefore we cannot qualitatively evaluate our free running simulation before 2000. We also appose here the SD simulation (~~SC1SD-base-02~~HIS-SD), which covers the period January 2000 – July 2018. This is useful and helpful to classify the results of the free running model system concerning the quality with respect to the SD simulation and the observations of the stations, and it serves as a "bridge" from the observations via the SD simulation results, to the results of the (longer-term) free-running model simulation.

Figure A1 shows the comparison between the simulations and SBUV data. Obviously, the RC1SD-base-10 simulation (period 1979–2013) compares much better with the SBUV data than the ~~RC2-base-04~~REF simulation. The same also holds for the ~~SC1SD-base-02~~HIS-SD simulation (period 2000–2018). This is expected since the SD simulation uses reanalyzed meteorology, whereas the free running simulation has its own meteorological/synoptical sequence. For comparison with the fixed GHG simulation, we need to switch to the pair of free running simulations. And the question is, if the evaluation (comparison with observations) also hold for the ~~RC2-base-04~~REF simulation, which is the basis for the comparison with the fixed GHG simulation (~~SC2-fGHG-01~~FIX). In the case of free running simulations, the evaluation is only possible for the trends and for the amplitude of the year-to-year variability, but not for the sign of the anomaly in a given nominal year and/or month. Figure A1 shows that the free running simulation (~~RC2-base-04~~REF) reflects correctly the negative ozone trends of the past, seen in the observations and in the SD simulation, and is therefore suitable for comparison with the fixed GHG simulation.

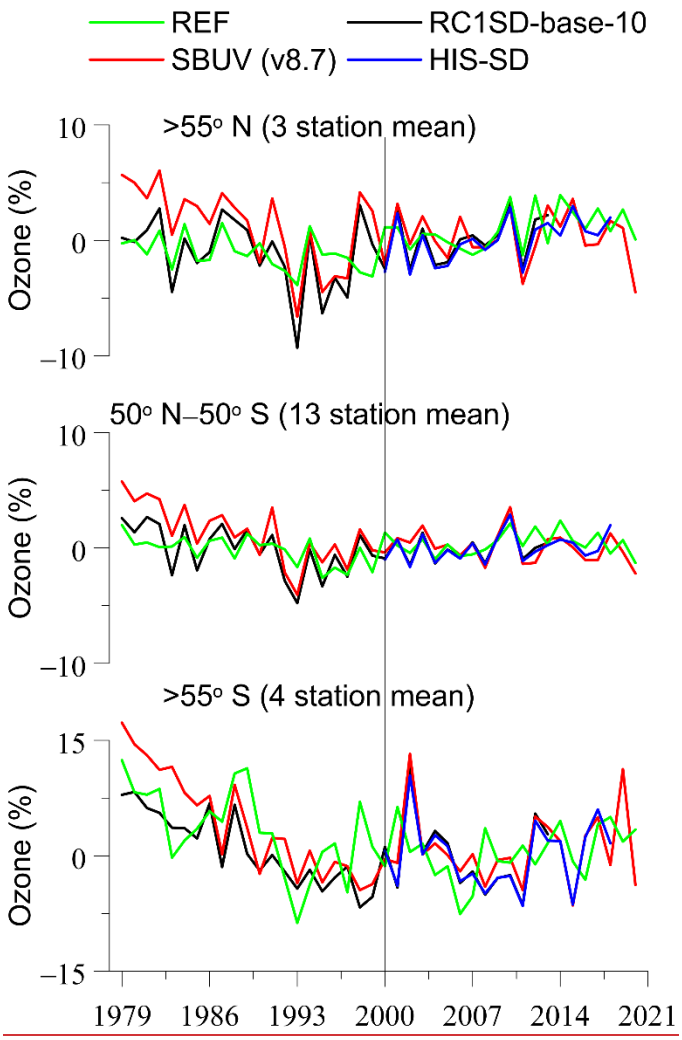
REF
RC1SD-base-10
SBUV (v8.7)
HIS-SD
>55° N (3 station mean)
50° N–50° S (13 station mean)
>55° S (4 station mean)
Ozone (%)
10
0
−10
15
−15
1979
1986
1993
2000
2007
2014
2021

861

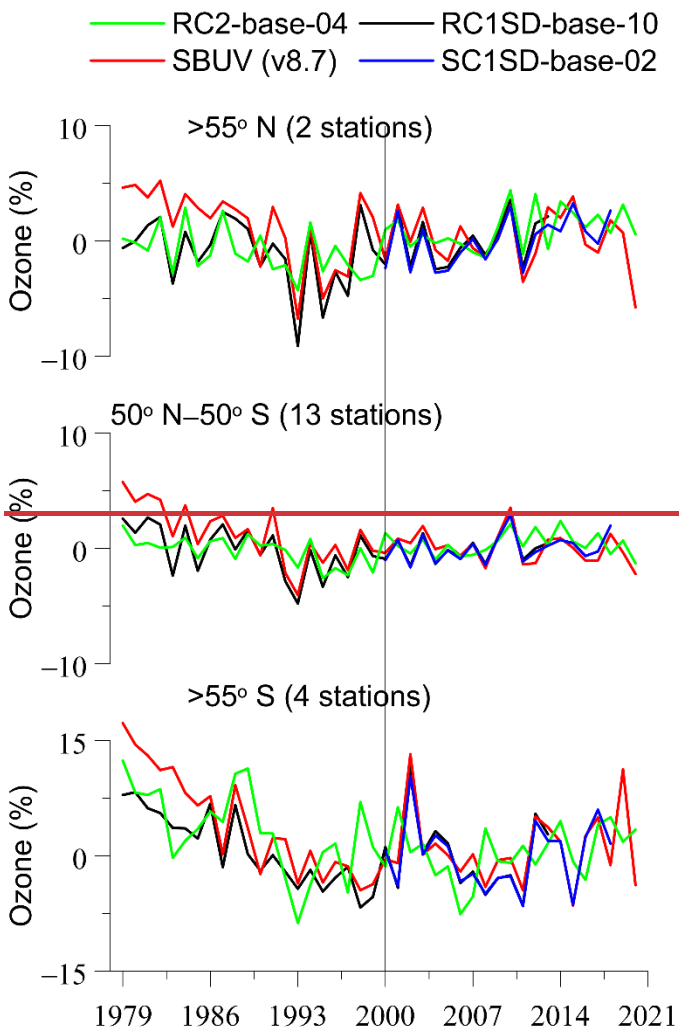

862

863 **Figure A1.** Comparison of REF~~RC2-base-04~~ (free running simulation; green line) with RC1SD-base-10
864 (SD simulation for 1979–2013; black line), ~~SC1SD-base-02~~HIS-SD (SD simulation for 2000–2018; blue
865 line) and SBUV (v8.7) satellite measurements (red line) for ~~2~~ 3 stations higher than 55° N (upper plot), 13
866 stations between 50° N–50° S (middle plot) and 4 stations higher than 55° S (lower plot). The vertical line
867 has been put in the year 2000. The y-axis shows yearly averaged total ozone data (in %) calculated from
868 de-seasonalized monthly data. The monthly data were de-seasonalized relative to the long-term monthly
869 mean (2000–2018) and were expressed in %. For the northern high latitude stations, the annual average
870 refers to the average of monthly anomalies from March to September, and for the southern high latitude
871 stations, it refers to the average of monthly anomalies from September to March. For the stations between
872 50° N–50° S we used all months to calculate the annual average.

873

Appendix B Model simulations of zonally averaged cloud cover between 50º and 80º N

Figure B1 shows the changes of the zonally averaged cloud cover based on ~~RC2-base-04~~REF (RCP-6.0) and ~~SC2-fGHG-02~~FIX simulations, and their differences (~~RC2-base-04~~REF minus ~~SC2-fGHG-01~~FIX), per 10-degree latitude zones from 50º to 80º N. For the period 1960 to 2100, the changes in cloud cover due to the evolution of GHGs (RCP-6.0) are presented in Table B1. The same picture with increasing trends as we move northward of 50º N is also found for the period 2050 to 2100.

Table B1. Changes in zonal mean cloud cover between 50º and 80º N due to the evolution of GHGs (RCP-6.0), for the periods 1960–2100 and 2050–2100.

	1960–2100			2050–2100		
	% Change	p-value	N	% Change	p-value	N
50º–60º N	0.9	< 0.0001	140	0.3	0.56064	50
60º–70º N	2.7	< 0.0001	140	0.7	0.27113	50
70º–80º N	4.3	< 0.0001	140	1.9	0.00012	50

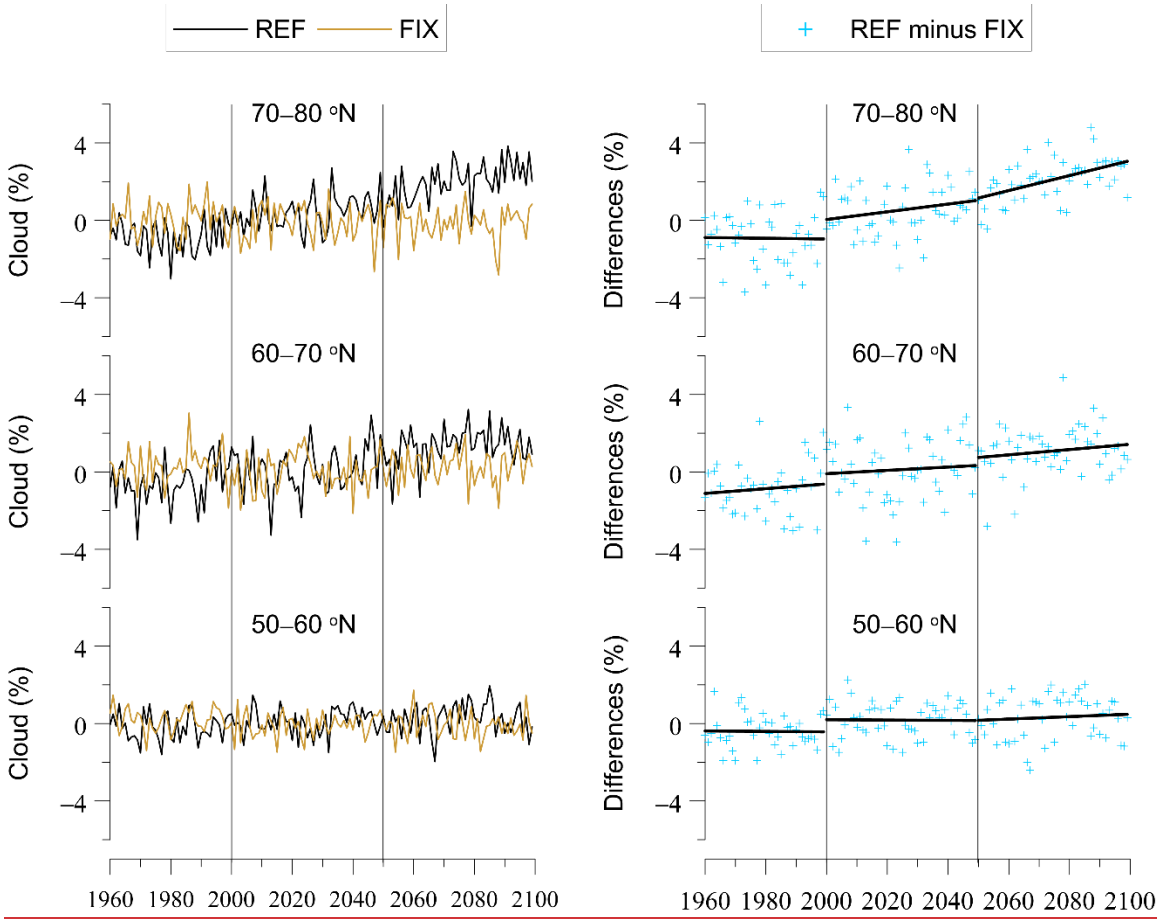

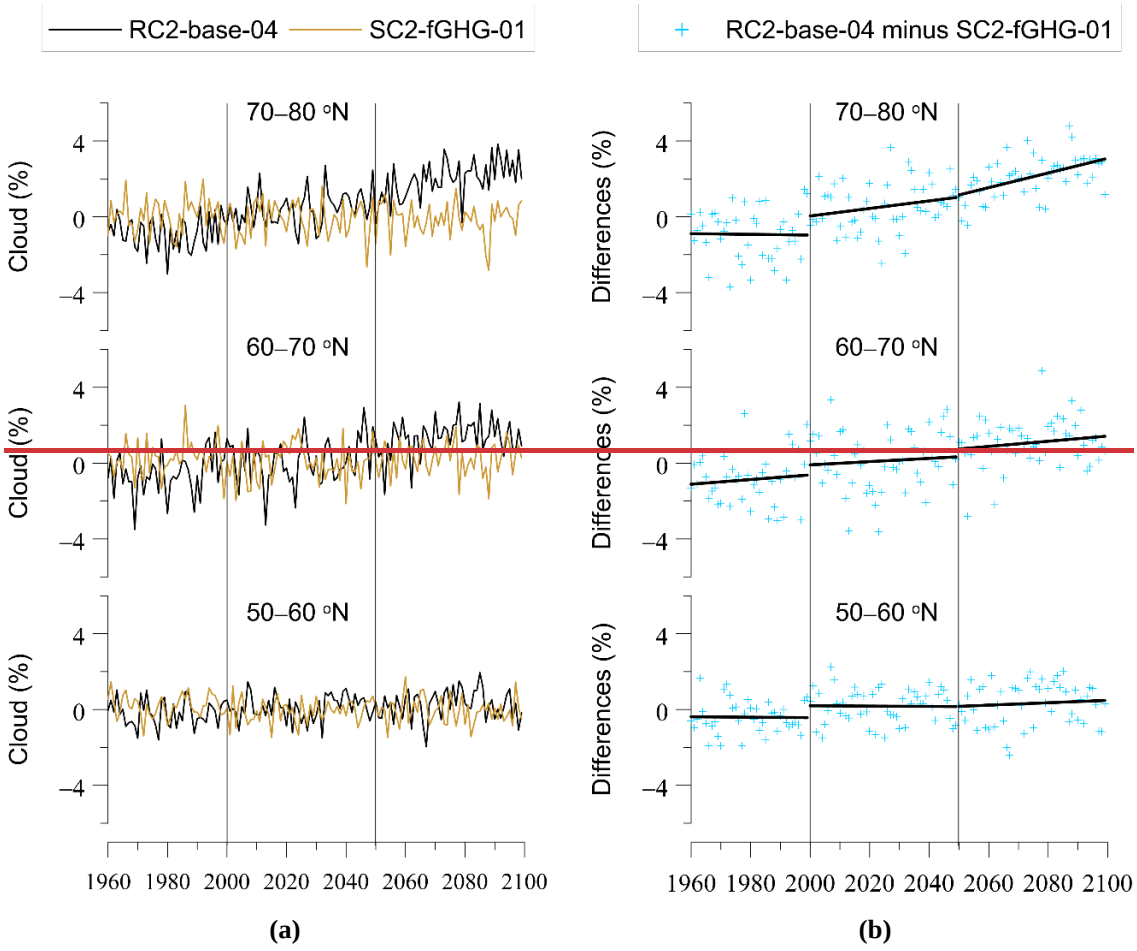

884 **Figure B1.** EMAC CCM projections of zonal mean cloud cover for 10-degree latitude zones (50º–60º N,
885 60º–70º N, 70º–80º N), based on simulations with increasing and fixed GHGs mixing ratios. **(a)** ~~RC2-base-~~
886 ~~04~~REF is the simulation with increasing GHGs according to RCP-6.0. ~~SC2-fGHG-01~~FIX is the simulation
887 with fixed GHGs emissions at 1960 levels. **(b)** Difference between the two model simulations, as an
888 indicator of the impact of increasing GHGs. The y-axis in the left figure (a) shows yearly averaged cloud
889 cover data (in %) calculated from de-seasonalized monthly data. The monthly data were de-seasonalized
890 relative to the long-term monthly mean (1990–2019) and were expressed in %. For the northern high
891 latitudes, the annual average refers to the average of monthly anomalies from March to September.

892

893 **Appendix C Model simulations of zonally averaged surface albedo between 50º and 80º N, and 50º**
894 **and 80º S**

895 Figure C1 shows the changes in zonally averaged surface albedo based on ~~RC2-base-04~~REF (RCP-6.0) and
896 ~~SC2-fGHG-02~~FIX simulations, and their differences (~~RC2-base-04~~REF minus ~~SC2-fGHG-01~~FIX), per 10-
897 degree latitude zones between 50º N and 80º N. Figure C2 shows the respective changes between 50º S and

898 80° S. The changes in surface albedo due to the evolution of GHGs (RCP-6.0) between 50° and 80° N, and
899 50° and 80° S, are summarized in Table C1.

900

901 **Table C1.** Changes in zonal mean surface albedo due to the evolution of GHGs (RCP-6.0) between 50° and
902 80° N, and 50° and 80° S, for the periods 1960–2100 and 2050–2100.

North	1960–2100			2050–2100		
	% Change	p-value	N	% Change	p-value	N
50°–60° N	–21.0	< 0.0001	140	–8.9	< 0.0001	50
60°–70° N	–18.3	< 0.0001	140	–9.2	< 0.0001	50
70°–80° N	–41.3	< 0.0001	140	–15.1	< 0.0001	50

903

South	1960–2100			2050–2100		
	% Change	p-value	N	% Change	p-value	N
50°–60° S	–12.5	< 0.0001	140	–3.7	0.00299	50
60°–70° S	–22.5	< 0.0001	140	–3.8	0.00298	50
70°–80° S	–6.1	< 0.0001	140	–1.3	0.00132	50

904

905

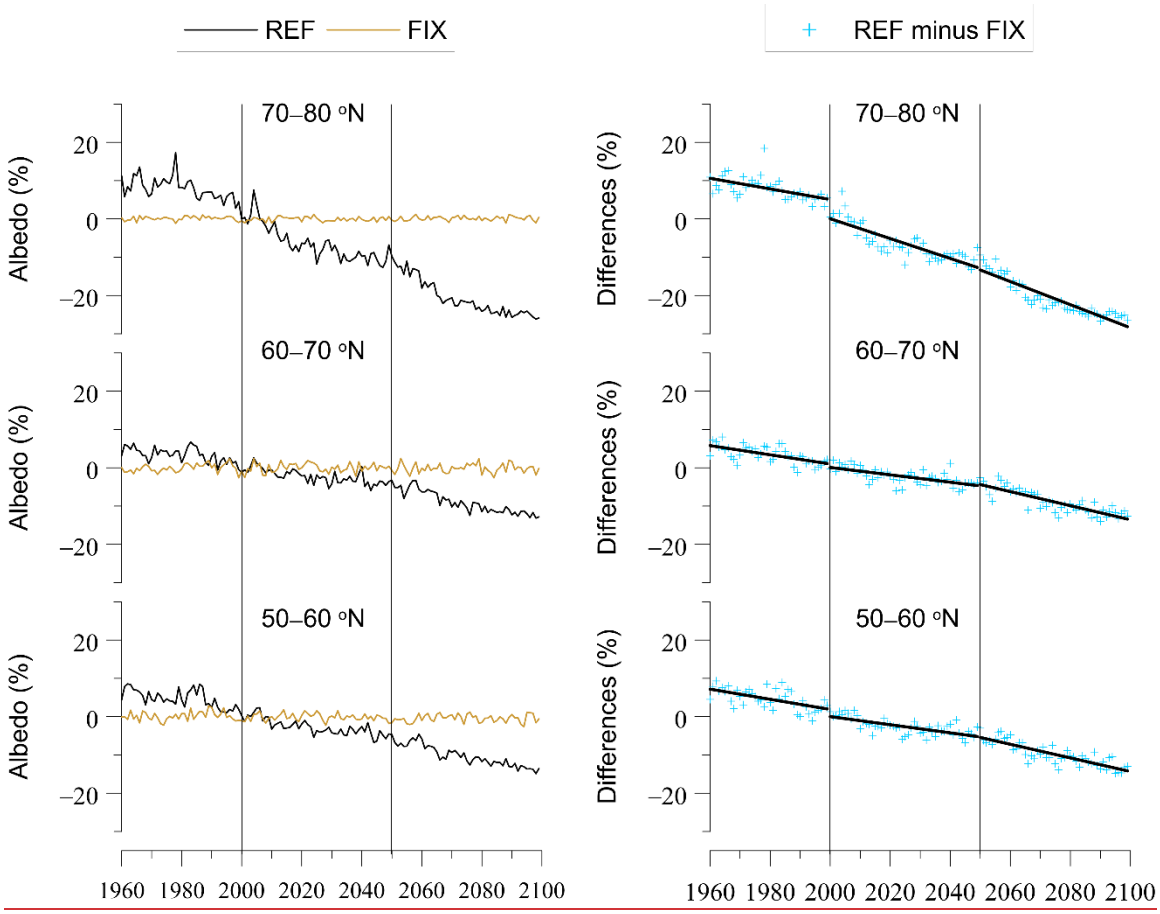
REF
FIX
REF minus FIX
70–80 °N
60–70 °N
50–60 °N
Albedo (%)
Differences (%)
20
0
–20
1960 1980 2000 2020 2040 2060 2080 2100

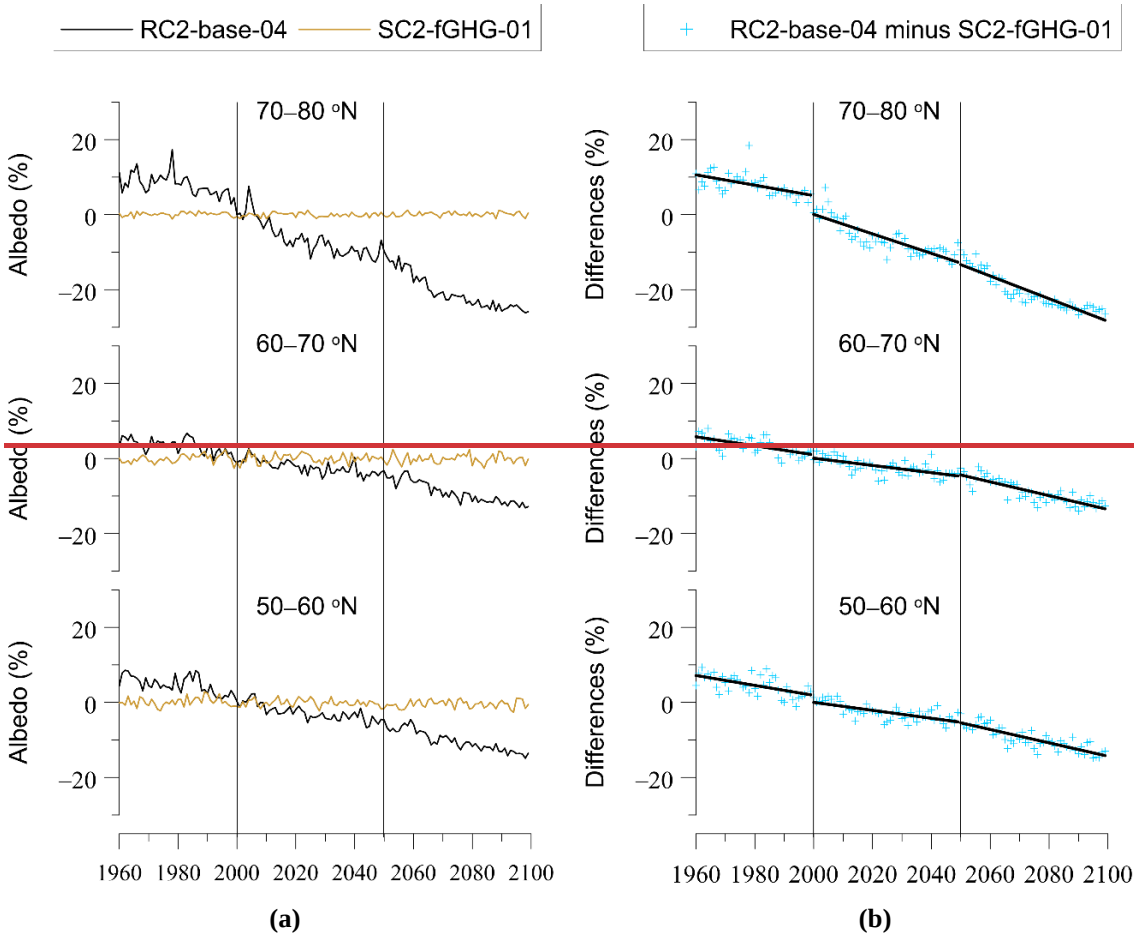

Figure C1. EMAC CCM projections of zonal mean surface albedo for 10-degree latitude zones (50-60° N, 60-70° N, 70-80° N), based on simulations with increasing and fixed GHGs mixing ratios. **(a)** ~~RC2-base-04~~REF is the simulation with increasing GHGs according to RCP-6.0. ~~SC2-fGHG-01~~FIX is the simulation with fixed GHGs emissions at 1960 levels. **(b)** Difference between the two model simulations, as an indicator of the impact of increasing GHGs. The y-axis in the left figure (a) shows yearly averaged surface albedo data (in %) calculated from de-seasonalized monthly data. The monthly data were de-seasonalized relative to the long-term monthly mean (1990–2019) and were expressed in %. For the northern high latitudes, the annual average refers to the average of monthly anomalies from March to September.

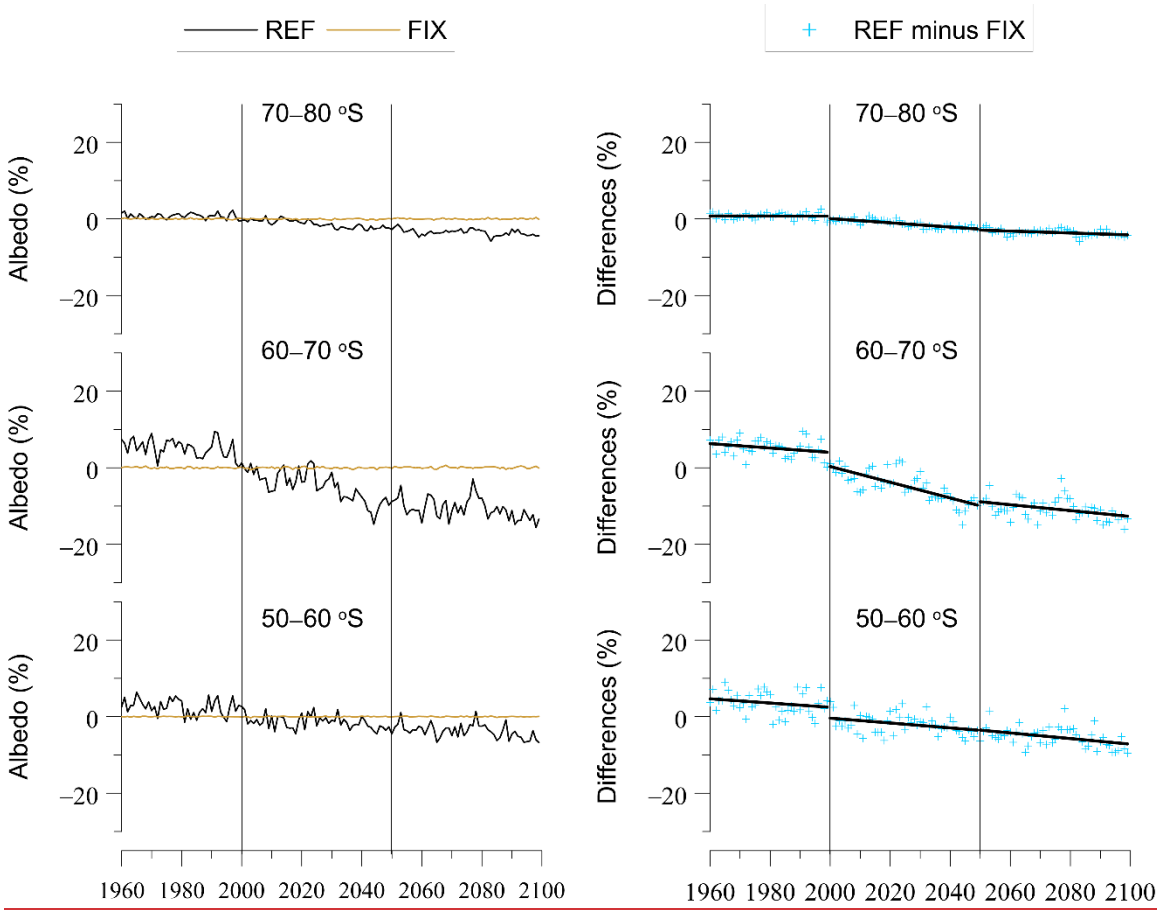
REF
FIX
REF minus FIX
70–80 °S
60–70 °S
50–60 °S
Albedo (%)
Differences (%)
20
0
–20
1960 1980 2000 2020 2040 2060 2080 2100

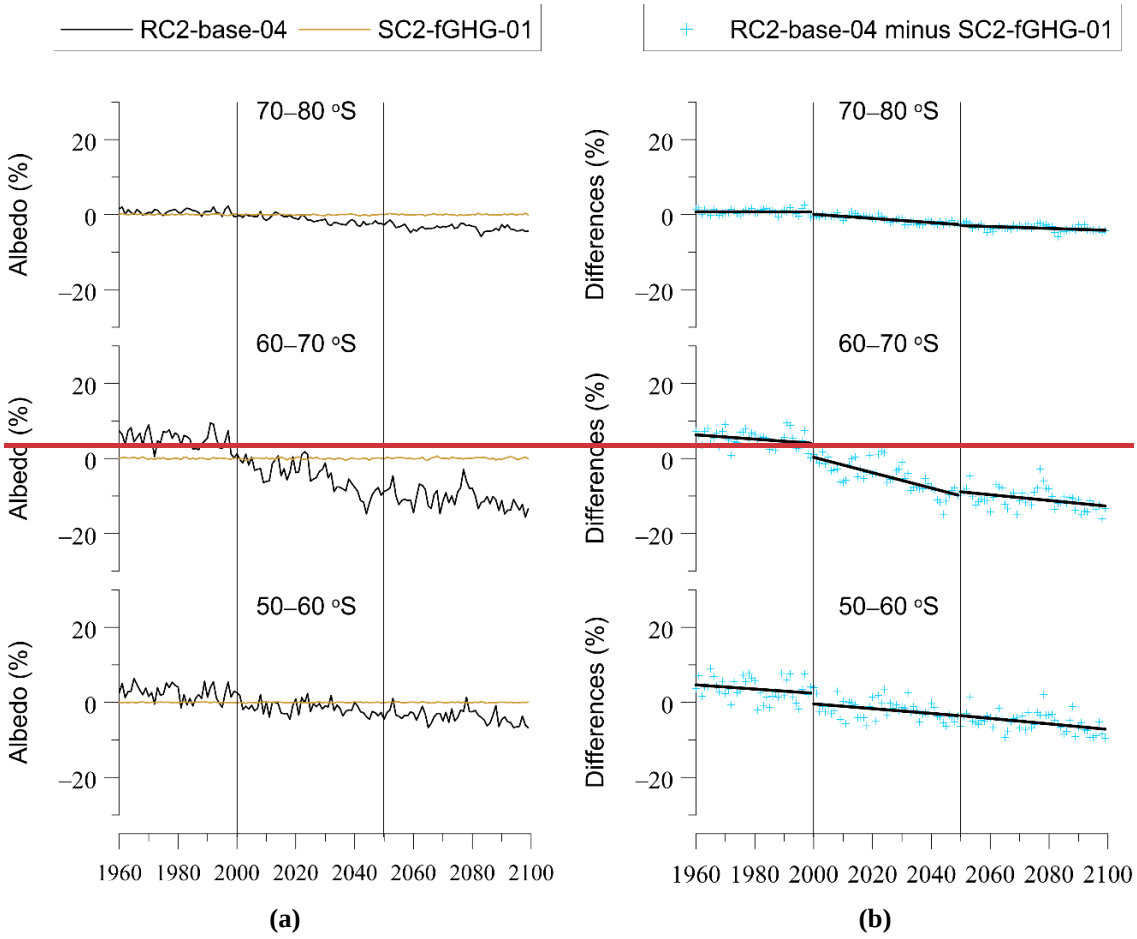

Figure C2. Same as Figure C1 but for 50-60° S, 60-70° S, and 70-80° S. The y-axis in the left figure (a) shows yearly averaged surface albedo data (in %) calculated from de-seasonalized monthly data. The monthly data were de-seasonalized relative to the long-term monthly mean (1990–2019) and were expressed in %. For the southern high latitudes, the annual average refers to the average of monthly anomalies from September to March.

Data Availability: The UV irradiance data are archived at the NDACC data repository, https://www-air.larc.nasa.gov/pub/NDACC/PUBLIC/stations/~~ftp://ftp.cpc.ncep.noaa.gov/ndacc/station/~~ (last access ~~27 July 2021~~4 September 2022). The SBUV (v8.~~6~~7) satellite ozone data are available at https://acd-ext.gsfc.nasa.gov/Data_services/merged/previous_mods.html (last access ~~18 March 2021~~4 September 2022). The MODIS/Terra v6.1 satellite cloud fraction monthly mean data (MOD08_M3 v6.1) are available at https://giovanni.gsfc.nasa.gov/giovanni/#service=TmAvMp&starttime=&endtime=&data=MOD08_M3_6_1_Cloud_Fraction_Mean_Mean (last access ~~6 April 2021~~4 September 2022).

Author Contribution: K.E. and C.Z. conceptualized the study. A.B., G.B., D.K., S.S., B.L., C.B., F.A., S.S. ~~and~~, H.D., and K.L. provided ground-based UV irradiance data. K.E., D.K., I.F. and K.T. analysed data. M.D. and P.J. provided the EMAC model simulations. J.K. and K.D. processed the model simulations. The manuscript was originally prepared by K.E. and was reviewed with comments and corrections from all co-authors.

Competing interests: One co-author (MD) is coordinator, and one co-author (IP) is co-organizer of the special issue "Atmospheric ozone and related species in the early 2020s: latest results and trends (ACP/AMT inter-journal SI), 2021".

Acknowledgments: The research work was partially funded by the Hellenic Foundation for Research and Innovation (H.F.R.I.) under the "First Call for H.F.R.I. Research Projects to support Faculty members and Researchers and the procurement of high-cost research equipment grant" (Atmospheric parameters affecting SPectral solar IRradiance and solar Energy (ASPIRE), Project Number: 300). We acknowledge support by the project "PANhellenic infrastructure for Atmospheric Composition and climatE change" (MIS 5021516) which is implemented under the Action "Reinforcement of the Research and Innovation Infrastructure", funded by the Operational Programme "Competitiveness, Entrepreneurship and Innovation" (NSRF 2014-2020), and co-financed by Greece and the European Union (European Regional Development Fund). The research contributes to the National Network for Climate Change and its Impact – CLIMPACT. We acknowledge the project Long-term Ozone Trends and Uncertainties in the Stratosphere (LOTUS) and the Mariolopoulos-Kanaginis Foundation for the Environmental Sciences. The EMAC simulations have been performed at the German Climate Computing Centre (DKRZ) through support from the Bundesministerium für Bildung und Forschung (BMBF). DKRZ and its scientific steering committee are gratefully acknowledged for providing the HPC and data archiving resources for this consortial project ESCiMo (Earth System Chemistry integrated Modelling). Measurements of French spectroradiometers are supported by CNES (French programme TOSCA); the Université de La Réunion and CNRS; the Région Hauts-de-France and the Ministère de l'Enseignement Supérieur et de la Recherche (CPER Climibio); and the European Fund for Regional Economic Development. Technicians at the three French and at the Finnish (Sodankylä) sites are acknowledged for the maintenance and calibration of the instruments. Kaisa Lakkala is supported by the CHAMPS project (grant no. 329225) of the Academy of Finland under the CLIHE programme. We acknowledge the SBUV science team for providing the satellite ozone profiles. NIWA UV spectrometer systems, serial numbers UV3 (Mauna Loa, HI) and UV5 (Boulder, CO) in the USA are owned and operated by NOAA/ESRL/Global Monitoring Division, Boulder CO. They are maintained, calibrated, and operated by NOAA. The final data from both of these instruments are quality controlled and produced by NIWA-Lauder, New Zealand. We thank NIWA and NOAA for the use of their data in this publication. Analyses and visualizations used in this study were produced with the Giovanni online data system, developed and maintained by the NASA GES DISC. We also acknowledge the MODIS mission scientists and associated NASA personnel for the production of the data used in this research

effort. We would like to thank the anonymous reviewer for summarizing the key findings which we incorporated at the end of the conclusions.

References

Armitage, P., Berry, G., and Matthews, J. N. S.: Statistical methods in medical research, 4th edition, Blackwell Publishing, ISBN 0-632-05257-0, pp.865, 2002.

Bais, A. F., Bernhard, G., McKenzie, R. L., Aucamp, P. J., Young, P. J., Ilyas, M., Jöckel, P., and Deushi, M.: Ozone-climate interactions and effects on solar ultraviolet radiation, Photochem. Photobiol. Sci., 18, 602-640, https://doi.org/10.1039/C8PP90059K, 2019.

Bais, A. F., McKenzie, R. L., Bernhard, G., Aucamp, P. J., Ilyas, M., Madronich, S., and Tourpali, K.: Ozone depletion and climate change: impacts on UV radiation, Photochem. Photobiol. Sci., 14(1), 19–52, doi:10.1039/c4pp90032d, 2015.

Bais, A. F., Tourpali, K., Kazantzidis, A., Akiyoshi, H., Bekki, S., Braesicke, P., Chipperfield, M. P., Dameris, M., Eyring, V., Garny, H., Iachetti, D., Jöckel, P., Kubin, A., Langematz, U., Mancini, E., Michou, M., Morgenstern, O., Nakamura, T., Newman, P. A., Pitari, G., Plummer, D. A., Rozanov, E., Shepherd, T. G., Shibata, K., Tian, W., and Yamashita, Y.: Projections of UV radiation changes in the 21st century: impact of ozone recovery and cloud effects, Atmos. Chem. Phys., 11, 7533–7545, https://doi.org/10.5194/acp-11-7533-2011, 2011.

Bais, A. F., and Zerefos C. S.: The effect of changes in ozone on solar UV-B radiation at Reykjavik, SPIE Vol. 2049 Atmospheric Radiation, 263–267, 1993.

Bais, A. F., Zerefos, C. S., Meleti, C., Ziomas I. C., and Tourpali, K.: Spectral measurements of solar UVb radiation and its relations to total ozone, SO_2, and clouds, J. Geophys. Res., 98(D3), 5199–5204, 1993.

Bernhard, G.: Trends of solar ultraviolet irradiance at Barrow, Alaska, and the effect of measurement uncertainties on trend detection, Atmos. Chem. Phys., 11, 13029–13045, https://doi.org/10.5194/acp-11-13029-2011, 2011.

Bernhard, G., Booth, C. R., Ehramjian, J. C., Stone, R., and Dutton, E. G.: Ultraviolet and visible radiation at Barrow, Alaska: Climatology and influencing factors on the basis of version 2 National Science Foundation network data, J. Geophys. Res., 112, D09101, doi:10.1029/2006JD007865, 2007.

Bernhard, G., Mayer, B., Seckmeyer, G., and Moise, A.: Measurements of spectral solar UV irradiance in tropical-Australia, J. Geophys. Res. Atmospheres, 102(D7), 8719 – 8730, https://doi.org/10.1029/97JD00072, 1997.

Bernhard, G., Neale, R. E., Barnes, P. W., Neale, P. J., Zepp, R. G., Wilson, S. R., Andrady, A. L., Bais, A. F., McKenzie, R. L., Aucamp, P. J., Young, P. J., Liley, J. B., Lucas, R. M., Yazar, S., Rhodes, L. E., Byrne, S. N., Hollestein, L. M., Olsen, C. M., Young, A. R., Robson, T. M., Bornman, J. F., Jansen, M. A.

K., Robinson, S. A., Ballaré, C. L., Williamson, C. E., Rose, K. C., Banaszak, A. T., Häder, D.-P., Hylander, S., Wängberg, S.-Å., Austin, A. T., Hou, W.-C., Paul, N. D., Madronich, S., Sulzberger, B., Solomon, K. R., Li, H., Schkowski, T., Longstreth, J., Pandey, K. K., Heikkilä, A. M., and White, C. C.: Environmental effects of stratospheric ozone depletion, UV radiation and interactions with climate change: UNEP Environmental Effects Assessment Panel, update 2019, Photochem. Photobiol. Sci., 19, 542–584, doi:10.1039/d0pp90011g, 2020.

Bernhard, G., and Stierle, S.: Trends of UV Radiation in Antarctica, Atmosphere, 11(8), 795, https://doi.org/10.3390/atmos11080795, 2020.

Bhartia, P. K., McPeters, R. D., Flynn, L. E., Taylor, S., Kramarova, N. A., Frith, S., Fisher, B., and DeLand, M.: Solar Backscatter UV (SBUV) total ozone and profile algorithm, Atmos. Meas. Tech., 6, 2533–2548, https://doi.org/10.5194/amt-6-2533-2013, 2013.

Blumthaler M., and Ambach, W.: Indication of increasing solar ultraviolet-B radiation flux in alpine regions, Science, 248(4952), 206-208, doi: 10.1126/science.2326634, 1990.

Brühl, C., and Crutzen, P. J.: On the disproportionate role of tropospheric ozone as a filter against solar UV-B radiation, Geophys. Res. Lett., 16, 703–706, 1989.

Butchart, N.: The Brewer-Dobson circulation, Rev. Geophys., 52, doi:10.1002/2013RG000448, 2014.

Collins, W. J., Bellouin, N., Doutriaux-Boucher, M., Gedney, N., Halloran, P., Hinton, T., Hughes, J., Jones, C. D., Joshi, M., Liddicoat, S., Martin, G., O'Connor, F., Rae, J., Senior, C., Sitch, S., Totterdell, I., Wiltshire, A., and Woodward, S.: Development and evaluation of an Earth-System model – HadGEM2, Geosci. Model Dev., 4, 1051–1075, doi:10.5194/gmd-4-1051-2011, 2011.

Dee, D. P., Uppala, S. M., Simmons, A. J., Berrisford, P., Poli, P., Kobayashi, S., Andrae, U., Balmaseda, M. A., Balsamo, G., Bauer, P., Bechtold, P., Beljaars, A. C. M., van de Berg, L., Bidlot, J., Bormann, N., Delsol, C., Dragani, R., Fuentes, M., Geer, A. J., Haimberger, L., Healy, S. B., Hersbach, H., Hólm, E. V., Isaksen, L., Kållberg, P., Köhler, M., Matricardi, M., McNally, A. P., Monge-Sanz, B. M., Morcrette, J.-J., Park, B.-K., Peubey, C., de Rosnay, P., Tavolato, C., Thépaut, J.-N., and Vitart, F.: The ERA-Interim reanalysis: configuration and performance of the data assimilation system, Q. J. Roy. Meteor. Soc., 137, 553–597, doi:10.1002/qj.828, 2011.

De Mazière, M., Thompson, A. M., Kurylo, M. J., Wild, J. D., Bernhard, G., Blumenstock, T., Braathen, G. O., Hannigan, J. W., Lambert, J.-C., Leblanc, T., et al. The Network for the Detection of Atmospheric Composition Change (NDACC): History, status and perspectives, Atmos. Chem. Phys., 18, 4935–4964, 2018.

den Outer, P. N., Slaper, H., Kaurola, J., Lindfors, A., Kazantzidis, A., Bais, A. F., Feister, U., Junk, J., Janouch, M., and Josefsson, W.: Reconstructing of erythemal ultraviolet radiation levels in Europe for the past 4 decades, J. Geophys. Res., 115, D10102, doi:10.1029/2009JD012827, 2010.

Dhomse, S. S., Kinnison, D., Chipperfield, M. P., Salawitch, R. J., Cionni, I., Hegglin, M. I., Abraham, N. L., Akiyoshi, H., Archibald, A. T., Bednarz, E. M., et al.: Estimates of ozone return dates from Chemistry-Climate Model Initiative simulations, Atmos. Chem. Phys., 18, 8409–8438, 2018.

Douglass, A., Fioletov, V. (Coordinating Lead Authors), Godin-Beekmann, S., Müller, R., Stolarski, R. S., Webb, A. (Lead Authors), Arola, A., Burkholder, J. B., Burrows, J. P., Chipperfield, M. P., Cordero, R., David, C., den Outer, P. N., Diaz, S. B., Flynn, L. E., Hegglin, M., Herman, J. R., Huck, P., Jánosi, I. M., Krzyscin, J. W., Liu, Y., Logan, J., Matthes, K., McKenzie, R. L., Muthama N. J., Petropavlovskikh, I., Pitts, M., Ramachandran, S., Rex, M., Salawitch, R. J., Sinnhuber, B.-M., Staehelin, J., Strahan, S., Tourpali, K., Valverde-Canossa, J., and Vigouroux, C.: Stratospheric ozone and surface ultraviolet radiation. In Scientific assessment of ozone depletion: 2010, Global Ozone Research and Monitoring Project (Report No. 52, Chapter 2). Geneva, Switzerland: World Meteorological Organization, 2011.

Eayrs, C., Li, X., Raphael, M. N., and Holland, D. M.: Rapid decline in Antarctic sea ice in recent years hints at future change, Nat. Geosci., 14, 460 – 464, doi:10.1038/s41561-021-00768-3, 2021.

Eleftheratos, K., Kazadzis, S., Zerefos, C., Tourpali, K., Meleti, C., Balis, D., Zyrichidou, I., Lakkala, K., Feister, U., Koskela, T., Heikkilä, A., and Karhu, J. M.: Ozone and spectroradiometric UV changes in the past 20 years over high latitudes, Atmosphere-Ocean, 53, 117-125, doi:10.1080/07055900.2014.919897, 2015.

Eleftheratos, K., Kapsomenakis, J., Zerefos, C. S., Bais, A. F., Fountoulakis, I., Dameris, M., Jöckel, P., Haslerud, A. S., Godin-Beekmann, S., Steinbrecht, W., Petropavlovskikh, I., Brogniez, C., Leblanc, T., Liley, J. B., Querel R., and Swart, D. P. J.: Possible Effects of Greenhouse Gases to Ozone Profiles and DNA Active UV-B Irradiance at Ground Level, Atmosphere, 11, 228, doi:10.3390/atmos11030228, 2020.

Eyring, V., Lamarque, J.-F., Hess, P., Arfeuille, F., Bowman, K., Chipperfield, M., Duncan, B., Fiore, A., Gettelman, A., Giorgetta, M., Granier, C., Hegglin, M., Kinnison, D., Kunze, M., Langematz, U., Luo, B., Martin, R., Matthes, K., Newman, P., Peter, T., Robock, A., Ryerson, A., Saiz-Lopez, A., Salawitch, R., Schultz, M., Shepherd, T., Shindell, D., Stähelin, J., Tegtmeier, S., Thomason, L., Tilmes, S., Vernier, J.-P., Waugh, D., and Young, P.: Overview of IGAC/SPARC Chemistry-Climate Model Initiative (CCMI) Community Simulations in Support of Upcoming Ozone and Climate Assessments, SPARC Newsletter, 40, 48-46, 2013.

Fountoulakis, I., and Bais, A. F.: Projected changes in erythemal and vitamin D effective irradiance over northern-hemisphere high latitudes, Photochem. Photobiol. Sci., 14(7), 1251–1264, doi:10.1039/c5pp00093a, 2015.

Fountoulakis, I., Bais, A. F., Tourpali, K., Fragkos, K. and Misios, S.: Projected changes in solar UV radiation in the Arctic and sub-Arctic Oceans: Effects from changes in reflectivity, ice transmittance, clouds, and ozone, J. Geophys. Res. Atmos., 119(13), 8073–8090, doi:10.1002/2014JD021918, 2014.

Fountoulakis, I., Diémoz, H., Siani, A. M., Hülsen, G., and Gröbner, J.: Monitoring of solar spectral ultraviolet irradiance in Aosta, Italy, Earth Syst. Sci. Data, 12, 2787–2810, https://doi.org/10.5194/essd-12-2787-2020, 2020a.

Fountoulakis, I., Diémoz, H., Siani, A.-M., Laschewski, G., Filippa, G., Arola, A., Bais, A. F., De Backer, H., Lakkala, K., Webb, A. R., De Bock, V., Karppinen, T., Garane, K., Kapsomenakis, J., Koukouli, M.-E., and Zerefos, C. S.: Solar UV Irradiance in a Changing Climate: Trends in Europe and the Significance of Spectral Monitoring in Italy, Environments, 7(1), https://doi.org/10.3390/environments7010001, 2020b.

Fountoulakis, I., Zerefos, C. S., Bais, A. F., Kapsomenakis, J., Koukouli, M.-E., Ohkawara, N., Fioletov, V., De Backer, H., Lakkala, K., Karppinen, T., Webb, A. R.: Twenty-five years of spectral UV-B measurements over Canada, Europe and Japan: Trends and effects from changes in ozone, aerosols, clouds, and surface reflectivity, Comptes Rendus Geoscience, 350(7), 393–402, https://doi.org/10.1016/j.crte.2018.07.011, 2018.

Gröbner J.: Ultraviolet Radiation: Distribution and Variability. In: Meyers R.A. (eds) Encyclopedia of Sustainability Science and Technology, Springer, New York, NY, https://doi.org/10.1007/978-1-4419-0851-3_453, 2012.

Jöckel, P., Tost, H., Pozzer, A., Kunze, M., Kirner, O., Brenninkmeijer, C. A. M., Brinkop, S., Cai, D. S., Dyro, C., Eckstein, J., et al.: Earth System Chemistry integrated Modelling (ESCiMo) with the Modular Earth Submodel System (MESSy) version 2.51, Geosci. Model Dev., 9, 1153–1200, 2016.

Jones, C. D., Hughes, J. K., Bellouin, N., Hardiman, S. C., Jones, G. S., Knight, J., Liddicoat, S., O'Connor, F. M., Andres, R. J., Bell, C., Boo, K.-O., Bozzo, A., Butchart, N., Cadule, P., Corbin, K. D., Doutriaux-Boucher, M., Friedlingstein, P., Gornall, J., Gray, L., Halloran, P. R., Hurtt, G., Ingram, W. J., Lamarque, J.-F., Law, R. M., Meinshausen, M., Osprey, S., Palin, E. J., Parsons Chini, L., Raddatz, T., Sanderson, M. G., Sellar, A. A., Schurer, A., Valdes, P., Wood, N., Woodward, S., Yoshioka, M., and Zerroukat, M.: The HadGEM2-ES implementation of CMIP5 centennial simulations, Geosci. Model Dev., 4, 543–570, https://doi.org/10.5194/gmd-4-543-2011, 2011.

IPCC, 2021: Summary for Policymakers. In: Climate Change 2021: The Physical Science Basis. Contribution of Working Group I to the Sixth Assessment Report of the Intergovernmental Panel on Climate Change [Masson Delmotte, V., Zhai, P., Pirani, A., Connors, S. L., Péan, C., Berger, S., Caud, N., Chen, Y., Goldfarb, L., Gomis, M. I., Huang, M., Leitzell, K., Lonnoy, E., Matthews, J. B. R., Maycock, T. K., Waterfield, T., Yelekçi, O., Yu R., and Zhou, B. (eds.)]. Cambridge University Press. In Press.

Kerr, J. B., and McElroy, C. T.: Evidence for large upward trends of ultraviolet-B radiation linked to ozone depletion, Science, 262(5136), 1035–1034, doi:10.1126/science.262.5136.1032, 1993.

Kosmopoulos, P. G., Kazadzis, S., Schmalwieser, A. W., Raptis, P. I., Papachristopoulou, K., Fountoulakis, I., Masoom, A., Bais, A. F., Bilbao, J., Blumthaler, M., Kreuter, A., Siani, A. M., Eleftheratos, K., Topaloglou, C., Gröbner, J., Johnsen, B., Svendby, T. M., Vilaplana, J. M., Doppler, L., Webb, A. R.,

Khazova, M., De Backer, H., Heikkilä, A., Lakkala, K., Jaroslawski, J., Meleti, C., Diémoz, H., Hülsen, G., Klotz, B., Rimmer, J., and Kontoes, C.: Real-time UV index retrieval in Europe using Earth observation-based techniques: system description and quality assessment, Atmos. Meas. Tech., 14, 5657–5699, https://doi.org/10.5194/amt-14-5657-2021, 2021.

Krzyścin, J. W. and Baranowski, D. B.: Signs of the ozone recovery based on multi sensor reanalysis of total ozone for the period 1979–2017, Atmospheric Environment, 199, 334–344, https://doi.org/10.1016/j.atmosenv.2018.11.050, 2019.

Lakkala, K., Arola, A., Heikkilä,A., Kaurola, J., Koskela, T., Kyrö, E., Lindfors, A., Meinander, O., Tanskanen, A., Gröbner, J. and Hülsen, G.: Quality assurance of the Brewer spectral UV measurements in Finland. Atmos. Chem. Phys., 8, 3369-3383, 2008.

Kylling, A., Dahlback, A., and Mayer, B.: The effect of clouds and surface albedo on UV irradiances at a high latitude site, Geophys. Res. Lett., 27(9), 1411–1414, 2000.

Lamy, K., Portafaix, T., Josse, B., Brogniez, C., Godin-Beekmann, S., Bencherif, H., Revell, L., Akiyoshi, H., Bekki, S., Hegglin, M. I., Jöckel, P., Kirner, O., Liley, B., Marecal, V., Morgenstern, O., Stenke, A., Zeng, G., Abraham, N. L., Archibald, A. T., Butchart, N., Chipperfield, M. P., Di Genova, G., Deushi, M., Dhomse, S. S., Hu, R.-M., Kinnison, D., Kotkamp, M., McKenzie, R., Michou, M., O'Connor, F. M., Oman, L. D., Pitari, G., Plummer, D. A., Pyle, J. A., Rozanov, E., Saint-Martin, D., Sudo, K., Tanaka, T. Y., Visioni, D., and Yoshida, K.: Clear-sky ultraviolet radiation modelling using output from the Chemistry Climate Model Initiative, Atmos. Chem. Phys., 19, 10087–10110, https://doi.org/10.5194/acp-19-10087-2019, 2019.

Lucas, R. M., Yazar, S., Young, A. R., Norval, M., de Gruijl F. R., Takizawa, Y., Rhodes, L. E., Sinclair, C. A., and Neale, R. E.: Human health in relation to exposure to solar ultraviolet radiation under changing stratospheric ozone and climate, Photochem. Photobiol. Sci., 18, 641, doi: 10.1039/c8pp90060d, 2019.

Madronich, S., McKenzie, R. L., Björn, L. O., and Caldwell, M. M.: Changes in biologically active ultraviolet radiation reaching the Earth's surface, Journal of Photochemistry and Photobiology B: Biology, 46, 5–19, 1998.

Maksym, T.: Arctic and Antarctic sea ice change: contrasts, commonalities, and causes. Annu. Rev. Mar. Sci. 11, 187–213, doi:10.1146/annurev-marine-010816-060610, 2019.

(The HadGEM2 Development Team): Martin, G. M., Bellouin, N., Collins, W. J., Culverwell, I. D., Halloran, P. R., Hardiman, S. C., Hinton, T. J., Jones, C. D., McDonald, R. E., McLaren, A. J., O'Connor, F. M., Roberts, M. J., Rodriguez, J. M., Woodward, S., Best, M. J., Brooks, M. E., Brown, A. R., Butchart, N., Dearden, C., Derbyshire, S. H., Dharssi, I., Doutriaux-Boucher, M., Edwards, J. M., Falloon, P. D., Gedney, N., Gray, L. J., Hewitt, H. T., Hobson, M., Huddleston, M. R., Hughes, J., Ineson, S., Ingram, W. J., James, P. M., Johns, T. C., Johnson, C. E., Jones, A., Jones, C. P., Joshi, M. M., Keen, A. B., Liddicoat, S., Lock, A. P., Maidens, A. V., Manners, J. C., Milton, S. F., Rae, J. G. L., Ridley, J. K., Sellar, A., Senior,

C. A., Totterdell, I. J., Verhoef, A., Vidale, P. L., and Wiltshire, A.: The HadGEM2 family of Met Office Unified Model climate configurations, Geosci. Model Dev., 4, 723–757, https://doi.org/10.5194/gmd-4-723-2011, 2011.

McKenzie, R., Bernhard, G., Liley, B., Disterhoft, P., Rhodes, S., Bais, A., Morgenstern, O., Newman, P., Oman, L., Brogniez, C., et al.: Success of Montreal Protocol Demonstrated by Comparing High Quality UV Measurements with "World Avoided" Calculations from Two Chemistry-Climate Models, Sci. Rep., 9, 12332, 2019.

McKenzie, R. L., Matthews, W. A., and Johnston, P. V.: The relationship between erythemal UV and ozone, derived from spectral irradiance measurements, Geophys. Res. Lett., 18(12), 2269–2272, 1991.

Neale, R. E., Barnes, P. W., Robson,·T. M., Neale,·P. J., Williamson,·C. E., Zepp, R. G., Wilson, S. R., Madronich,·S., Andrady,·A. L., Heikkilä, A. M., Bernhard, G. H., Bais, A. F., Aucamp, P. J., Banaszak, A. T., Bornman, J. F., Bruckman, L. S., Byrne, S. N., Foereid, B., Häder, D.-P., Hollestein, L. M., Hou, W.-C., Hylander, S., Jansen, M. A. K., Klekociuk, A. R., Liley, J. B., Longstreth, J., Lucas, R. M., Martinez-Abaigar, J., McNeill, K., Olsen, C. M., Pandey, K. K., Rhodes, L. E., Robinson, S. A., Rose, K. C., Schikowski, T., Solomon, K. R., Sulzberger, B., Ukpebor, J. E., Wang, Q.-W., Wängberg, S.-Å., White, C. C., Yazar, S., Young, A. R., Young, P. J., Zhu, L., Zhu, M.: Environmental effects of stratospheric ozone depletion, UV radiation, and interactions with climate change: UNEP Environmental Effects Assessment Panel, Update 2020, Photochemical & Photobiological Sciences, 20, 1–67, https://doi.org/10.1007/s43630-020-00001-x, 2021.

Nichol, S. E., Pfister, G., Bodeker, G. E., McKenzie, R. L., Wood, S. W., and Bernhard, G.: Moderation of cloud reduction of UV in the Antarctic due to high surface albedo, J. Applied Meteorology, 42, 1174–1183, 2003.

Norris, J. R., Allen, R. J., Evan, A. T., Zelinka, M. D., O'Dell, C. W., and Klein, S. A.: Evidence for climate change in the satellite cloud record, Nature, 536, 72–75, doi: 10.1038/nature18273, 2016.

Parkinson, C. L.: A 40-y record reveals gradual Antarctic sea ice increases followed by decreases at rates far exceeding the rates seen in the Arctic. Proc. Natl Acad. Sci. USA, 116, 14414–14423, doi:10.1073/pnas.1906556116, 2019.

Pisoft, P., Sacha, P., Polvani, L. M., Añel, J. A., de la Torre, L., Eichinger, R., Foelsche, U., Huszar, P., Jacobi, C., Karlicky, J., Kuchar, A., Miksovsky, J., Zak, M., and Rieder, H. E.: Stratospheric contraction caused by increasing greenhouse gases, Environ. Res. Lett., 16, 064038, https://doi.org/10.1088/1748-9326/abfe2b, 2021.

Riihelä, A., Bright, R. M., and Anttila, K.: Recent strengthening of snow and ice albedo feedback driven by Antarctic sea-ice loss, Nat. Geosci., 14, 832–836, doi:10.1038/s41561-021-00841-x, 2021.

Sander, R., Jöckel, P., Kirner, O., Kunert, A. T., Landgraf, J., and Pozzer, A.: The photolysis module JVAL-14, compatible with the MESSy standard, and the JVal PreProcessor (JVPP), Geosci. Model Dev., 7, 2653–2662, 2014.

Santer B. D., Wehner, M. F., Wigley, T. M. L., Sausen, R., Meehl, G. A., Taylor, K. E., Ammann., C., Arblaster, J., Washington, W. M., Boyle, J. S., and Brüggemann, W.: Contributions of Anthropogenic and Natural Forcing to Recent Tropopause Height Changes, Science, Vol 301, Issue 5632, 479–483, doi:10.1126/science.1084123, 2003.

Schneider, T., Kaul, C. M., and Pressel, K. G.: Possible climate transitions from breakup of stratocumulus decks under greenhouse warming, Nature Geoscience, 12, 163–167, https://doi.org/10.1038/s41561-019-0310-1, 2019.

Setlow, R. B.: The Wavelengths in Sunlight Effective in Producing Skin Cancer: A Theoretical Analysis, Proc. Nat. Acad. Sci. USA, 71(9), 3363–3366, https://doi.org/10.1073/pnas.71.9.3363, 1974.

Solomon, S., Ivy, D. J., Kinnison, J., Mills, M. J., Neely, R. R., and Schmidt, A.: Emergence of healing in the Antarctic ozone layer, Science 353, 269–274. https://doi.org/10.1126/science.aae0061, 2016.

Stocker, T. F., Qin, D., Plattner, G. K., Tignor, M. M. B., Allen, S. K., Boschung, J., Nauels, A., Xia, Y., Bex, V., and Midgley, P. M.: Climate change 2013 the physical science basis: Working Group I contribution to the fifth assessment report of the intergovernmental panel on climate change vol 9781107057999, 2013.

von der Gathen, P., Kivi, R., Wohltmann, I., Salawitch, R. J., and Rex, M.: Climate change favours large seasonal loss of Arctic ozone, Nature Communications, 12, 3886, https://doi.org/10.1038/s41467-021-24089-6, 2021.

von Storch, H. and Zwiers, F. W.: Statistical analysis in climate research, Cambridge University Press, Cambridge, 1999, ISBN 0 521 45071 3, 484 pp.

Weatherhead, B., Tanskanen, A., Stevermer, A. (Lead Authors), Andersen, S. B., Arola, A., Austin, J., Bernhard, G., Browman, H., Fioletov, V., Grewe, V., Herman, J., Josefsson, W., Kylling, A., Kyrö, E., Lindfors, A., Shindell, D., Taalas, P., and Tarasick, D.: Ozone and ultraviolet radiation, In Arctic Climate Impact Assessment (ACIA), (Chapter 5, pp. 151–182), Cambridge University Press, 2005, Retrieved from https://acia.amap.no/ (last access: ~~23~~ 4 September ~~2021~~2022).

Weber, M., Coldewey-Weber, M., Coldewey-Egbers, M., Fioletov, V. E., Frith, S. M., Wild, J. D., Burrows, J. P., Long, C. S., Loyola, D.: Total ozone trends from 1979 to 2016 derived from five merged observational datasets – the emergence into ozone recovery, Atmos. Chem. Phys., 18, 2097–2117, https://doi.org/10.5194/acp-18-2097-2018, 2018.

Weihs, P., Simic, S., Laube, W., Mikielewicz, W., Rengarajan, G., and Mandl, M.: Albedo Influences on Surface UV Irradiance at the Sonnblick High-Mountain Observatory (3106-m Altitude), J. Applied

Meteorology, 38, 1599–1610, https://doi.org/10.1175/1520-0450(1999)038<1599:AIOSUI>2.0.CO;2, 1999.

Wild, M., Gilgen, H., Roesch, A., Ohmura, A., Long, C. N., Dutton, E. G., Forgan, B., Kallis, A., Russak, V., and Tsvetkov, A.: From dimming to brightening: decadal changes in solar radiation at Earth's surface, Science, Vol. 308, Issue 5723, 847–850, doi: 10.1126/science.1103215, 2005.

Zerefos, C., Kapsomenakis, J., Eleftheratos, K., Tourpali, K., Petropavlovskikh, I., Hubert, D., Godin-Beekmann, S., Steinbrecht, W., Frith, S., Sofieva, V., et al.: Representativeness of single lidar stations for zonally averaged ozone profiles, their trends and attribution to proxies, Atmos. Chem. Phys., 18, 6427–6440, 2018.

Zerefos, C., Meleti, C., Balis, D., Tourpali, K., Bais, A. F.: Quasi-biennial and longer-term changes in clear sky UV-B solar irradiance, Geophys. Res. Lett., Vol. 25, No. 23, 4345-4348, 1998.

Zerefos, C. S., Tourpali, K., Zanis, P., Eleftheratos, K., Repapis, C., Goodman, A., Wuebbles, D., Isaksen, I. S. A., and Luterbacher, J.: Evidence for an earlier greenhouse cooling effect in the stratosphere before 1980 over the Northern Hemisphere, Atmospheric Chemistry and Physics, 14, 7705–7720, doi: 10.5194/acp-14-7705-2014, 2014.

Zhang, R., Wang, H., Fu, Q., Rasch, P. J., and Wang, X.: Unraveling driving forces explaining significant reduction in satellite-inferred Arctic surface albedo since the 1980s, Proc. Natl. Acad. Sci. USA, 116(48), 23947–23953, doi:10.1073/pnas.1915258116, 2019.

Table 1. Ground-based stations with long-term UV measurements used for the evaluation of EMAC CCM DNA active irradiance simulations. Stations are listed from northern to southern high latitudes and are grouped as follows: ~~2~~3 stations at latitudes greater than 55° N, 13 stations between 50° N – 50° S and 4 stations at latitudes greater than 55° S.

Station name	Latitude	Longitude	Period
1. Summit, Greenland*	72.58	-38.45	08/2004-08/2017
2. Barrow, AK, United States*	71.32	-156.68	02/1991-07/2016
3. Sodankylä, Finland	67.37	26.63	01/1990-12/2021
~~3~~4. Villeneuve d'Ascq, France*	50.61	3.14	01/2000-12/2019
~~4~~5. Groß-Enzersdorf, Austria*	48.20	16.56	05/1998-11/2019
~~5~~6. Zugspitze, Germany*	47.42	10.98	08/1995-06/2007
~~6~~7. Hoher Sonnblick, Austria*	47.05	12.95	01/1997-06/2020
~~7~~8. Aosta, Italy	45.74	7.36	08/2006-09/2020
~~8~~9. Observatoire de Haute Provence, France*	43.94	5.70	01/2009-11/2018
~~9~~10. Thessaloniki, Greece	40.63	22.95	08/1993-12/2019
~~10~~11. Boulder, CO, United States*	39.99	-105.26	01/2004-12/2019
~~11~~12. Athens, Greece	37.99	23.78	07/2004-12/2020
~~12~~13. Mauna Loa, HI, United States*	19.53	-155.58	07/1995-12/2019
~~13~~14. Reunion Island, St. Denis, France*	-20.90	55.50	03/2009-12/2019
~~14~~15. Alice Springs, Australia*	-23.80	133.87	01/2005-12/2019
~~15~~16. Lauder, New Zealand*	-45.04	169.68	01/1991-12/2019
~~16~~17. Ushuaia, Argentina*	-54.82	-68.32	01/1990-11/2008
~~17~~18. Palmer, Antarctica*	-64.77	-64.05	03/1990-05/2021
~~18~~19. Arrival Heights, Antarctica*	-77.83	166.67	01/1990-04/2021
~~19~~20. South Pole, Antarctica*	-90	0	11/1990-03/2021

*NDACC sites

Table 2. (a) Correlation results between model simulations (~~SC1SD-base-02~~HIS-SD) and ground-based DNA active irradiance data for the northern high latitude stations (>55° N), the southern high latitude stations (>55° S), and the stations between 50° N – 50° S. **(b)** Same as (a) but for the ~~SC1SD-base-02~~HIS-SD simulation and satellite SBUV (v8.~~6~~7) total ozone data. **(c)** Same as (a) but for the ~~SC1SD-base-02~~HIS-SD simulation and satellite MODIS/Terra cloud fraction data. Error, t-value, and p-value refer to slope; t-value should be higher than 2.576 for 99% statistical significance.

~~(a) DNA active irradiance~~							
	~~R~~	~~Slope~~	~~Error~~	~~t-value~~	~~p-value~~	~~N~~	~~RMSE~~
~~>55° N~~	~~+0.518~~	~~0.657~~	~~0.129~~	~~5.105~~	~~<0.0001~~	~~73~~	~~9.543~~
~~>55° S~~	~~+0.746~~	~~0.879~~	~~0.070~~	~~12.629~~	~~<0.0001~~	~~129~~	~~14.766~~
~~50° N – 50° S~~	~~+0.499~~	~~0.387~~	~~0.045~~	~~8.564~~	~~<0.0001~~	~~223~~	~~4.215~~
~~**(b) Total ozone**~~							
	~~R~~	~~Slope~~	~~Error~~	~~t-value~~	~~p-value~~	~~N~~	~~RMSE~~
~~>55° N~~	~~+0.908~~	~~0.839~~	~~0.034~~	~~24.627~~	~~<0.0001~~	~~131~~	~~1.359~~
~~>55° S~~	~~+0.892~~	~~0.888~~	~~0.040~~	~~22.211~~	~~<0.0001~~	~~129~~	~~3.414~~
~~50° N – 50° S~~	~~+0.894~~	~~0.817~~	~~0.028~~	~~29.672~~	~~<0.0001~~	~~223~~	~~0.872~~
~~**(c) Cloud cover**~~							
	~~R~~	~~Slope~~	~~Error~~	~~t-value~~	~~p-value~~	~~N~~	~~RMSE~~
~~>55° N~~	~~+0.480~~	~~0.405~~	~~0.065~~	~~6.215~~	~~<0.0001~~	~~131~~	~~6.367~~
~~>55° S~~	~~+0.485~~	~~0.806~~	~~0.129~~	~~6.230~~	~~<0.0001~~	~~128~~	~~5.003~~
~~50° N – 50° S~~	~~+0.703~~	~~0.721~~	~~0.049~~	~~14.674~~	~~<0.0001~~	~~222~~	~~5.162~~

(a) DNA active irradiance							
	R	Slope	Error	t-value	p-value	N	RMSE
>55° N	+0.504	0.807	0.125	6.447	<0.0001	124	11.527
>55° S	+0.746	0.879	0.070	12.629	<0.0001	129	14.766
50° N – 50° S	+0.499	0.387	0.045	8.564	<0.0001	223	4.215
(b) Total ozone							
	R	Slope	Error	t-value	p-value	N	RMSE
>55° N	+0.899	0.858	0.037	23.264	<0.0001	131	1.308
>55° S	+0.892	0.888	0.040	22.211	<0.0001	129	3.414
50° N – 50° S	+0.894	0.817	0.028	29.672	<0.0001	223	0.872
(c) Cloud cover							
	R	Slope	Error	t-value	p-value	N	RMSE
>55° N	+0.453	0.362	0.063	5.775	<0.0001	131	4.483
>55° S	+0.485	0.806	0.129	6.230	<0.0001	128	5.003
50° N – 50° S	+0.703	0.721	0.049	14.674	<0.0001	222	5.162

1242

Table 3. Trends (% per decade) in total ozone, DNA active irradiance, and cloudiness from the two model simulations and the differences between them, i.e., free-running simulation with increasing GHGs (RC2-base-04REF) minus the simulation with fixed GHGs at 1960 levels (SC2-fGHG-01FIX), averaged at 23 stations in the northern high latitudes (>55° N), 4 stations in the southern high latitudes (>55° S), and 13 stations between 50° N – 50° S. The trends are estimated from the annual mean anomalies shown in Figures 3, 4, 54, 5, 6.

	>55° N (2 stations)								
Trends (% per decade)	RC2-base-04			SC2-fGHG-01			Difference		
	1960-1999	2000-2049	2050-2099	1960-1999	2000-2049	2050-2099	1960-1999	2000-2049	2050-2099
Ozone	−0.56 ± 0.24	0.53 ± 0.16	0.49 ± 0.17	−1.28 ± 0.27	0.42 ± 0.14	0.02 ± 0.16	0.72 ± 0.27	0.12 ± 0.16	0.47 ± 0.18
DNA active irradiance	0.29 ± 0.88	−2.79 ± 0.62	−2.54 ± 0.68	2.99 ± 0.91	−1.18 ± 0.49	−0.34 ± 0.57	−2.70 ± 1.16	−1.54 ± 0.63	−2.11 ± 0.74
Clouds	0.09 ± 0.40	−0.13 ± 0.30	0.18 ± 0.28	−0.05 ± 0.44	0.23 ± 0.19	−0.06 ± 0.29	0.14 ± 0.63	−0.36 ± 0.36	0.25 ± 0.39
	>55° S (4 stations)								
Trends (% per decade)	RC2-base-04			SC2-fGHG-01			Difference		
	1960-1999	2000-2049	2050-2099	1960-1999	2000-2049	2050-2099	1960-1999	2000-2049	2050-2099
Ozone	−3.78 ± 0.57	2.63 ± 0.31	1.42 ± 0.29	−4.65 ± 0.48	2.28 ± 0.41	0.58 ± 0.31	0.87 ± 0.56	0.35 ± 0.46	0.84 ± 0.42
DNA active irradiance	5.70 ± 0.97	−4.92 ± 0.55	−1.68 ± 0.43	7.61 ± 0.92	−4.81 ± 0.75	−0.72 ± 0.38	−1.91 ± 0.95	−0.10 ± 0.82	−0.97 ± 0.58
Clouds	−0.36 ± 0.39	−0.71 ± 0.28	−0.28 ± 0.26	0.18 ± 0.31	−0.05 ± 0.22	−0.01 ± 0.26	−0.54 ± 0.47	−0.53 ± 0.35	−0.21 ± 0.35
	50° N – 50° S (13 stations)								
Trends (% per decade)	RC2-base-04			SC2-fGHG-01			Difference		
	1960-1999	2000-2049	2050-2099	1960-1999	2000-2049	2050-2099	1960-1999	2000-2049	2050-2099
Ozone	−0.61 ± 0.14	0.42 ± 0.11	0.02 ± 0.12	−1.27 ± 0.16	0.36 ± 0.10	0.12 ± 0.09	0.66 ± 0.10	0.06 ± 0.08	−0.10 ± 0.09
DNA active irradiance	1.55 ± 0.44	−0.53 ± 0.35	0.86 ± 0.35	1.75 ± 0.48	−0.54 ± 0.32	0.05 ± 0.28	−0.20 ± 0.58	0.01 ± 0.44	0.81 ± 0.39
Clouds	−1.15 ± 0.29	−0.30 ± 0.27	−0.60 ± 0.25	0.16 ± 0.30	−0.25 ± 0.23	−0.16 ± 0.19	−1.21 ± 0.42	−0.12 ± 0.30	−0.50 ± 0.27

	>55° N (3 stations)								
Trends (% per decade)	REF			FIX			Difference		
	1960-1999	2000-2049	2050-2099	1960-1999	2000-2049	2050-2099	1960-1999	2000-2049	2050-2099
Ozone	−0.55 ± 0.21	0.50 ± 0.16	0.41 ± 0.17	−1.35 ± 0.26	0.36 ± 0.15	0.05 ± 0.15	0.79 ± 0.24	0.14 ± 0.16	0.36 ± 0.17
DNA active irradiance	1.03 ± 0.77	−1.75 ± 0.56	−2.47 ± 0.60	2.61 ± 0.78	−1.15 ± 0.46	−0.83 ± 0.57	−1.57 ± 0.96	−0.59 ± 0.68	−1.64 ± 0.76
Clouds	−0.21 ± 0.30	−0.10 ± 0.23	0.32 ± 0.20	−0.20 ± 0.43	0.02 ± 0.25	0.19 ± 0.27	−0.29 ± 0.45	−0.39 ± 0.25	0.29 ± 0.27

	>55º S (4 stations)								
Trends (% per decade)	**REF**			**FIX**			**Difference**		
	1960-1999	**2000-2049**	**2050-2099**	**1960-1999**	**2000-2049**	**2050-2099**	**1960-1999**	**2000-2049**	**2050-2099**
Ozone	–3.78 ± 0.57	2.63 ± 0.31	1.42 ± 0.29	–4.65 ± 0.48	2.28 ± 0.41	0.58 ± 0.31	0.87 ± 0.56	0.35 ± 0.46	0.84 ± 0.42
DNA active irradiance	5.70 ± 0.97	–4.92 ± 0.55	–1.68 ± 0.43	7.61 ± 0.92	–4.81 ± 0.75	–0.72 ± 0.38	–1.91 ± 0.95	–0.10 ± 0.82	–0.97 ± 0.58
Clouds	–0.36 ± 0.39	–0.71 ± 0.28	–0.28 ± 0.26	0.18 ± 0.31	–0.05 ± 0.22	–0.01 ± 0.26	–0.54 ± 0.47	–0.53 ± 0.35	–0.21 ± 0.35
	50º N – 50º S (13 stations)								
Trends (% per decade)	**REF**			**FIX**			**Difference**		
	1960-1999	**2000-2049**	**2050-2099**	**1960-1999**	**2000-2049**	**2050-2099**	**1960-1999**	**2000-2049**	**2050-2099**
Ozone	–0.61 ± 0.14	0.42 ± 0.11	0.02 ± 0.12	–1.27 ± 0.16	0.36 ± 0.10	0.12 ± 0.09	0.66 ± 0.10	0.06 ± 0.08	–0.10 ± 0.09
DNA active irradiance	1.55 ± 0.44	–0.53 ± 0.35	0.86 ± 0.35	1.75 ± 0.48	–0.54 ± 0.32	0.05 ± 0.28	–0.20 ± 0.58	0.01 ± 0.44	0.81 ± 0.39
Clouds	–1.15 ± 0.29	–0.30 ± 0.27	–0.60 ± 0.25	0.16 ± 0.30	–0.25 ± 0.23	–0.16 ± 0.19	–1.21 ± 0.42	–0.12 ± 0.30	–0.50 ± 0.27

1251

1252

1253

Table 4. Same as Table 3 but for the winter months, January (J), February (F), and March (M) for the northern high latitude stations. Due to the polar night, UV results for January and February are not shown due to large standard errors.

Trends (% per decade)	>55° N (2 stations)								
	RC2-base-04			SC2-fGHG-01			Difference		
	1960-1999	2000-2049	2050-2099	1960-1999	2000-2049	2050-2099	1960-1999	2000-2049	2050-2099
Ozone (J)	−1.85 ± 0.91	1.72 ± 0.59	−0.02 ± 0.63	−1.09 ± 0.93	0.33 ± 0.58	0.61 ± 0.64	−0.76 ± 1.36	1.39 ± 0.71	−0.63 ± 0.88
Ozone (F)	−2.36 ± 0.78	2.09 ± 0.63	1.39 ± 0.62	−2.15 ± 0.84	0.21 ± 0.61	0.17 ± 0.48	−0.21 ± 1.08	1.88 ± 0.81	1.22 ± 0.76
Ozone (M)	−3.16 ± 0.53	0.65 ± 0.49	0.83 ± 0.39	−2.79 ± 0.71	0.84 ± 0.38	−0.82 ± 0.48	−0.37 ± 0.81	−0.18 ± 0.55	1.65 ± 0.59
DNA active irradiance (J)	Polar night	Polar night	Polar night	Polar night	Polar night	Polar night	Polar night	Polar night	Polar night
DNA active irradiance (F)	Polar night	Polar night	Polar night	Polar night	Polar night	Polar night	Polar night	Polar night	Polar night
DNA active irradiance (M)	5.49 ± 1.77	−1.70 ± 1.40	−3.00 ± 1.22	8.28 ± 1.90	−0.82 ± 1.23	1.30 ± 1.19	−2.80 ± 2.41	−0.49 ± 1.81	−4.29 ± 1.64
Clouds (J)	−0.67 ± 0.67	1.38 ± 0.62	0.41 ± 0.54	1.21 ± 0.66	−0.31 ± 0.52	0.43 ± 0.51	−1.84 ± 0.93	1.70 ± 0.98	0.11 ± 0.74
Clouds (F)	−0.71 ± 0.99	0.99 ± 0.72	0.83 ± 0.68	0.47 ± 0.91	−0.54 ± 0.71	−0.26 ± 0.65	−1.58 ± 1.11	−0.60 ± 1.12	0.09 ± 0.88
Clouds (M)	0.47 ± 0.88	1.34 ± 0.92	1.61 ± 0.73	0.72 ± 1.35	0.31 ± 0.94	−0.27 ± 0.78	−0.25 ± 1.44	1.03 ± 1.30	1.92 ± 0.95

Trends (% per decade)	>55° N (3 stations)								
	REF			FIX			Difference		
	1960-1999	2000-2049	2050-2099	1960-1999	2000-2049	2050-2099	1960-1999	2000-2049	2050-2099
Ozone (J)	−1.66 ± 0.74	1.81 ± 0.53	0.49 ± 0.53	−1.32 ± 0.72	0.28 ± 0.50	0.28 ± 0.54	−0.34 ± 1.09	1.53 ± 0.64	0.21 ± 0.73
Ozone (F)	−2.27 ± 0.74	2.00 ± 0.59	0.88 ± 0.58	−1.65 ± 0.83	0.21 ± 0.54	0.31 ± 0.44	−0.62 ± 0.96	1.79 ± 0.78	0.58 ± 0.71
Ozone (M)	−2.98 ± 0.53	0.75 ± 0.50	0.66 ± 0.35	−3.04 ± 0.71	0.58 ± 0.39	−0.54 ± 0.41	0.06 ± 0.83	0.17 ± 0.58	1.20 ± 0.51
DNA active irradiance (J)	Polar night	Polar night	Polar night	Polar night	Polar night	Polar night	Polar night	Polar night	Polar night
DNA active irradiance (F)	Polar night	Polar night	Polar night	Polar night	Polar night	Polar night	Polar night	Polar night	Polar night
DNA active irradiance (M)	3.03 ± 1.97	−0.63 ± 1.52	−2.83 ± 1.22	7.20 ± 1.77	−0.09 ± 1.44	−0.98 ± 1.27	−3.28 ± 2.55	−0.06 ± 2.18	−1.90 ± 1.51
Clouds (J)	−0.67 ± 0.61	1.29 ± 0.63	0.94 ± 0.48	1.11 ± 0.77	0.03 ± 0.53	0.52 ± 0.49	−1.77 ± 0.92	1.25 ± 0.88	0.39 ± 0.68
Clouds (F)	−0.07 ± 0.86	0.60 ± 0.68	1.30 ± 0.57	0.55 ± 0.81	−0.14 ± 0.66	0.06 ± 0.58	−0.62 ± 1.11	0.74 ± 0.93	1.24 ± 0.82
Clouds (M)	0.35 ± 0.70	1.15 ± 0.60	1.33 ± 0.61	0.23 ± 1.02	0.21 ± 0.69	−0.17 ± 0.64	0.12 ± 1.12	0.94 ± 0.88	1.49 ± 0.79

Table 5. Statistical test results for the difference between two trends in DNA active irradiance (trend of 1960-2049 minus trend of 2050-2099), for the northern high latitude stations (>55° N), the southern high latitude stations (>55° S), and the stations between 50° N – 50° S.

~~Latitudes~~	~~>55° N (2 stations)~~		~~>55° S (4 stations)~~		~~50° N – 50° S (13 stations)~~	
	~~1960–2049~~	~~2050–2099~~	~~1960–2049~~	~~2050–2099~~	~~1960–2049~~	~~2050–2099~~
~~N~~	~~605~~	~~336~~	~~630~~	~~350~~	~~1080~~	~~600~~
~~slope, b/year (Eq. 4)~~	~~–0.200~~	~~–0.204~~	~~–0.116~~	~~–0.096~~	~~–0.033~~	~~0.081~~
~~S_b (Eqs. 5 and 6)~~	~~0.027~~	~~0.061~~	~~0.026~~	~~0.048~~	~~0.015~~	~~0.037~~
~~S_{b1-b2} (Eq. 3)~~	~~0.067~~		~~0.054~~		~~0.040~~	
~~t (Eq. 3)~~	~~0.061~~		~~–0.376~~		~~–2.844~~	
~~degrees of freedom~~	~~937~~		~~976~~		~~1676~~	
~~significance level~~	~~0.05~~		~~0.05~~		~~0.05~~	
~~p-value~~	~~0.951~~		~~0.707~~		~~0.005~~	
~~t-critical~~	~~1.96~~		~~1.96~~		~~1.96~~	
~~Significantly different trends~~	~~No~~		~~No~~		~~Yes~~	

Latitudes	**>55° N (3 stations)**		**>55° S (4 stations)**		**50° N – 50° S (13 stations)**	
	1960–2049	**2050–2099**	**1960–2049**	**2050–2099**	**1960–2049**	**2050–2099**
N	553	315	630	350	1080	600
slope, $b/year$ (Eq. 4)	–0.173	–0.186	–0.116	–0.096	–0.033	0.081
s_b (Eqs. 5 and 6)	0.027	0.062	0.026	0.048	0.015	0.037
$s_{(b_1-b_2)}$ (Eq. 3)	0.068		0.054		0.040	
$t-value$ (Eq. 3)	0.185		–0.376		–2.844	
degrees of freedom	864		976		1676	
significance level	0.05		0.05		0.05	
$p-value$	0.853		0.707		0.005	
$t-critical$	1.96		1.96		1.96	
Significantly different trends	No		No		Yes	

Table 6. (a) Coefficients of multiple regression analysis according to Eq. (7), applied to the differences between the two model simulations, ~~RC2-base-04~~REF and ~~SC2-fGHG-01~~FIX, for the period 2050–2099, for the northern high latitude stations (>55° N), the southern high latitude stations (>55° S), and the stations between 50° N – 50° S. **(b)** Trends (% per decade) for the period 2050-2099 in the DNA active irradiance, the ozone-related DNA active irradiance component and the cloud-related DNA active irradiance component.

~~(a) MLR coefficients (2050–2099)~~			
	~~>55° N (2 stations)~~	~~>55° S (4 stations)~~	~~50° N – 50° S (13 stations)~~
~~$a \pm error$~~	~~–4.305 ± 0.885~~	~~–1.994 ± 0.670~~	~~–0.557 ± 0.336~~
~~$\beta_{O_3} \pm error$~~	~~–2.068 ± 0.187~~	~~–0.667 ± 0.071~~	~~–2.831 ± 0.128~~
~~$\beta_{cloud} \pm error$~~	~~–0.593 ± 0.068~~	~~–0.367 ± 0.065~~	~~–0.642 ± 0.035~~
~~(b) Trends (% per decade) (2050–2099)~~			
	~~>55° N (2 stations)~~	~~>55° S (4 stations)~~	~~50° N – 50° S (13 stations)~~
~~DNA active irradiance~~	~~–2.04 ± 0.61%~~	~~–0.96 ± 0.48%~~	~~0.81 ± 0.37%~~
~~Ozone-related DNA active irradiance component~~	~~–0.96 ± 0.30%~~	~~–0.57 ± 0.21%~~	~~0.27 ± 0.20%~~
~~Cloud-related DNA active irradiance component~~	~~–0.14 ± 0.23%~~	~~0.07 ± 0.13%~~	~~0.33 ± 0.17%~~

(a) MLR coefficients (2050–2099)			
	>55° N (3 stations)	>55° S (4 stations)	50° N – 50° S (13 stations)
$a \pm error$	–4.473 ± 0.976	–1.994 ± 0.670	–0.557 ± 0.336
$\beta_{O_3} \pm error$	–2.017 ± 0.220	–0.667 ± 0.071	–2.831 ± 0.128
$\beta_{cloud} \pm error$	–0.749 ± 0.090	–0.367 ± 0.065	–0.642 ± 0.035
(b) Trends (% per decade) (2050–2099)			
	>55° N (3 stations)	>55° S (4 stations)	50° N – 50° S (13 stations)
DNA active irradiance	–1.86 ± 0.61%	–0.96 ± 0.48%	0.81 ± 0.37%
Ozone-related DNA active irradiance component	–0.72 ± 0.25%	–0.57 ± 0.21%	0.27 ± 0.20%
Cloud-related DNA active irradiance component	–0.21 ± 0.24%	0.07 ± 0.13%	0.33 ± 0.17%

Table 7. Trends and their standard errors (% per decade) in the differences between the two model simulations, ~~RC2-base-04~~REF and ~~SC2-fGHG-01~~FIX, for the DNA active irradiance, total ozone, cloud cover and surface albedo at Barrow (Alaska) and Palmer (Antarctica) for the periods 1960–1999, 2000–2049 and 2050–2099.

Trends (% per decade)	**Barrow, Alaska**			**Palmer, Antarctica**		
	1960-1999	**2000-2049**	**2050-2099**	**1960-1999**	**2000-2049**	**2050-2099**
DNA active irradiance	–2.88 ± 1.67	–2.18 ± 1.17	–2.14 ± 1.12	0.75 ± 1.47	–1.79 ± 1.08	–0.33 ± 0.90
Ozone	0.39 ± 0.24	0.06 ± 0.17	0.44 ± 0.19	–0.02 ± 0.54	0.23 ± 0.37	0.54 ± 0.40
Clouds	–0.96 ± 0.78	0.42 ± 0.54	0.60 ± 0.52	–1.60 ± 0.65	0.41 ± 0.49	–0.46 ± 0.48
Surface albedo	0.88 ± 1.33	–6.42 ± 0.80	–2.73 ± 0.89	0.08 ± 0.82	–1.52 ± 0.51	–1.60 ± 0.53

1286

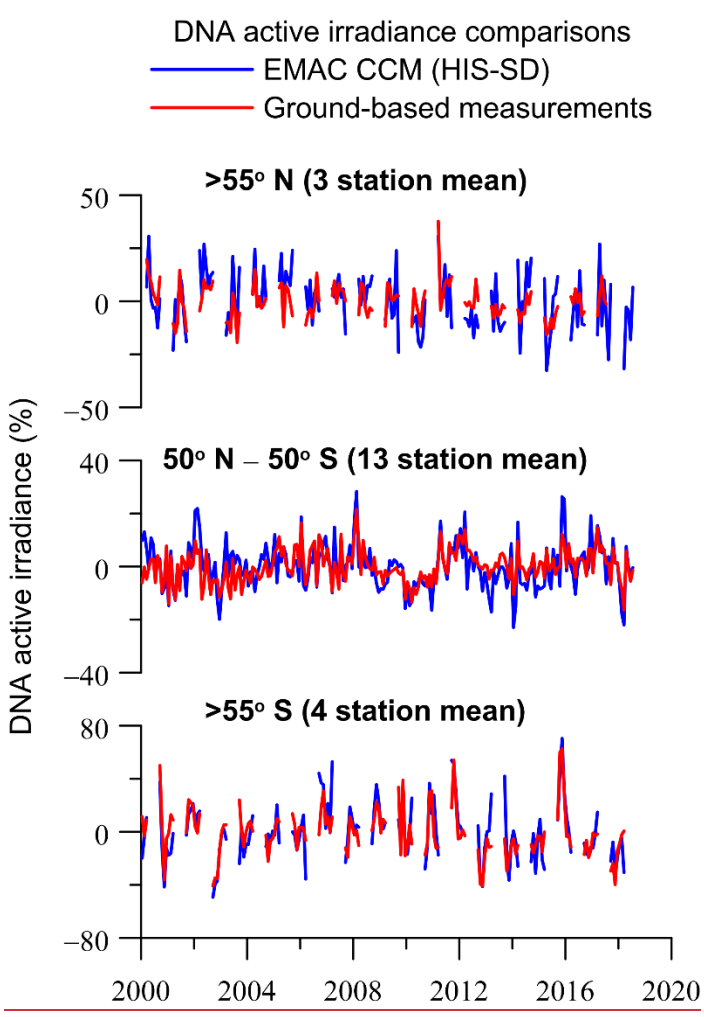
DNA active irradiance comparisons
EMAC CCM (HIS-SD)
Ground-based measurements
>55° N (3 station mean)
50° N – 50° S (13 station mean)
>55° S (4 station mean)
DNA active irradiance (%)
50
0
−50
40
0
−40
80
0
−80
2000
2004
2008
2012
2016
2020

1287

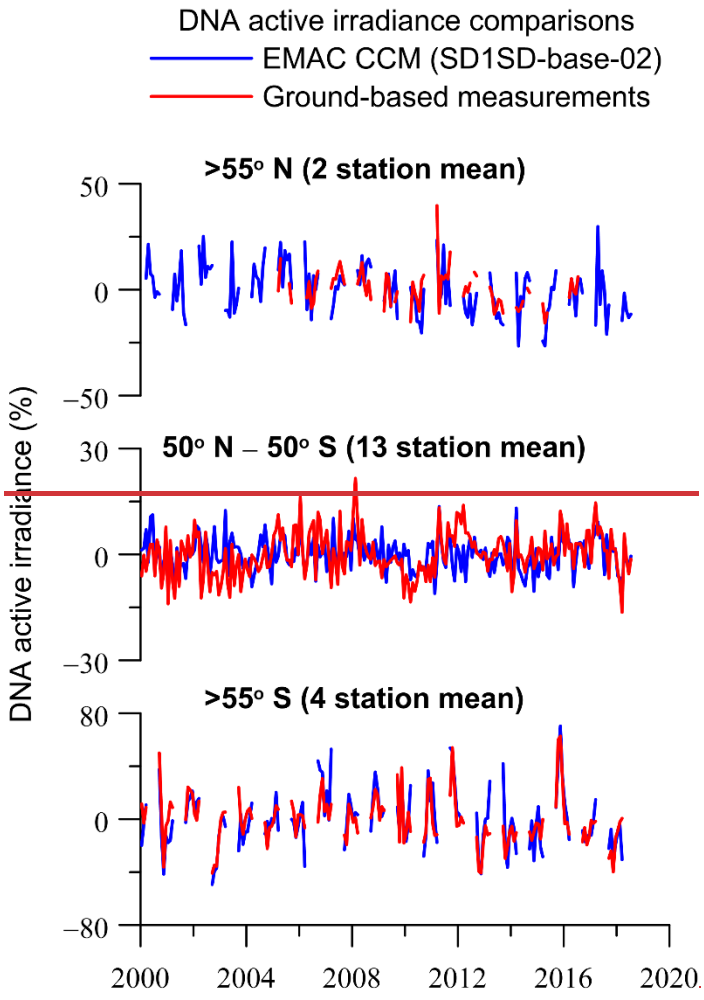

Figure 1. Comparison of model simulations of DNA active irradiance with averages of ground-based measurements at ~~2~~ 3 UV stations in the northern high latitudes (>55° N) (upper panel), 13 UV stations from 50° N to 50° S (middle panel) and 4 UV stations in the southern high latitudes (>55° S) (lower panel). ~~Shown are data from March to September for the northern high latitudes and from September to March for the southern high latitudes.~~ The y-axis shows ~~yearly averaged~~monthly de-seasonalized DNA active irradiance data (in %) ~~calculated from de-seasonalized monthly data~~. The monthly data at each station were de-seasonalized by subtracting the long-term monthly mean (2000–2018) pertaining to the same calendar month and were expressed in %. Then, the average over each geographical zone was estimated by averaging the de-seasonalized data of the stations belonging to each geographical zone. Shown are data from March to September for the northern high latitudes and from September to March for the southern high latitudes. ~~For the northern high latitude stations, the annual average refers to the average of monthly anomalies from March to September, and for the southern high latitude stations, it refers to the average of monthly anomalies from September to March. For the stations between 50° N–50° S we used all months to calculate the annual average.~~

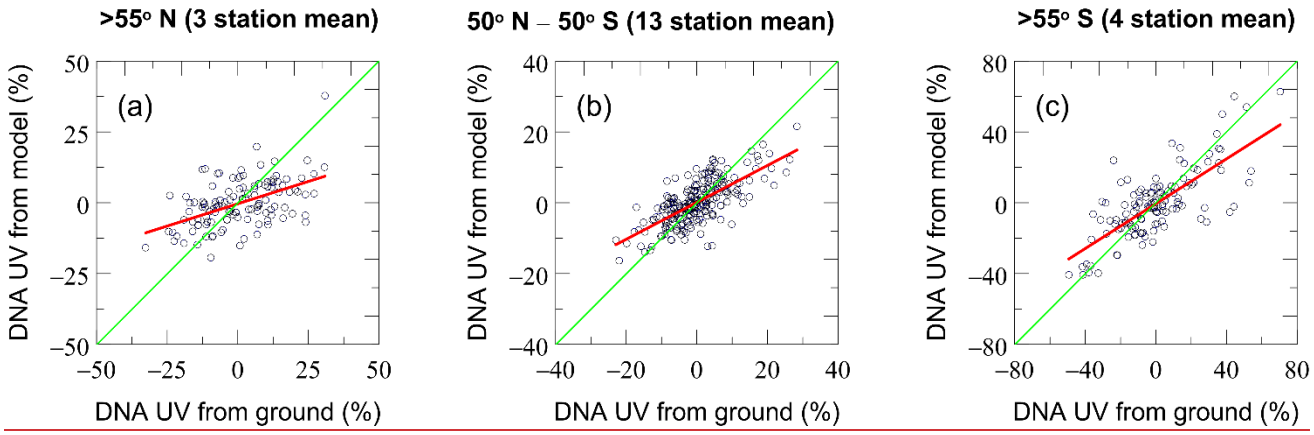

Figure 2. Scatter plots of DNA active irradiance from simulated and ground-based data shown in Figure 1 for **(a)** 3 UV stations in the northern high latitudes (>55° N), **(b)** 13 UV stations from 50° N to 50° S and **(c)** 4 UV stations in the southern high latitudes (>55° S).

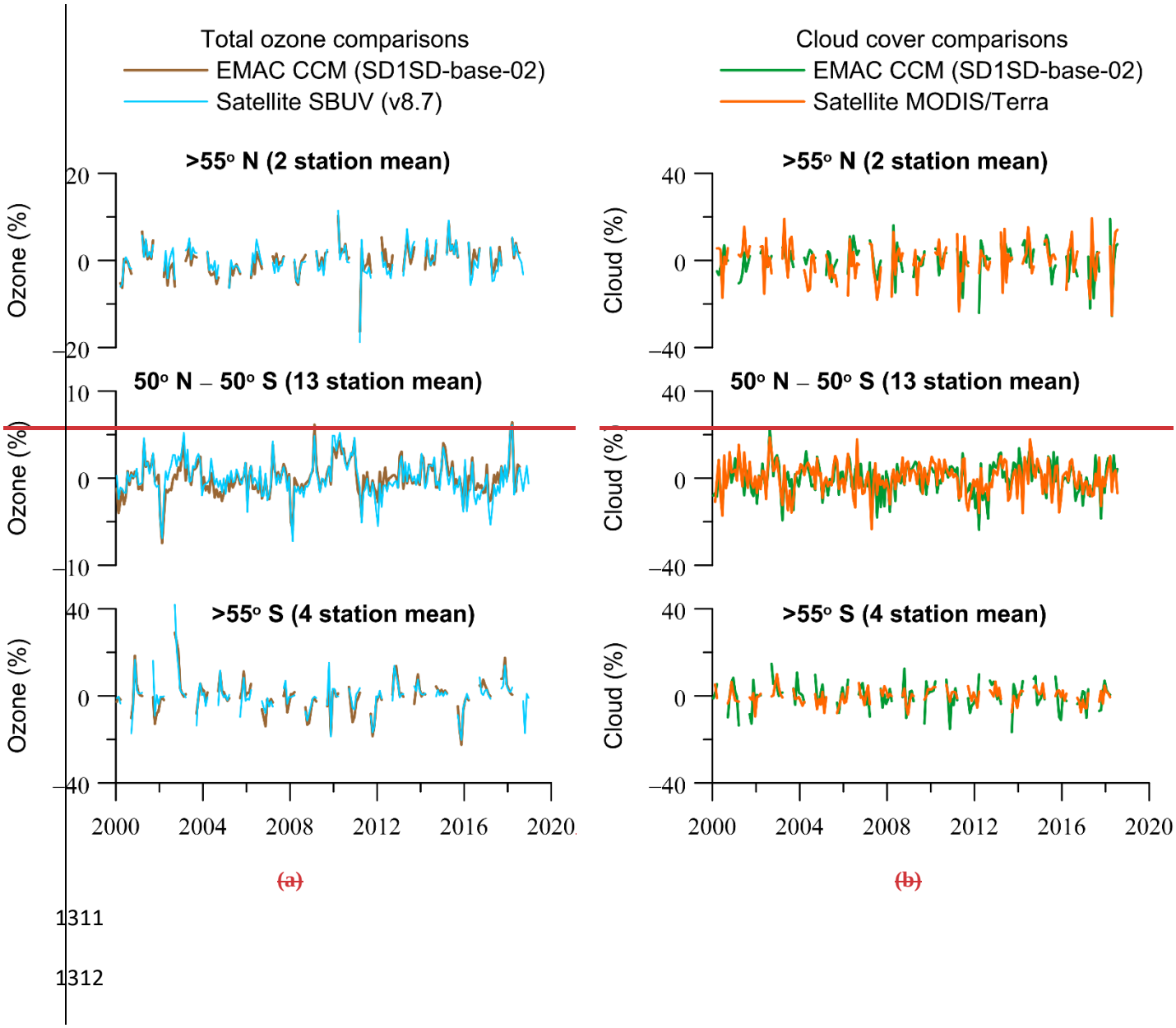
Total ozone comparisons
EMAC CCM (SD1SD-base-02)
Satellite SBUV (v8.7)
>55° N (2 station mean)
50° N – 50° S (13 station mean)
>55° S (4 station mean)
Ozone (%)
20
0
–20
10
–10
40
–40
2000
2004
2008
2012
2016
2020
Cloud cover comparisons
EMAC CCM (SD1SD-base-02)
Satellite MODIS/Terra
Cloud (%)

~~(a)~~ ~~(b)~~

1311

1312

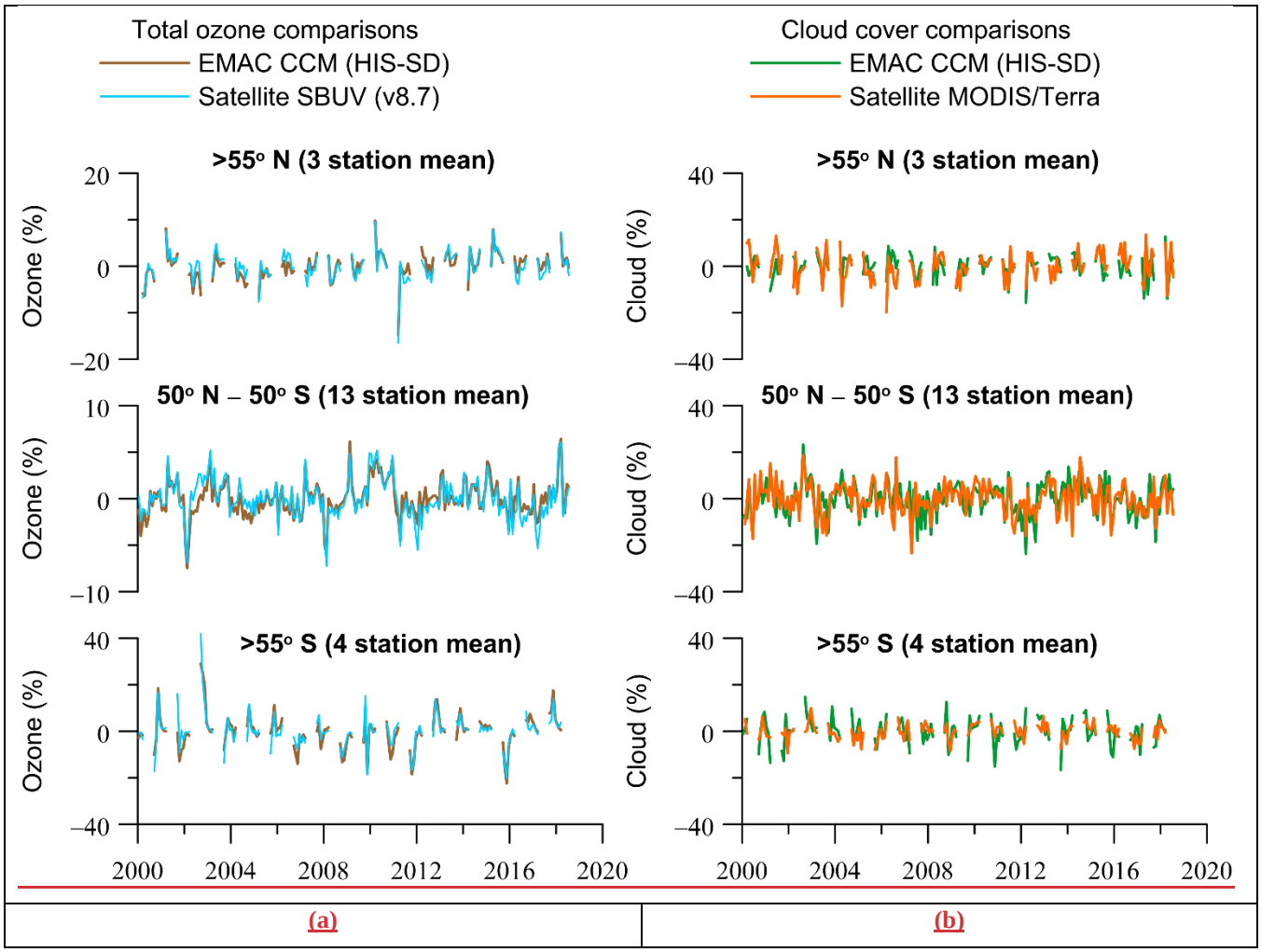

Figure ~~2~~3. (a) Same as in Figure 1 but for ozone column. **(b)** For cloud cover. The y-axes show monthly de-seasonalized anomalies (in %) ~~yearly averaged data (in %) calculated from de-seasonalized monthly data. The monthly data were de-seasonalized~~ relative to the long-term monthly mean (2000–2018) ~~and were expressed in %~~. Shown are monthly anomalies from March to September for the northern high latitudes, and from September to March for the southern high latitudes. For 50° N–50° S, we present all months.~~For the northern high latitude stations, the annual average refers to the average of monthly anomalies from March to September, and for the southern high latitude stations, it refers to the average of monthly anomalies from September to March. For the stations between 50° N–50° S we used all months to calculate the annual average.~~

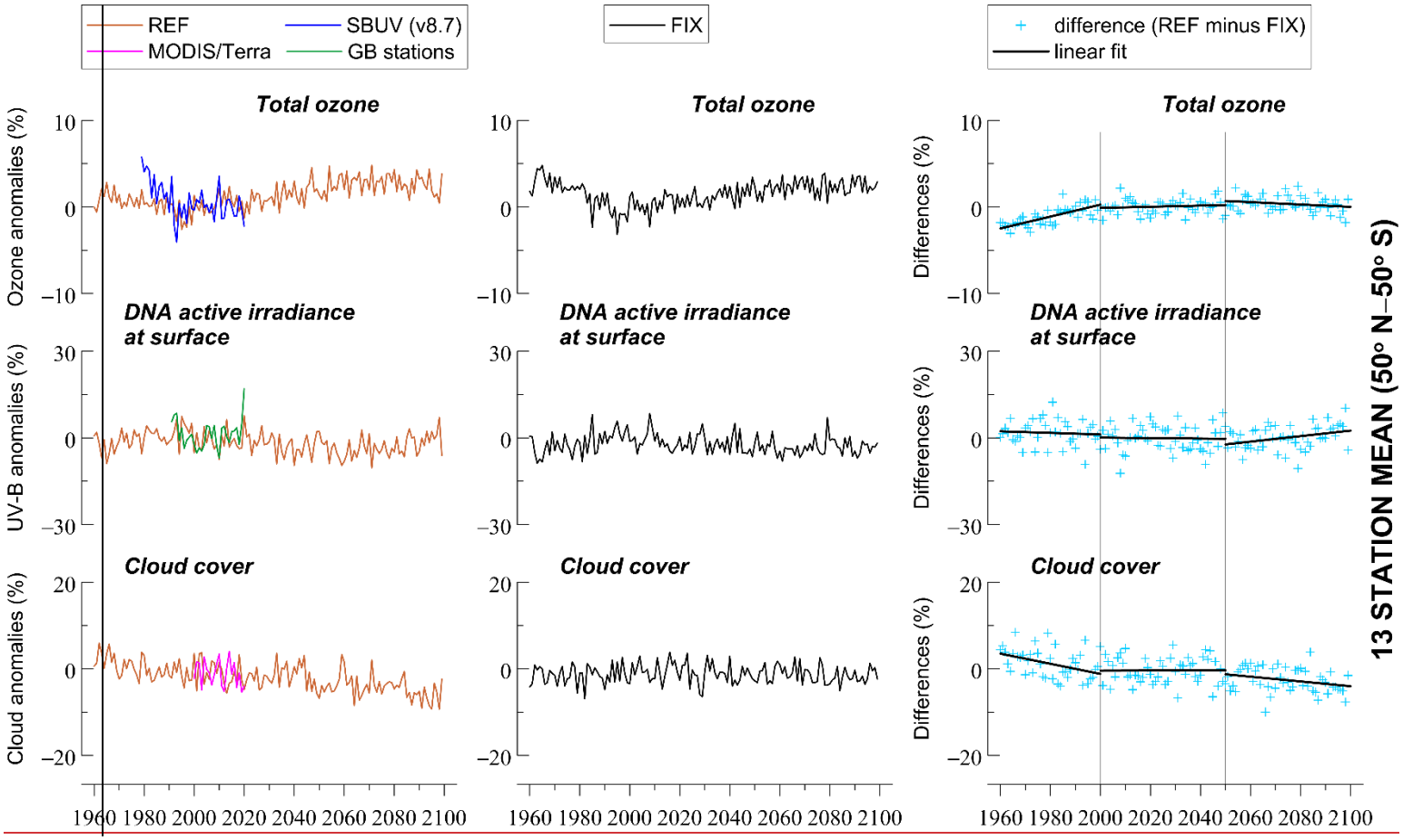
REF
SBUV (v8.7)
MODIS/Terra
GB stations
FIX
difference (REF minus FIX)
linear fit
Total ozone
DNA active irradiance at surface
Cloud cover
Ozone anomalies (%)
UV-B anomalies (%)
Cloud anomalies (%)
Differences (%)
13 STATION MEAN (50° N–50° S)
1960 1980 2000 2020 2040 2060 2080 2100

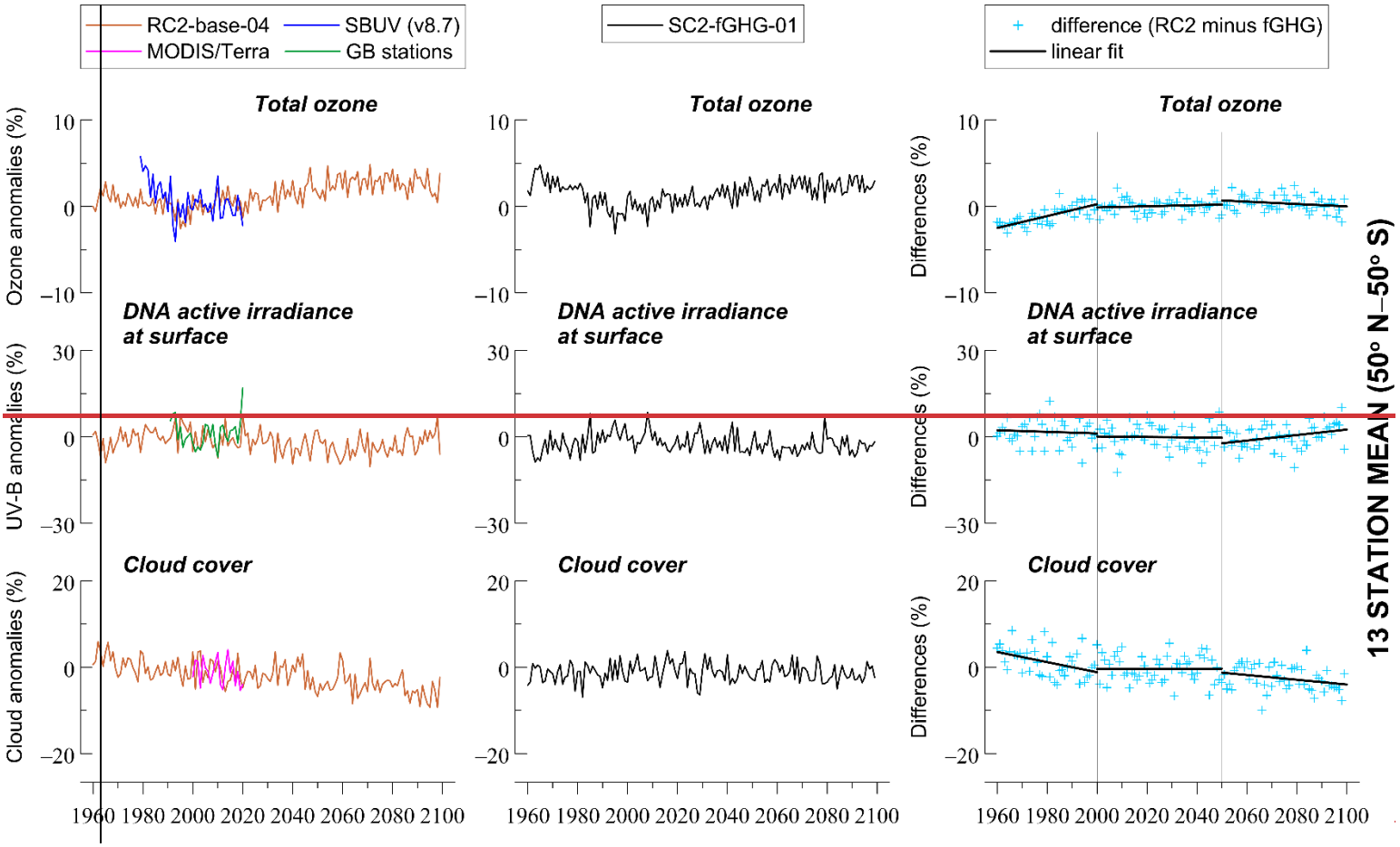

Figure ~~3~~4. Changes in total ozone, DNA active irradiance and cloud cover averaged at 13 UV stations from 50° N to 50° S, based on simulations with increasing and fixed GHGs mixing ratios. **(a)** ~~RC2-base-04~~REF is the simulation with increasing GHGs according to RCP-6.0. **(b)** ~~SC2-fGHG-01~~FIX is the simulation with fixed GHGs emissions at 1960 levels. **(c)** Difference between the two model simulations, indicating the impact of increasing GHGs. The y-axes in (a) and (b) show yearly averaged data (in %) calculated from de-seasonalized monthly data. The monthly data were de-seasonalized relative to the long-term monthly mean (1990–2019) and were expressed in %. For stations between 50° N–50° S we used all months to calculate the annual average.

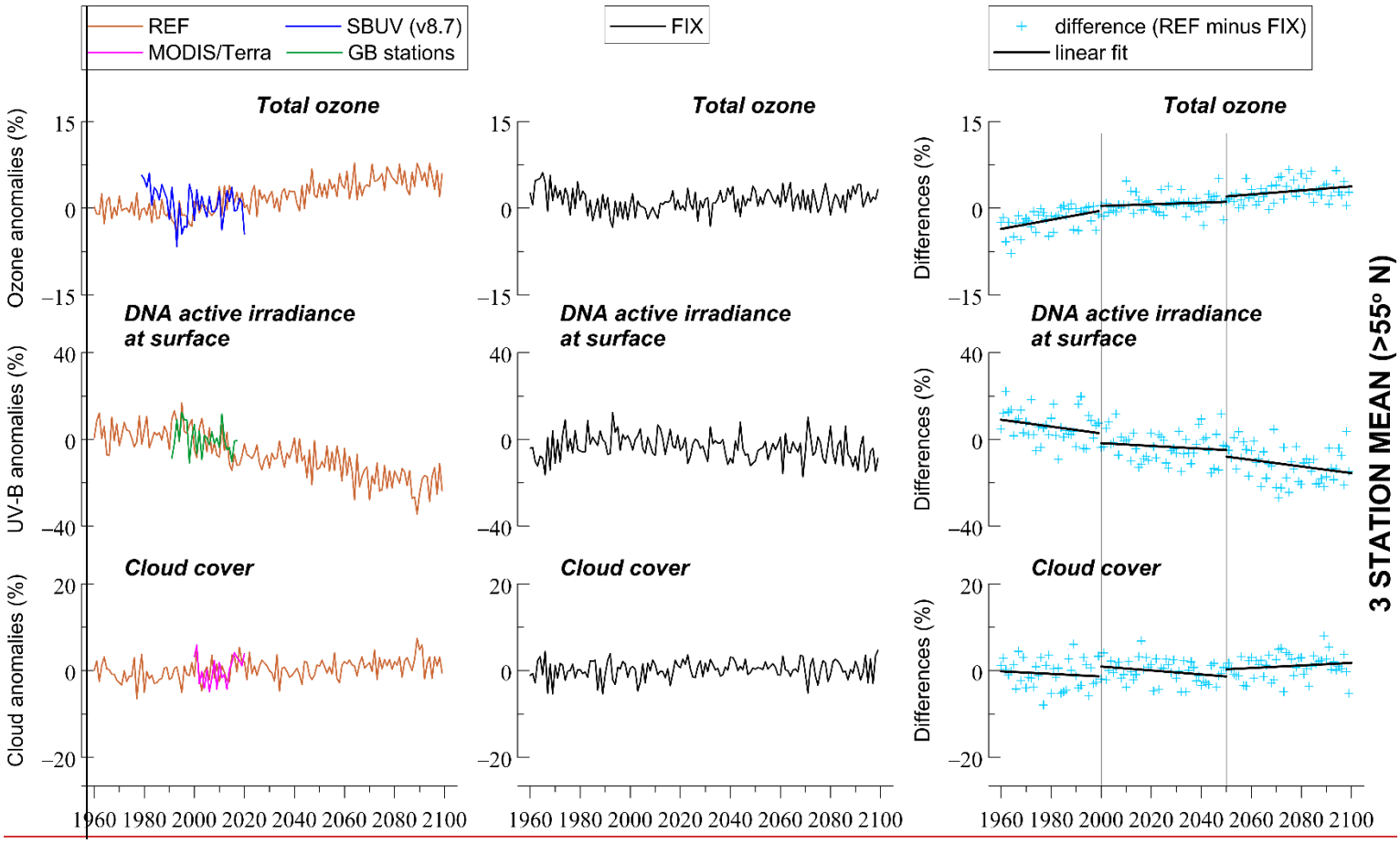
REF
SBUV (v8.7)
MODIS/Terra
GB stations
FIX
difference (REF minus FIX)
linear fit
Total ozone
DNA active irradiance at surface
Cloud cover
Ozone anomalies (%)
UV-B anomalies (%)
Cloud anomalies (%)
Differences (%)
3 STATION MEAN (>55° N)
15
0
−15
40
−40
20
−20
1960 1980 2000 2020 2040 2060 2080 2100

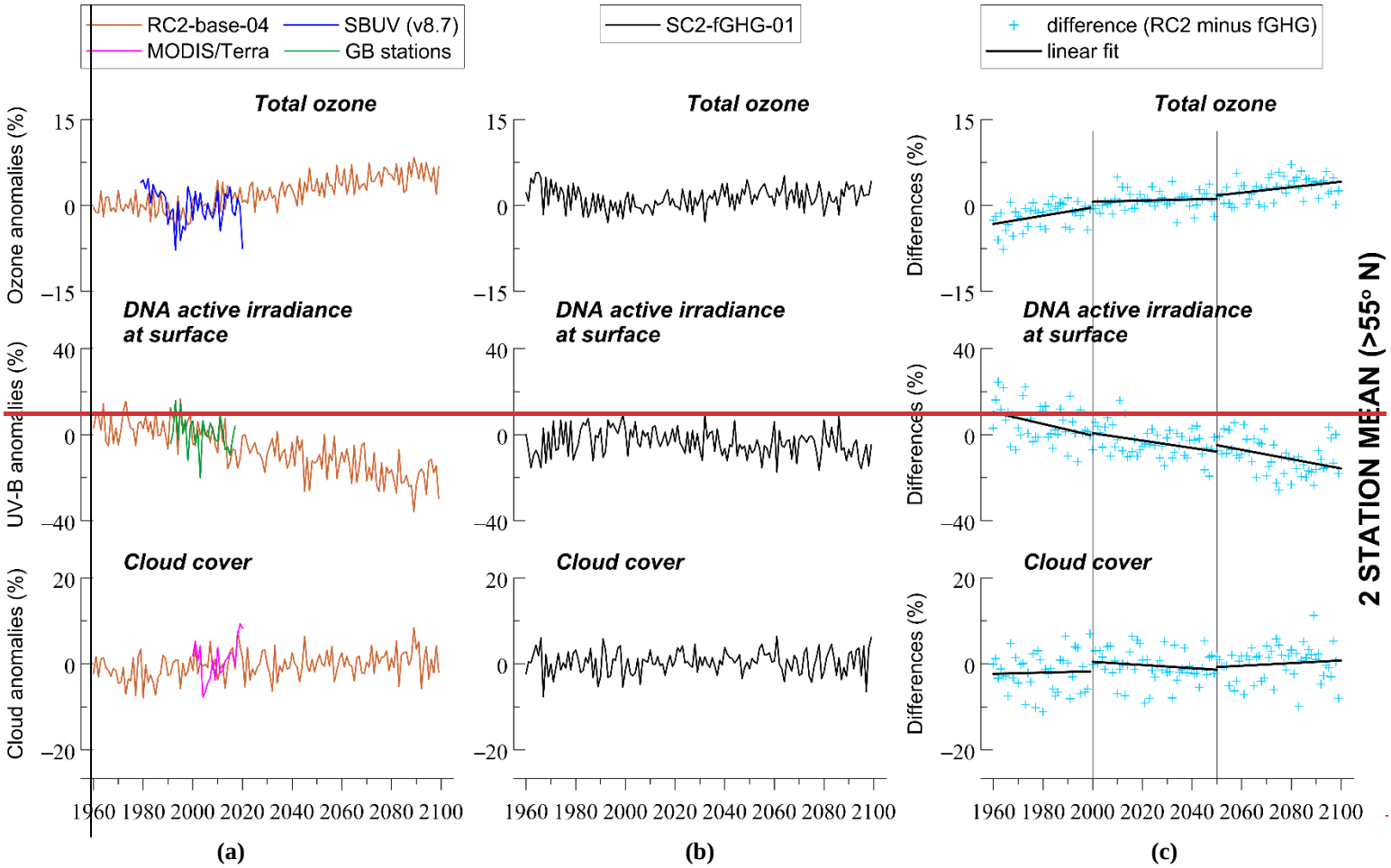

Figure 45. ~~Changes in total ozone, DNA active irradiance and cloud cover averaged at 2~~ Same as Figure 4 but for 3 UV stations in the northern high latitudes (>55° N). The y-axes in (a) and (b) show averages of monthly de-seasonalized anomalies from March to September.~~, based on simulations with increasing and fixed GHGs mixing ratios. **(a)** RC2-base-04 is the simulation with increasing GHGs according to RCP 6.0. **(b)** SC2-fGHG-01 is the simulation with fixed GHGs emissions at 1960 levels. **(c)** Difference between the two model simulations, indicating the impact of increasing GHGs. The y-axes in (a) and (b) show yearly averaged data (in %) calculated from de-seasonalized monthly data. The monthly data were de-seasonalized relative to the long-term monthly mean (1990-2019) and were expressed in %. For the northern high latitude stations, the annual average refers to the average of monthly anomalies from March to September.~~

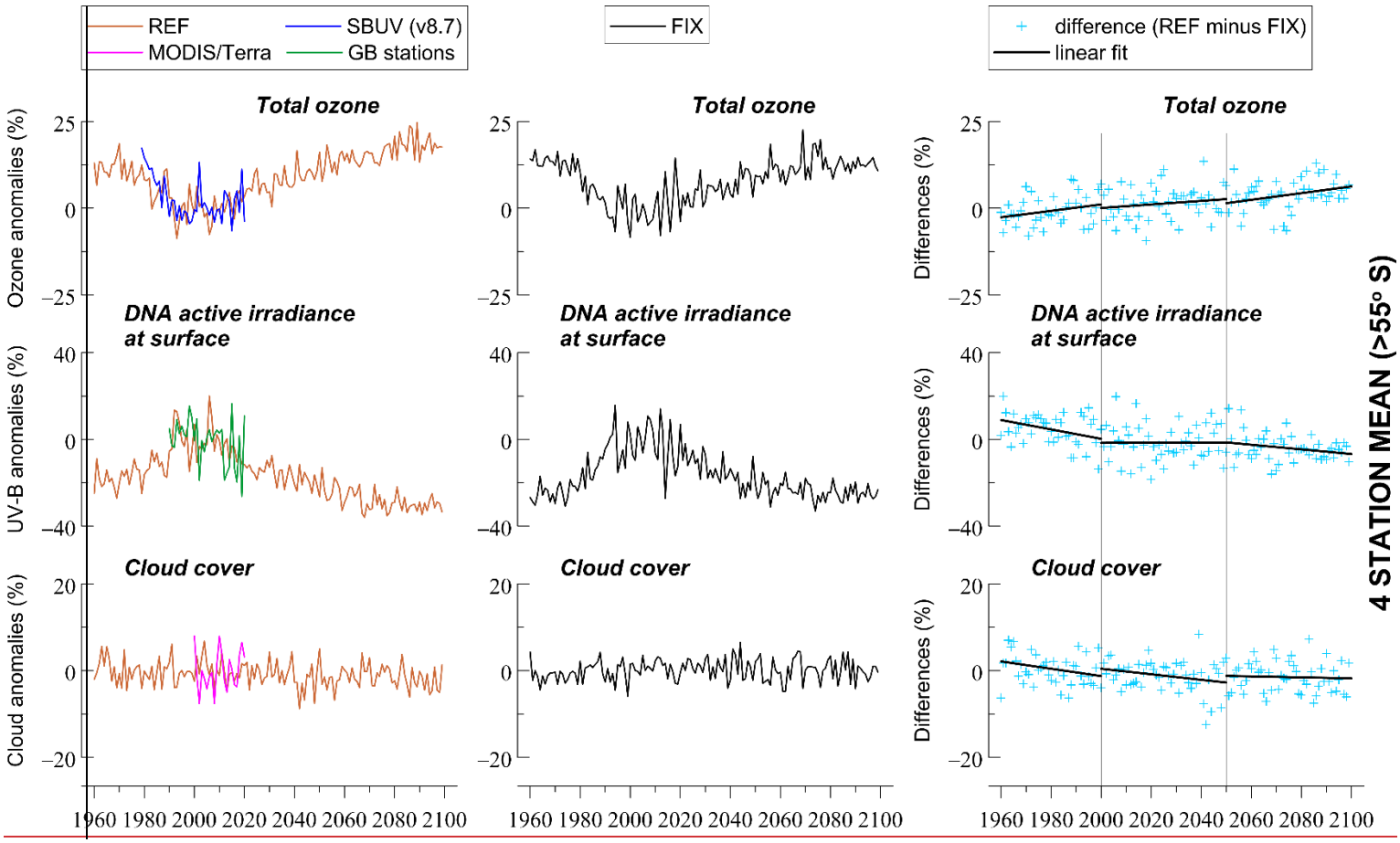
REF
SBUV (v8.7)
MODIS/Terra
GB stations
FIX
difference (REF minus FIX)
linear fit
Total ozone
DNA active irradiance at surface
Cloud cover
Ozone anomalies (%)
UV-B anomalies (%)
Cloud anomalies (%)
Differences (%)
4 STATION MEAN (>55° S)
1960 1980 2000 2020 2040 2060 2080 2100

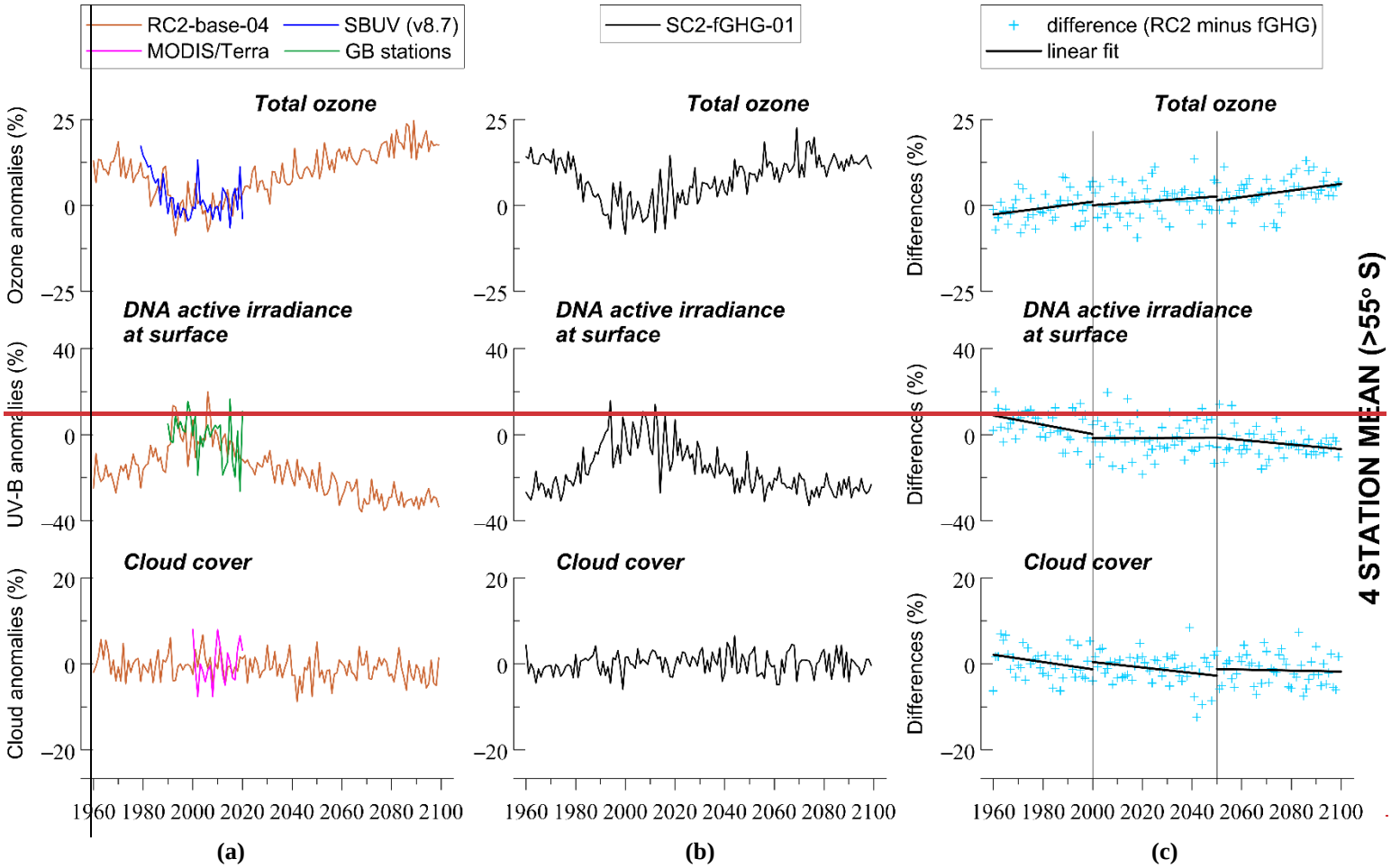

Figure ~~5~~6. ~~Changes in total ozone, DNA active irradiance and cloud cover averaged at~~ Same as Figure 4 but for 4 UV stations in the southern high latitudes (>55° S). The y-axes in (a) and (b) show averages of monthly de-seasonalized anomalies from September to March.~~, based on simulations with increasing and fixed GHGs mixing ratios. (a) RC2-base-04 is the simulation with increasing GHGs according to RCP 6.0. (b) SC2-fGHG-01 is the simulation with fixed GHGs emissions at 1960 levels. (c) Difference between the two model simulations, indicating the impact of increasing GHGs. The y-axes in (a) and (b) show yearly averaged data (in %) calculated from de-seasonalized monthly data. The monthly data were de-seasonalized relative to the long-term monthly mean (1990-2019) and were expressed in %. For the southern high latitude stations, the annual average refers to the average of monthly anomalies from September to March.~~

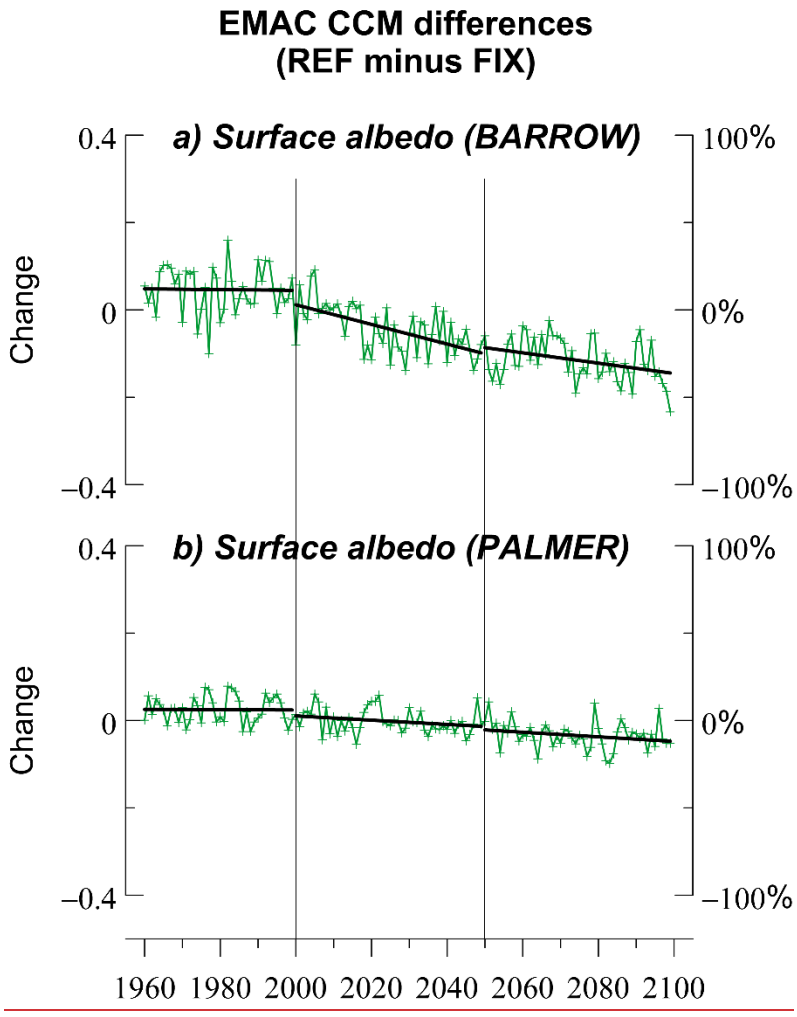
EMAC CCM differences
(REF minus FIX)
a) Surface albedo (BARROW)
b) Surface albedo (PALMER)
Change
0.4
0
−0.4
100%
0%
−100%
1960 1980 2000 2020 2040 2060 2080 2100

1352

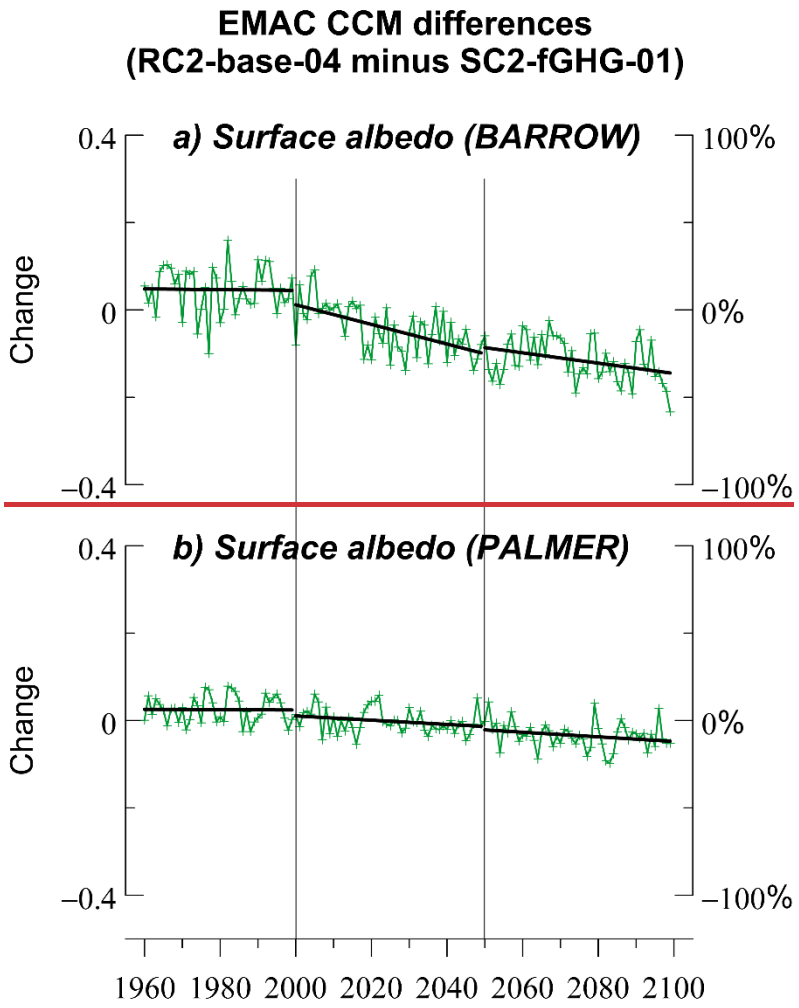

Figure ~~6~~7. (a) Changes in surface albedo at Barrow, Alaska, and **(b)** at Palmer, Antarctica, derived from the differences between the two model simulations: the one with increasing GHGs (~~RC2-base-04~~REF) and the one with fixed GHGs (~~SC2-fGHG-01~~FIX). Results refer to the summer season. Data were de-seasonalized with respect the period 1990–2019 and then were averaged from March to September at Barrow, and from September to March at Palmer. The left y-axis shows the differences in surface albedo values and the right y-axis shows the respective differences in % of the mean.